Title
Contributions of inhibition and physiological noise in a model of cat primary visual cortex

Author
Lauritzen, Thomas Zaccarin

Publication Date
2003

Peer reviewed|Thesis/dissertation

Contributions of inhibition and physiological noise in a model of cat primary visual cortex.

by

Thomas Zaccarin Lauritzen

DISSERTATION

Submitted in partial satisfaction of the requirements for the degree of

DOCTOR OF PHILOSOPHY

in

Biophysics

in the

GRADUATE DIVISION

of the

UNIVERSITY OF CALIFORNIA, SAN FRANCISCO

Contributions of inhibition and physiological noise in a model of cat primary visual cortex.

Thomas Zaccarin Lauritzen
Department of Physiology
Biophysics Graduate Program
W.M. Keck Center for Integrative Neuroscience
University of California, San Francisco

November 22, 2003

To my parents.

Acknowledgements

Sitting here rounding up approximately five years of graduate school I am surprised how fast time passed by. It is easy to get lost thinking about everything that has happened from world changing events and down to simple discussions in the Keck Center or a night out in town.

The person who have influenced me the most in shaping me as a scientist is, of course, my fearless advisor, Ken Miller. I learned about Ken's work about two years before I started at UCSF and after visiting him in the lab - at 8pm - I was sure I wanted to come to UCSF to work with him. It has been great working with Ken. He is both an excellent scientist and mentor. I especialy enjoyed how our discussons have gone from being Ken's monologues when I had just started in the lab to being more and more two-way communication as I learned more and more. All in all, I owe Ken a lot of thanks both for my past work and for stirring an interest that makes me keep on in the field of theoretical neuroscience.

Thanks too to the two other members of my thesis committee, Michael Stryker and Christoph Schreiner. Both have provided great feedback and discussions, Michael as an expert in cat V1 and Christoph as the more physics minded sensory systems person.

In my research I have not been working alone. Many people in the Miller lab have been helpfull. When I joined the lab especially Anton Krukowski and Todd Troyer taught me a lot, both about neuroscience in general and specifically about my project. Anton and I worked together on my first paper (chapter 1) and I remember that when he graduated he told me he was glad that someone continued his research. Now some years later I must say that I did not just continue his research, my whole thesis is based on his work. Anton, Todd and Andy Kayser also gave me valuable indsight and advise on how to function in the lab. Later on I have enjoyed working with Stephanie Palmer as she did a lot of the noise analysis I have used, fully trusting her. Most of my work have been computer simulations and it would not have been possible if I have not had Brian Wright around to help me. Besides Brian I shared office with Brendan Murphy and I have had good talks with him as well as we have been the two students carrying the biophysics flag in the lab and Keck center.

Which brings me to the Keck Center, with all its great people that I have hung out with and discussed science and what not. I will not be able to mention all, but I will name Andrew Tan and Matt Caywood that I have spent most of my time with, as well as the Sloan-Swartz fellows, that being a theorist, I had a lot of contact with.

A couple of earlier mentors deserves mention as well, John Hertz, my M.Sc. thesis advisor that introduced me to theoretical neuroscience and John Miller and Harold Lecar for letting me work in their labs for my academic year spent abroad. All three helped give me a get solid base for starting in graduate school.

All work and no play makes Thomas a dull boy, and luckily I have had an abundance of friends around. Of fear of leaving someone out I will not mention specific names, but most have been part of Drengene, the Berkeley group, the party posse or Qoöl regulars.

Research statement

The material in the first chapter resulted from a collaboration with Anton Krukowski and was published in Lauritzen et al. (2001). The second chapter was published in Lauritzen and Miller (2003a), and chapter three is part of a draft to be submitted. The results from that chapter were presented at the Society for Neuroscience annual meeting in 2003 (Lauritzen and Miller, 2003b).

Abstract

Contributions of inhibition and physiological noise in a model of cat primary visual cortex

Thomas Zaccarin Lauritzen

Several response properties distinguish cortical simple cells of cat primary visual cortex (V1) from the lateral geniculate nucleus (LGN) cells that provide their input. Understanding these differences is a central problem for understanding cerebral cortical circuitry. This dissertation uses a model of the excitatory and inhibitory cells in layer 4 of cat V1, and their thalamocortical and intracortical connections, to explore what patterns of circuitry and physiological mechanisms can explain the observed response properties of the cortex.

In chapter one, we show how a correlation-based circuitry can account responses to multi-grating stimuli. The response to a visual stimulus of the preferred orientation is partially suppressed by simultaneous presentation of stimulus at the orthogonal orientation, an effect known as "cross-orientation inhibition". We explain how this phenomenon can occur despite evidence that cells in V1 do not receive inhibitory connections from cells preferring orientations orthogonal to their own preferred orientation as well as address other non-linear properties of multi-grating stimuli.

The above model predicted that inhibitory cells respond to stimuli of all orientations with increased contrast despite being tuned for a single orientation. Recent experiments have revealed cat V1 layer 4 inhibitory cells with two distinct types of receptive fields (RFs): complex RFs with mixed ON/OFF responses, lacking in orientation tuning; and simple RFs with sharp orientation tuning. In chapter two, we include both these inhibitory cell types in the model and show that complex inhibitory neurons can account for sharp contrast-invariant orientation tuning of simple cells. Given this, antiphase inhibition acts to sharpen spatial frequency tuning, lower responses to low-temporal-frequency stimuli and increase the stability of cortical activity.

Physiological noise levels can convert contrast-invariant voltage tuning to contrast-invariant spike tuning. In chapter three, we introduce physiological levels of noise in the model and show that the network connectivity can provide the contrast-invariant voltage tuning and verify that this yields contrast-invariant spike tuning. We further address the effect of correlations of noise in the network and show that these decrease the spontaneous activity of the cells, while increasing their response as well as temporal frequency tuning in the presence of visual stimuli.

Contents

List of Figures

Chapter 1

Multi-grating stimuli

Abstract

In cortical simple cells of cat striate cortex, the response to a visual stimulus of the preferred orientation is partially suppressed by simultaneous presentation of a stimulus at the orthogonal orientation, an effect known as "cross-orientation inhibition". It has been argued that this is due to the presence of inhibitory connections between cells tuned for different orientations, but intracellular studies suggest that simple cells only receive inhibitory input from cells with similar orientation tuning. Furthermore, response suppression can be elicited by a variety of non-preferred stimuli at all orientations. Here we study a model circuit that was presented previously to address many aspects of simple cell orientation tuning, which is based on local intracortical connectivity between cells of similar orientation tuning. We show that this model circuit can account for many aspects of cross-orientation inhibition and, more generally, of response suppression by non-preferred stimuli and of other non-linear properties of responses to stimulation with multiple gratings.

1.1 Introduction

Cells in cat primary visual cortex (V1) are tuned for the orientation of light/dark borders (Hubel and Wiesel, 1962). Understanding the circuity underlying this orientation selectivity remains a central problem in systems neuroscience (reviewed in Ferster and Miller, 2000).

Clues to the underlying circuitry are provided by experiments involving the superposition of two drifting sinusoidal luminance gratings. A typical simple cell in layer 4 of cat V1 responds to a drifting grating shown at its preferred orientation and is silent in response to a drifting grating of the perpendicular (null) orientation. However, superposition of the null grating with the preferred causes a reduction in response relative to the response to the preferred grating alone, a phenomenon known as "cross-orientation inhibition" (Bonds, 1989; DeAngelis et al., 1992; Morrone et al., 1982). More generally, superposition of a non-preferred grating can suppress responses to a preferred grating (Bonds, 1989; DeAngelis et al., 1992).

This suppression suggests that a non-preferred grating recruits inhibition and/or disrupts the cell's excitatory drive. In particular, the existence of cross-orientation inhibition has led to the suggestion that inhibition from cells tuned to dissimilar orientations plays an important role in cortical orientation selectivity (Carandini and Heeger, 1994; Carandini et al., 1997, 1999; Heeger, 1992; Heeger et al., 1996; Somers et al., 1995). However, evidence from intracellular recordings argues against this idea. Such recordings show that the excitation and the inhibition received by simple cells in cat layer 4 show similar orientation tuning, with both peaked at the preferred orientation and falling to small values at the orthogonal orientation (Anderson et al., 2000a; Ferster, 1986), and that the orientation selectivity of voltage responses is neither created, nor sharpened, by intracortical circuitry (Chung and Ferster, 1998; Ferster et al., 1996).

In this paper, we show that a simple model circuit that is consistent with the intracellular data can account for many of the two-grating suppression effects, including cross-orientation inhibition. This model circuit was originally inspired by the findings that the inhibition and excitation received by a layer 4 simple cell have similar orientation tuning (Anderson et al., 2000a; Ferster, 1986), but are in a "push-pull" or spatially opponent relationship (Ferster, 1988; Hirsch et al., 1998): in ON-subregions, where light evokes excitation, dark evokes inhibition, and similarly dark evokes excitation and light evokes inhibition in OFF-subregions. Accordingly, we proposed (Troyer et al., 1998) that excitatory cells tend to make connections onto cells of similar preferred orientation and similar absolute spatial phase (similar locations in visual space of ON-subregions and of OFF-subregions), while inhibitory cells tend to project to cells of similar preferred orientation and opposite absolute spatial phase. In addition, we assumed that the LGN connections to a simple cell are organized in an oriented, subregion-specific manner (Chung and Ferster, 1998; Ferster et al., 1996; Hubel and Wiesel, 1962; Reid and Alonso, 1995; Tanaka, 1983): ON-center LGN inputs have receptive fields aligned over the simple cell's ON subregions, and OFF-center inputs are aligned on OFF subregions. We showed (Troyer et al., 1998) that, provided that the LGN-driven inhibition

was stronger than the direct LGN excitation, this circuitry could account for the invariance with stimulus contrast of orientation tuning (Sclar and Freeman, 1982; Skottun et al., 1987) and for a number of other intracellular and extracellular observations. Here we show that this circuitry can also account for cross-orientation inhibition, and more generally for a variety of two-grating suppression phenomena.

One of the more extensive experimental studies of such suppression was done by Bonds (1989). He used as a visual stimulus a preferred (base) grating at one temporal frequency and a superposed mask grating at a different temporal frequency. By analyzing the two corresponding temporal components of the response, he separated the base-driven and mask-driven response components, and studied how each component depended on the orientation, contrast, and spatial frequency of the mask grating. In our modeling studies we follow this procedure to determine how closely our model is able to reproduce these experimental observations. We also address two other experiments examining responses to superpositions of gratings with different temporal frequencies at the preferred orientation (Dean et al., 1982; Reid et al., 1992). These experiments found that the modulation of the cell response to low-temporal-frequency stimuli is suppressed by the superposition of high-temporal-frequency stimuli, while the modulation of the cell response to high-temporal-frequency stimuli is enhanced by superposition of low-temporal-frequency stimuli. Here we reproduce these results and explain some of the findings by a toy model.

1.2 Methods

We study a model previously described ("computational model" of Troyer et al., 1998). The major difference in the present work is that NMDA receptors have been included at excitatory synapses onto excitatory cells. Here we present only the basics of that model along with details of any differences in the present implementation.

Our LGN model consists of 7200 LGN X-cells arranged in four overlying 30×30 sheets of ON cells and four similar sheets of OFF cells, with ON and OFF lattices offset by one-half square lattice spacing, covering $6.8 \times 6.8°$ of the visual field. LGN firing rates in response to a single grating were calculated by assuming rates were sinusoidally modulated, up to rectification at zero rate, about background rates of 10 and 15 Hz for ON and OFF cells respectively, with the amplitude of the sinusoidal modulation chosen so that the first harmonic of the rectified responses matched values at a given contrast and temporal frequency reported by Sclar (1987). To compute responses to multiple gratings, we added the sinusoidal rate modulations induced by each grating and then rectified the result. Spikes were then generated from these rates in a random (Poisson) fashion. Overlaying cells have 25% correlation in their spike trains (each of four overlaying cells picked spikes with probability 1/4 from a common set of four Poisson spike trains), to match data showing correlations among LGN cells with overlapping RFs (Alonso et al., 1996).

The cortical model includes 1600 excitatory- and 400 inhibitory layer 4 simple cells, representing

a 2/3 × 2/3 mm patch of cortex, corresponding to 0.75 × 0.75° in visual angle. Each cortical cell was assigned a Gabor-function describing its receptive field, with orientation given by a measured orientation map from cat V1, spatial frequency of 0.8 cycles/degree, retinotopic position progressing uniformly across the sheet, and spatial phase assigned randomly to each cell. The precise parameters used for the Gabor functions were those specifying the "broadly tuned" cells in Troyer et al. (1998), which were designed to reproduce the observed (Anderson et al., 2000a; Ferster et al., 1996) 35^o half-width at half-height of the orientation tuning of intracellular voltage modulations in response to optimal sinusoidal gratings. The connection strength from LGN cells to a cortical cell was determined as in Troyer et al. (1998) by a probabilistic sampling of the cell's Gabor function, where positive regions of the Gabor are converted to probabilities of a connection from an ON-cell centered on that point, and negative regions converted to probabilities of OFF-cells connecting.

Cortical cells were modeled as single-compartment conductance-based integrate-and-fire neurons as in Troyer et al. (1998), with the following differences. The cortical background excitatory input (Poisson) received by all cells was set to a rate of 6000 Hz, resulting in background firing rates of approximately 0.5 Hz for excitatory cells and 20-30 Hz for inhibitory cells. The amplitude of the adaptation conductance, $\bar{g}_{\text{adapt}}$, was reduced by a factor of 5 from a value of 3 nS to 0.6 nS, to bring firing rates up to more realistic levels (as discussed in Troyer et al., 1998); this yielded reasonable levels of excitatory cell gain as measured from plots of firing rate versus instantaneous membrane potential. Finally, synaptic conductances were identical to those used in Troyer et al. (1998) except that we have included NMDA-mediated conductances, in addition to the AMPA-mediated conductances, in all of the excitatory synapses except for the thalamocortical synapses onto inhibitory cells, which were purely AMPA mediated. The decay of the NMDA conductances is modeled as a double exponential with a fast and a slow time constant:

$$g_{\text{NMDA}}(t) = \sum_{t_j<t} \bar{g}_{\text{NMDA}}(V) \left(f_{fast} e^{-(t-t_j)/\tau^{fall}_{\text{NMDA},fast}} + (1 - f_{fast}) e^{-(t-t_j)/\tau^{fall}_{\text{NMDA},slow}} - e^{-(t-t_j)/\tau^{rise}_{\text{NMDA}}} \right)$$

where the sum is over presynaptic spike times t_j, and f_{fast} represents the contribution of the faster exponential to the total decay term. Parameters were taken from data for adult rats in a developmental study of NMDA conductances in the rat visual cortex (Carmignoto and Vicini, 1992): $\tau^{\text{fall}}_{\text{NMDA,fast}} = 63$ msec, $\tau^{\text{fall}}_{\text{NMDA,slow}} = 200$ msec, $f_{\text{fast}} = 88\%$. We chose $\tau^{\text{rise}}_{\text{NMDA}} = 5.5$ msec to set the 10-90% rise time of the NMDA EPSC to be equal to 7.8 msec as has been observed experimentally (Lester et al., 1990). The voltage dependence of $\bar{g}_{\text{NMDA}}$ followed the model described in Jahr and Stevens (1990). The relative strength of NMDA and AMPA conductances were set in terms of the integrated current (*i.e.*, the total charge transfer) through excitatory conductances when the postsynaptic cell is clamped at the spike-threshold voltage. 90% of the integrated current in thalamocortical synapses to excitatory cells was mediated by NMDA, which is the value obtained by matching AMPA and NMDA amplitudes to those observed at thalamocortical synapses at the oldest ages studied in thalamocortical slices (Crair and Malenka, 1995), and 95% of the current in

intracortical excitatory synapses was mediated by NMDA.

The probability that a cortical cell connected to any other cortical cell depended on the correlation between their sets of LGN inputs, as in Troyer et al. (1998): the probability of a connection from an excitatory cell monotonically increased with the degree of correlation, while the probability of a connection from an inhibitory cell monotonically increased with the degree of anticorrelation. This connectivity rule yields the basic cortical circuit structure within a single iso-orientation column shown in cartoon form in figure 1.1A. For simplicity, the inhibitory cells received only thalamocortical input. Previous simulations have demonstrated that intracortical excitatory connections onto inhibitory cells do not have a significant effect on the behavior of the model (Krukowski, 2000; Troyer et al., 1998). An important feature of the model is that the inhibition is dominant over feedforward excitation, rather than precisely balancing it.

Simulations for a given grating or multi-grating stimulus were run as follows. We first allowed the network to run for one second of simulated time while LGN cells fired at their background rates. We then started the grating stimulus and allowed the simulation to run an additional 0.25 seconds to suppress transients, then recorded data for 1 second of simulated time as the grating stimulus continued. PSTHs of 20 such simulations (each with different seeds for the random number generator controlling the Poisson sampling of LGN spikes) were made for the spiking results. Cells of all orientation preferences are represented in the cortical network. To be certain of avoiding artifacts of alignment of the grid with the stimulus, the preferred-orientation stimulus was always at an orientation of 128°, and we sampled our results from the 35 excitatory cells with preferred orientations within ±2.5° of 128°.

1.2.1 Toy rate model

In modeling responses to sums of two grating stimuli at the preferred orientation at different temporal frequencies, we considered both the full model as described above and a simple toy model. The toy model was based on the DC and F1 of the feedforward input (the LGN-driven input, both direct LGN excitation and indirect inhibition via interneurons) observed in the full model. We assumed that the feedforward inputs due to the two sinusoids were simply added and the result passed through a linear threshold input/output curve. We considered 2 sine curves: $y_{2Hz}(t) = \sin(4\pi t/sec) - \beta_{2Hz}$, $y_{8Hz}(t) = \alpha(\sin(16\pi t/sec) - \beta_{8Hz})$, where α is the amplitude of the 8 Hz grating relative to that of the 2 Hz grating, and the β's are the *inhibitory* total feedforward DC (the sum of LGN excitation and inhibition from LGN-driven inhibitory interneurons). We estimated the size of the β's in the full model by examining the total synaptic current evoked when the membrane potential is clamped at spike threshold. We considered response to a 2 Hz grating alone and an 8 Hz grating alone, where grating contrasts were chosen so that evoked current F1's were comparable (2 Hz grating at 20% contrast, 8 Hz grating at 40% contrast, ratio of 2Hz F1 to 8 Hz F1 is 0.8). Defining β as DC/F1 of the resulting currents, we found $\beta_{8Hz} = 0.42$ and

$\beta_{2Hz} = 0.019$. We considered a linear rectified model of response $r(t)$ to an input waveform $i(t)$: $r(t) = [i(t) - \theta]^+$, where θ is a threshold (values used given in Results) and $[x]^+ = x$, $x > 0$; $[x]^+ = 0$, $x \leq 0$. To model single sinusoids, $i(t)$ is set equal to $y_{2Hz}(t)$ or $y_{8Hz}(t)$; for double sinusoids, $i(t) = y_{2Hz}(t) + y_{8Hz}(t)$. We then examined the Fourier component of $r(t)$ at 2 Hz and/or 8 Hz.

1.3 Results

1.3.1 Basic concepts of the model circuit

To understand our results, it is important to recall the main ideas of our circuit model, which will figure prominently in the following results (Fig. 1.1). We define feedforward input to excitatory cells as the sum of the direct LGN excitatory input and the LGN-driven input from inhibitory neurons. Due to the dominant antiphase inhibition, the mean feedforward input evoked by grating stimuli is inhibitory. Cortical excitatory simple cells can only be driven to fire by the temporal modulation of this input: inhibition and excitation are driven at opposite phases of the modulation, so that one goes up when the other goes down. This modulation allows excitation to periodically dominate over inhibition and drive responses, even though inhibition dominates in the mean (Fig. 1.1B).

The mean LGN input evoked by a grating does not depend on grating orientation (because this mean is just the weighted sum of the mean rates of the individual LGN inputs to the simple cell, and the responses of LGN cells are assumed to be untuned for orientation). But the modulation of the LGN input varies strongly with orientation. In response to a preferred orientation stimulus, all of the LGN inputs to a cell modulate their firing rates together, so the total LGN input to the cell is strongly modulated and the cell periodically fires (Fig. 1.1B). As the stimulus orientation is moved away from the preferred, the different LGN inputs to a cell come to be increasingly desynchronized in their rate modulations. These modulations at different phases wash out, so that the net input to the cell becomes temporally steady and unmodulated, albeit with the same mean, and the cell is inhibited (Fig. 1.1C).

The net feedforward input - that is, the sum of the LGN input and the antiphase inhibition - is determined by the LGN input as follows. The mean LGN input evokes a net inhibitory mean feedforward input, due to the dominance of inhibition in our circuit. The anti-phase inhibition amplifies the modulation of the LGN input, yielding a stronger modulation of the net feedforward input. We previously showed that this combination of net inhibitory mean feedforward input, which is untuned for stimulus orientation, and the orientation tuning of the modulation of the feedforward input could account for the contrast-invariance of cortical orientation tuning (Troyer et al., 1998). Here we show that the same principles can explain suppression effects such as cross-orientation inhibition.

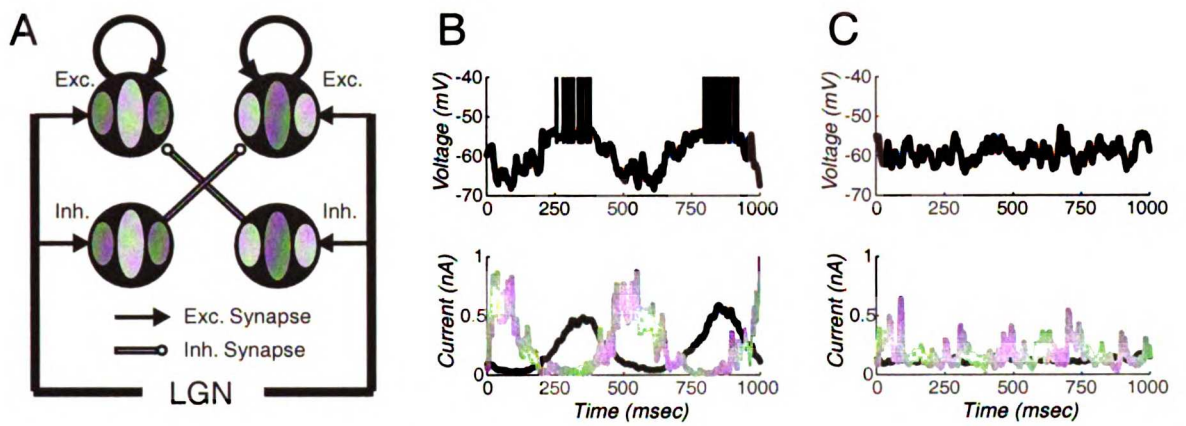

Figure 1.1:

A: Cartoon figure of the correlation-based local cortical circuitry used in our model. Four cell pools – two excitatory (top) and two inhibitory (bottom), each with two opposite preferred spatial phases (left vs. right) – are depicted. The four cell pools are at the same retinotopic position, but have been separated for visibility. Light gray represents ON subfields and dark grey OFF subfields. Cells receive input from LGN and from other cortical cells preferring similar orientations. Connections are assigned probabilistically. ON-center LGN inputs with centers overlying a cell's ON-subregions, and OFF inputs with centers overlying OFF subregions, are likely to connect to the cell. The cells receive excitatory intracortical connections with highest probability from other excitatory cells they are most correlated with (same absolute placement of ON and OFF subfields). Inhibitory connections are received with highest probability from inhibitory interneurons they are most anti-correlated with (opposite absolute placement of ON and OFF subfields). Unlike the cartoon, the actual model includes cells of all orientations and spatial phases and spanning a range of retinotopic positions. The probabilistic sampling leads cells to receive input from other cells differing in preferred orientation by up to about 30°, and differing in phase from identical (excitatory connections) or opposite (inhibitory connections) by up to about 60°; the cartoon illustrates the most probable connections. The feedforward inhibition (LGN→inhibitory cell→ excitatory cell) is stronger than the feedforward excitation (LGN→excitatory cell). B: Membrane potential (top) and synaptic currents (bottom) of a single cell as a function of time when stimulated by a drifting grating at its preferred orientation. The excitatory (black) and inhibitory (gray) synaptic currents are modulated out of phase with one another, resulting in an oscillatory membrane potential. The cell spikes during the excitatory peak of the oscillations. C: Membrane potential (top) and synaptic currents (bottom) of a single cell when stimulated by a drifting grating orthogonal to its preferred orientation. There is little modulation of the synaptic current or membrane potential in time. Since the feedforward inhibition is stronger than the feedforward excitation, the membrane potential does not reach threshold.

Finally, we introduce our terminology. We characterize a response to a periodic stimulus by the mean response, referred to as the "DC" of the response; and the amplitude of the response modulation at the temporal frequency of the stimulus, referred to as the "F1" of the response (for

"first harmonic"). Note that the *peak* value of the response is roughly given by the sum DC+F1.

1.3.2 Cross-orientation inhibition

In the model circuit, the response to a base grating at the preferred orientation is suppressed by simultaneous presentation of a mask grating at the null orientation (the orientation perpendicular to the preferred). Two factors contribute to this suppression (Fig. 1.2) First, the preferred-

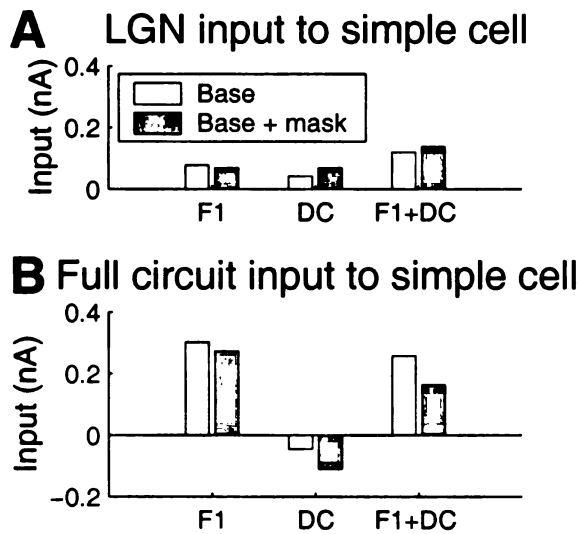

Figure 1.2:
F1, DC and peak (F1+DC) input current to a model simple cell (mean over cells with similar orientation preference, 4 degree bins) from LGN alone (A) and LGN + cortex (B) in response to stimulus grating at preferred orientation, 40% contrast alone (base); or to superposition of preferred (base) and orthogonal (mask) orientation gratings, each at 40% contrast.

orientation stimulus evokes synchronized modulation of the firing rates of the LGN inputs to a simple cell, but superposition of the null stimulus disrupts this synchronization. This reduces the F1 of the net LGN input to a simple cell. This is a small effect in this example, but can be more significant, as we will see later (Fig. 1.10). Second, superposition of the null stimulus increases the mean spiking rate of the LGN inputs and thus the DC of the net LGN input to a simple cell. This is converted by the dominant antiphase inhibition in the circuit into an increased *negative* feedforward DC input to the simple cell. The combination of these two effects provides sufficient suppression to match many aspects of the suppression observed experimentally, including the illustrated cross-orientation inhibition. Note that the superposition of the second grating yields an increase in the peak input (DC+F1) of the LGN input, so that simple cell responses would be increased by addition of the second grating if only LGN input were considered.

1.3.3 Contrast dependence of cross-orientation inhibition

The amount of suppression is dependent on the mask contrast. The mean spike response to a base grating at the preferred orientation decreases with the contrast of a mask grating at a non-preferred orientation, both in a cell from Bonds (1989) (Fig. 1.3A) and in simulations (Fig. 1.3C). The

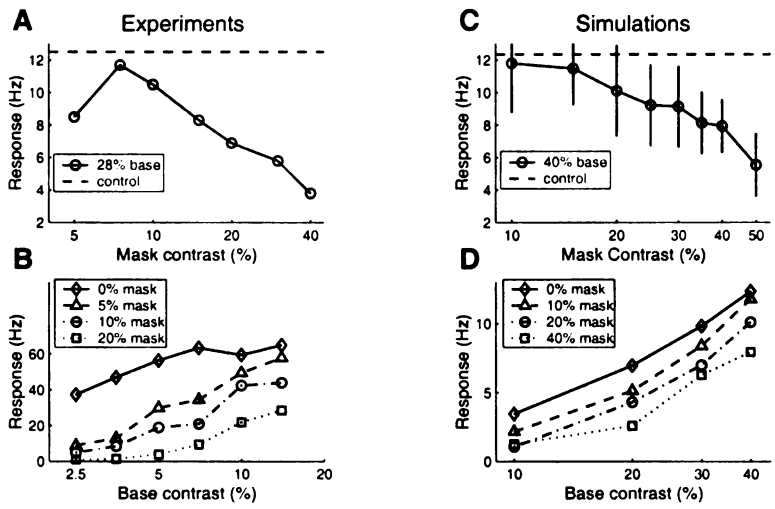

Figure 1.3:

Experiments reproduced from (Bonds, 89) (A, B – each shows data for a single simple cell), and corresponding simulation results (C, D – mean over cells with similar orientation preference; error bars in C show standard deviation, error bars omitted in D for visual clarity). A, C: Suppression of mean spiking response to a base grating of optimal orientation (expt. 28% contrast, sim. 40% contrast) with varying contrast of mask at non-preferred orientation ("inhibiting" orientation in experiments; orthogonal to preferred in simulations). Dashed line is response with base alone. B, D: Response versus log contrast of base shows downward shift that increases with mask contrast, with little change in slope. Note, overall spiking rate differences are not meaningful: experimentally there is high variability between cells (compare A,B); in simulations, overall spiking rate can be modified by parameter changes without otherwise altering network behavior (Troyer et al., 1998).

curve of response vs. base contrast is shifted downward or rightward with increasing mask contrast, with little change in slope, both in an experimental cell (Fig. 1.3B) and in simulation (Fig. 1.3D). Both response vs. base contrast and suppression vs. mask contrast are stronger in the experimental cells illustrated than in simulation, but the degree of suppression for a given ratio of base to mask contrast is more comparable.

Recent experiments by Sengpiel et al. (1998) also addressed the effect of inhibition by a sec-

ond grating on the contrast-response curve. They described the contrast-response function by a hyperbolic ratio function, $R = R_{max}\frac{c^n}{c_{50}^n+c^n}$, where R_{max} is the maximal response, c_{50} is the contrast that elicts a half-maximal response, and n is the power exponent. For a majority of cells, cross-orientation inhibition caused a rightward shift of the contrast-response function, that is, a change in c_{50} but not in R_{max} or n. This is seen in the normalized population response for 48 cells (both simple and complex cells), with and without cross-orientation inhibition, from Sengpiel et al. (1998) (Fig. 1.4A). The inhibition in the model is similarly described well by a rightward shift

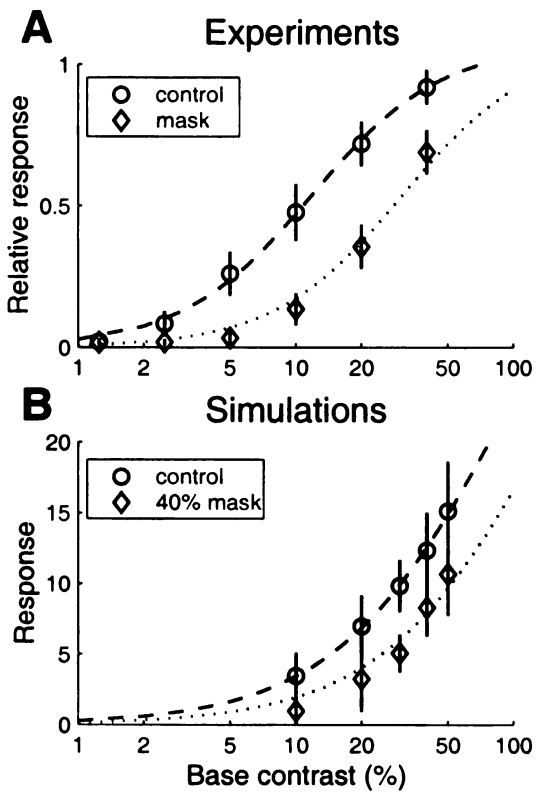

Figure 1.4:

Experiments reproduced from (Sengpiel et al., 1998) (A - mean response of pool of 48 cells, simple and complex from all layers, each cell's response expressed relative to its maximal response), and corresponding simulation results (B - mean spike response, ±1 stdev, over cells in simulation with similar orientation preference). Response R vs. base contrast c fitted to hyperbolic rate functions $R = R_{\max}c^n/(c^n + c_{50}^n)$, shown as dashed lines (control responses, base grating alone) and dotted lines (base plus mask gratings). Experiments, control: $R_{\max} = 1.072$, $c_{50} = 0.118$, $n = 1.46$ ($\chi^2 = 0.097$, 3 degrees of freedom (d.f.)); plus cross-oriented mask: $c_{50} = 0.308$ with $R_{\max}$ and n held fixed ($\chi^2 = 2.49$, 5 d.f.). Simulations, control: $R_{\max} = 42.8013$, $c_{50} = 0.8564$, $n = 1.126$ ($\chi^2 = 0.1131$, 2 d.f.); plus cross-oriented mask (40 % contrast): $c_{50} = 1.5707$ with $R_{\max}$ and n held fixed ($\chi^2 = 3.6672$, 4 d.f.). For both experiments and simulations, cross-orientation inhibition is well described by a rightward shift of the contrast response function.

of the contrast response function (Fig. 1.4B).

1.3.4 Effect of cross-orientation inhibition on orientation tuning

We examined the effects of a mask stimulus at the null orientation on the response tuning for the orientation of a base grating (Fig. 1.5).

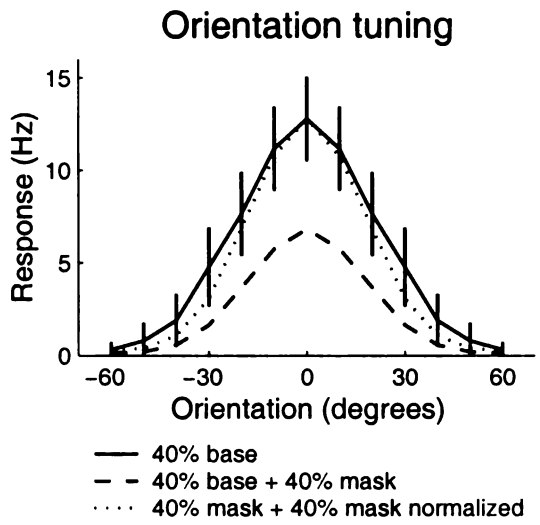

Figure 1.5:

Model orientation tuning curves, with and without mask stimulation. Solid line is orientation tuning curve when stimulated with a single base grating alone (mean ±1 SD). Dashed line is the tuning (mean) for base grating orientation while simultaneously stimulating with a mask grating at the orientation orthogonal to the cell's preferred orientation. Dotted line is the same as the dashed, except scaled so that the peak response matches that of the tuning curve for the base grating alone. The response reduction due to the mask grating is mainly multiplicative.

The mask-induced suppression does not significantly alter the orientation tuning in the model: when the response tuning curve in the presence of the mask is scaled to have the same height as the response tuning curve in the absence of the mask, the two curves become almost identical. Thus, the effect of the suppressing grating on the orientation tuning curve is predicted to be mainly divisive.

1.3.5 Dependence of suppression on mask orientation

The initial concept of cross-orientation inhibition has been broadened by several experiments to that of a more general, nonspecific suppression of the response to a preferred stimulus by superposition of a second stimulus (Bonds, 1989; DeAngelis et al., 1992). Here we focus on the experiments of Bonds (1989), who used as stimuli superimposed pairs of sine gratings: a base grating at the preferred orientation and 2 Hz temporal frequency, and a mask grating at 3 Hz (or other temporal frequencies, considered later) and various orientations, as illustrated in figure 1.6. By decomposing the cell's response into two F1's, one at each temporal frequency, as well as a DC, the separate response to each grating was assessed: the F1 at 2 Hz represents response to the base grating, while the F1 at 3 Hz represents response to the mask grating. This allowed Bonds (1989) to determine the effect of the orientation of the mask grating on the suppression of the response to the base grating.

We have mimicked this procedure in our simulations (Fig. 1.7). In both experiments and simulations, the mask grating at non-preferred orientations suppressed the DC spike response, and the tuning of this DC response with mask orientation is similar to the excitatory orientation tuning curve to a single grating (Fig. 1.7A,E). Similarly, both experiment and simulation show tuning of the 3 Hz (mask) F1 component of the response with the mask orientation, again following

Figure 1.6:

Bonds (1989) experimental procedure. Bonds created his compound gratings by adding two simple gratings, a base grating always at the preferred orientation with a temporal frequency of 2 Hz and a mask grating at various orientations and a temporal frequency of 3 Hz (in later experiments the mask has other temporal frequencies). He could then look at the mean (DC) response, the 2 Hz F1 response defined as the base response and the 3 Hz F1 response defined to be the mask response.

the excitatory orientation-tuned response of the cell (Fig. 1.7B,F). The effects of the mask on the 2 Hz (base) F1 component of the response is more complex. Experimentally, Bonds (1989) found 11 of 14 cells showed suppression of the base component that was untuned for mask orientation (Fig. 1.7C), while 3 of 14 cells showed broad tuning for mask orientation (Fig. 1.7D). In simulations, we find that the 2 Hz component of the intracellular current shows suppression that is untuned for mask orientation (Fig. 1.7G), but the 2 Hz component of the spiking response shows broadly tuned suppression (Fig. 1.7H) akin to that seen in a minority of cells by Bonds. This tuning of the base spike response arises from the addition of an untuned base current component and a tuned mask current component followed by a rectification to give the spike response.

Neither simulation results nor experimental results (Bonds, 1989) depended on the relative spatial phase of the two gratings (not shown).

1.3.6 Temporal frequency dependence of the suppression

By keeping the base grating at 2 Hz and varying the temporal frequency of the mask grating, Bonds (1989) investigated the temporal characteristics of the cortical suppression. We first examine the dependence of suppression on mask contrast and temporal frequency (Figure 1.8). In the experiments, strong suppression is found for lower temporal frequencies (2 and 8 Hz), with a decrease in suppression at 16 Hz. In simulations, 8 and 16 Hz masks evoke greater suppression than the 2 Hz mask, but the suppression does decrease between 8 and 16 Hz.

We next examine the dependence of suppression on mask orientation and temporal frequency (Fig. 1.9). In experiments, the total (DC) response (Fig. 1.9A) shows suppression for masks at

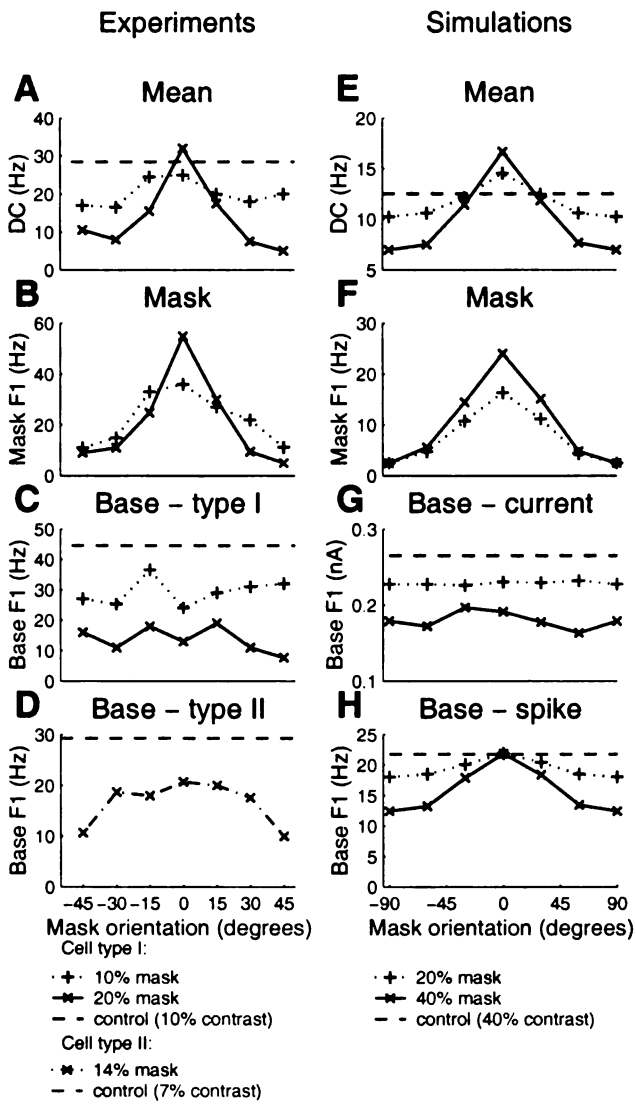

Figure 1.7:

Experiments reproduced from (Bonds, 1989) (A, B, C – data for a single simple cell, dashed line is base, 10% contrast at preferred orientation, dotted line is adding a 10% mask grating, and solid line is adding a 20% mask grating at various orientations, D – data from another single simple cell, dashed line is base, 7% contrast at preferred orientation, dash-dotted line is adding a 14% mask grating), and corresponding simulation results (E, F, G, H – each shows mean response over cells in simulation with similar orientation preference; dashed line is base, 40% contrast at preferred orientation, dotted line is adding a 20% mask grating, and solid line is adding a 40% mask grating at various orientations). A, E: Mean spike response vs. mask orientation. B, F: 3 Hz F1 (mask component) of the cell response is similar for experiment and simulations. C: 2 Hz F1 (base component) of the cell from A and B is untuned with the mask orientation (type I, 11/14 simple cells studied). D: 2 Hz F1 component of another simple cell shows some tuning with the mask orientation (type II, 3/14 simple cells). G: 2 Hz F1 component of the synaptic current in simulations is untuned with mask orientation, similar to type I cells. H: 2 Hz F1 component of spike response in simulations shows tuning with the mask orientation, similar to type II cells.

off-orientations that decreases with mask temporal frequency until, for a mask of 32 Hz, there is no inhibitory effect at all. When the mask is at the preferred orientation, the lowest frequencies evoke no suppression. The mask response (Fig. 1.9B) is, not surprisingly, tuned with mask orientation, and the excitation decreases with temporal frequency. The excitation actually cuts off earlier than the suppression: at 16 Hz there is little excitatory effect of the mask, while there is still a significant inhibition of the DC and base responses. The suppression of the base response (Fig. 1.9C) is untuned

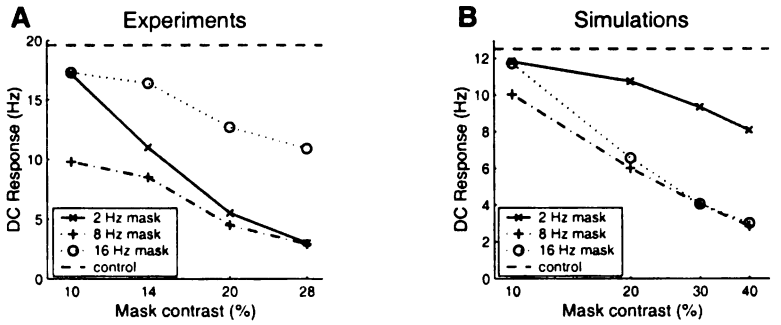

Figure 1.8:

Experiments reproduced from (Bonds, 1989) (A – data for a single simple cell), and corresponding simulation results (B – mean response over cells in simulation with similar orientation preference). Plots show mean spike response vs. mask contrast for a combination of a 2 Hz base grating at preferred orientation and a mask grating oriented at an inhibitory orientation (experiments), which we have taken to be orthogonal to the preferred (simulations). Dashed lines, response to base grating alone; solid lines, response with 2 Hz mask; dash-dotted lines, response with 8 Hz mask; dotted lines, response with 16 Hz mask. The inhibitory effect of the mask grating decreases with the temporal frequency of the mask in experiments, whereas in the simulations the inhibitory effect of the mask grating is tuned towards higher temporal frequencies, thus peaking at 8 to 16 Hz, but decreasing with further increase in temporal frequency (not shown).

with mask orientation, and the inhibition is highest for low temporal frequencies and decreases with increasing temporal frequencies, as in Fig. 1.8. Our simulations (Fig. 1.9D-F) are similar except that, again, 3 Hz gratings evoke less suppression than higher temporal frequencies, and the base component of the spiking response shows orientation tuning (although again, the base component of the current response is untuned).

To understand the temporal-frequency tuning of suppression in our model, we examined the thalamocortical and full-circuit input to cells when adding a varying-temporal-frequency mask grating at the orientation orthogonal to a preferred-orientation 2Hz base grating (Fig. 1.10). We assume that the 2 Hz component of the response is roughly determined by the sum of the DC and the 2 Hz F1, representing the peak reached by the 2 Hz component when ignoring the other modulating components. The LGN input shows an increased DC component for 8 and 16 Hz masks relative to that for a 3 Hz mask, while the 2 Hz F1 component is slightly reduced. The cortical circuit amplifies both the DC and 2 Hz F1 component and reverses the DC component. The superposition of the 2 Hz F1 and DC then results in a peak input (F1+DC) that is lower for the higher-temporal-frequency masks. According to the experiments, the peak input should increase for the higher mask temporal frequencies, suggesting flaws in our models either of the LGN DC and/or F1 or of inhibitory cell temporal tuning; we return to this in the discussion.

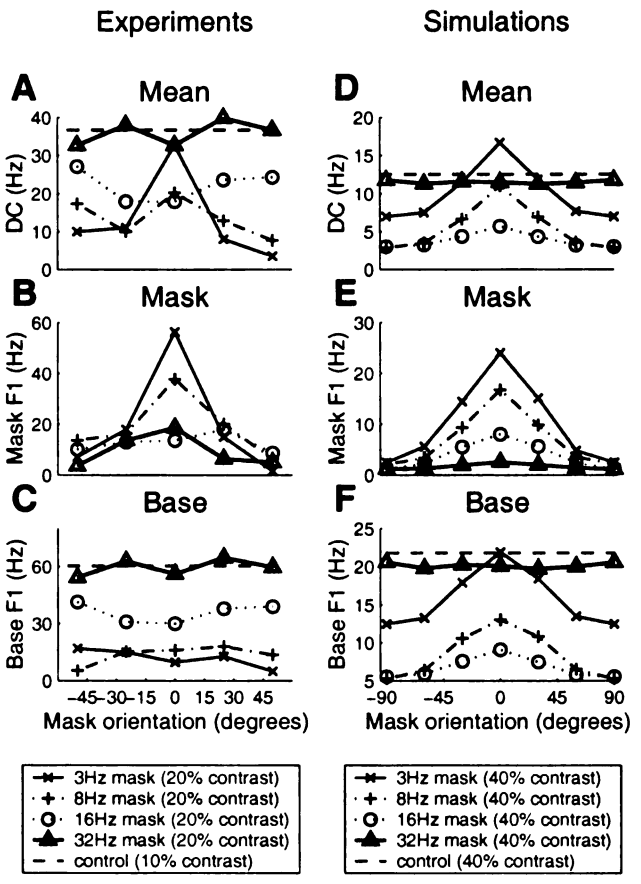

Figure 1.9:

Dependence of suppression on orientation and temporal frequency of mask grating, added to base grating at preferred orientation and 2Hz. Experiments reproduced from (Bonds, 1989) (A, B, C - data for a single simple cell), and corresponding simulation results (D, E, F - mean response over cells with similar orientation preference). "Control" is response to base grating alone. A, D: Mean (DC) spike response. B, E: F1 of the spike response at the mask temporal frequency. C, F: F1 of spike response at the base temporal frequency. In general, inhibition peaks at higher temporal frequencies in the simulations than in the experimental cell. As earlier, the simulated base response is tuned with the mask orientation, while the experimental base response is not. Simulated base current response is untuned (not shown).

1.3.7 Spatial-frequency dependence of the suppression

Cortical cells show bandpass tuning for the spatial frequency of a grating. This bandpass tuning is expected to also influence suppressive effects. Figure 1.11 shows experiments (Bonds, 1989) and simulations of cell responses with varying spatial frequency of the base and mask. The experiments show that tuning of the suppression for mask spatial-frequency is broader than the cell's excitatory spatial tuning bandwith. Furthermore the bandwith of the suppression increases with mask contrast. In our simulations, inhibitory cells and excitatory cells have identical spatial frequency tuning (they have identical Gabor-functions defining their receptive fields), and as a result, the suppression and excitatory tuning have similar bandwidth, again suggesting a flaw in our model of inhibitory cell receptive fields. The simulations do show a bit of the broadening of inhibition with contrast.

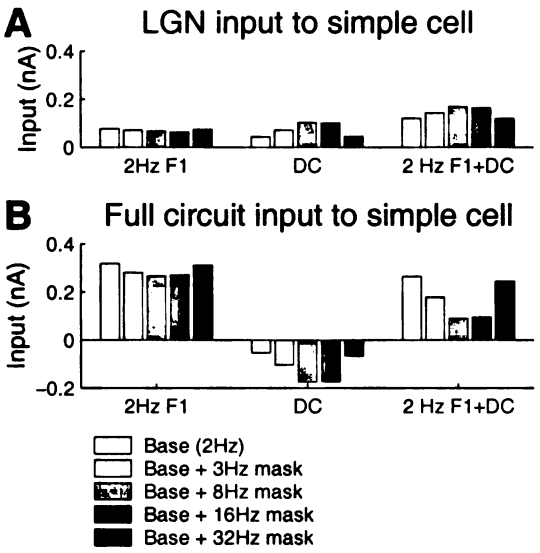

Figure 1.10:

Base (2 Hz) F1, DC, and peak (2 Hz F1+DC) input current to a model simple cell from LGN alone (A) and LGN + cortex (B) in response to stimulus grating at preferred orientation, 40% contrast alone (base); or to superposition of preferred (base) and orthogonal orientation (mask) gratings of various temporal frequencies, each at 40% contrast. The DC input from LGN alone increases with higher frequencies up to 16 Hz, following the tuning of our model LGN cells (Sclar, 1987). This results in an increased (inhibitory) DC for the full network which, added to a slightly smaller base modulation (F1), results in a significantly decreased peak input to the cell, thus explaining the temporal tuning of the inhibition of the base component of response in the simulations.

1.3.8 Modulation changes with multiple gratings

When stimulating simple cells with a superposition of a high- and a low-temporal-frequency grating, the F1 of the spike response of the lower frequency is decreased relative to that evoked by the low temporal frequency grating alone. At the same time the F1 of the high temporal frequency is enhanced compared to its value for a single grating. This was shown by Dean et al. (1982), who obtained results for 18 simple cells at 1.25 and 7.75 Hz temporal frequency using counter-phase gratings. When restricted to cells for which the ratio of the response amplitudes to each frequency presented alone was between 0.8-1.2, they found a mean relative response modulation (ratio of F1 when two gratings shown together to F1 of single grating alone) of 0.77 at 1.25 Hz and 1.23 at 7.75 Hz. Across all cells, they found mean changes in the same directions (Dean et al., 1982, fig 2). In our simulations we choose drifting gratings so the modeled responses will not depend on the absolute spatial phase of the cells. Using 2Hz and 8Hz gratings with contrasts chosen to yield similar responses to each grating alone, we find a relative response modulation of 0.60 at 2 Hz and 1.09 at 8 Hz (Fig. 1.12A). Thus the strength of suppression and the direction, though not the strength, of enhancement are roughly replicated by our model.

This can be understood from a simple toy model as illustrated in figure 1.13. We assume that each grating alone evokes both a sinusoidal oscillation and a negative DC; the superposition of the gratings is modeled simply by adding their oscillations and DC's. The resulting waveform

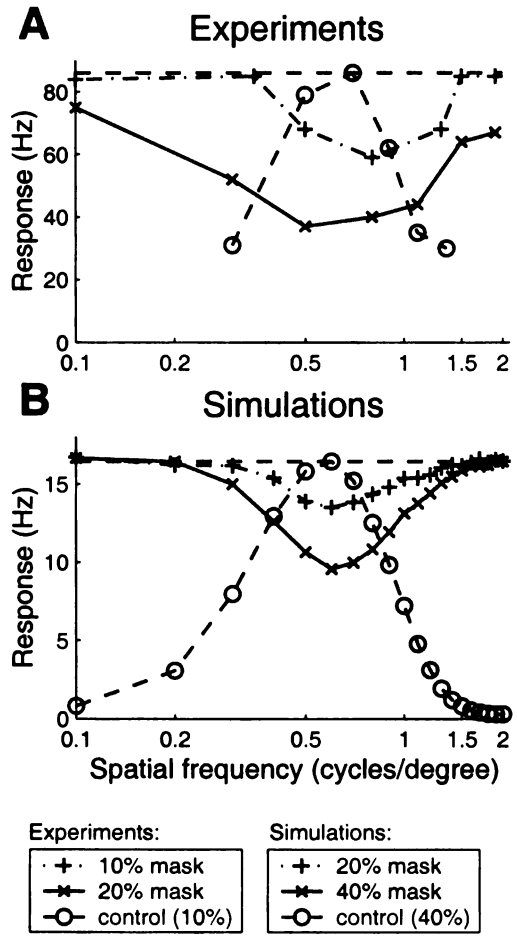

Figure 1.11:

Experiments reproduced from (Bonds, 1989) (A – data for a single simple cell), and corresponding simulation results (B – each shows mean response over cells with similar orientation preference). Response vs. spatial frequency of base and mask; base is at cell's preferred orientation, mask is at an inhibitory orientation (experiment) or orthogonal to the preferred (simulation). Dashed lines with circles show response to base alone, vs. base spatial frequency; horizontal dashed lines show response to base alone at its preferred spatial frequency. Inhibitory curves show the response, vs. mask spatial frequency, when adding a mask at high (solid) and low (dash-dotted) contrast to the base at its preferred spatial frequency. The inhibition has broader spatial frequency tuning for the experiments than in the simulations.

is rectified at a threshold and the F1 of the rectified response is computed. The model has four parameters: the threshold, expressed as a percentage of the amplitude of the 2 Hz oscillation; the sizes β_{2Hz} and β_{8Hz} of the negative DC's, relative to the amplitude of their respective sinusoidal oscillations; and the amplitude α of the 8 Hz oscillation relative to that of the 2 Hz. In simulations of the full model, we find $\beta_{8Hz} = 0.4232$ and $\beta_{2Hz} = 0.0187$ (see Methods), and so accordingly in our toy model we initially consider $\beta_{8Hz} = 0.4$ and $\beta_{2Hz} = 0$. We first choose α so that, after rectification, the 2Hz grating alone and the 8Hz grating alone evoke similar F1's. Examining results across values of the threshold (Fig. 1.12B), we find that for thresholds less than 0.3, this simple model replicates the basic result of the experiment: the low-frequency F1 decreases, and the high-

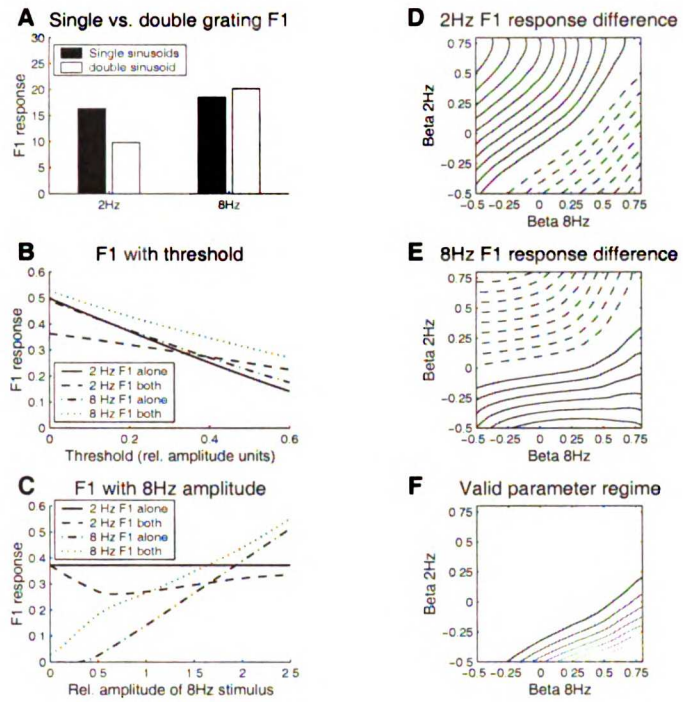

Figure 1.12:

A: F1 response at 2 and 8 Hz for a single drifting grating at the preferred orientation, at a temporal frequency of 2 Hz (20% contrast) and 8 Hz (40% contrast) respectively (white bars), compared with the 2 and 8 Hz F1 response to a superposition of the two gratings (both at the preferred orientation) (grey bars). B-F: Toy model of the effect in A: see Results for details. B-C: Solid: 2 Hz F1 response to 2 Hz grating alone; dash-dotted: 8 Hz F1 response to 8 Hz grating alone; dashed: 2 Hz F1 response to double grating; dotted: 8 Hz F1 response to double grating. Negative DC's are matched to data from the full model; $\beta_{2Hz} = 0$, $\beta_{8Hz} = 0.4$. B: $\alpha = 1.95$. For thresholds less than around 0.3, the model displays the biologically observed behaviour (Dean et al., 1982): the 2 Hz F1 for the double grating is less than for the single grating, while the 8 Hz F1 for the double grating is higher than for the single grating. C: Threshold is fixed at 0.2. For all values of α, the F1 responses are modified in the double gratings in the directions observed biologically. For higher values of α, the double grating F1 responses approach their respective single grating F1 responses. D-F: Dependence of results on the negative DC's, β_{2Hz} and β_{8Hz}, for a fixed threshold ($\theta = 0.2$) and relative amplitude ($\alpha = 2$). D: Contour plot of the relative change in the 2 Hz F1 (F1 given both sinusouds minus F1 given 2 Hz sinusoid alone). Solid lines are positive values and dashed lines are negative values, each line indicates an increment of 0.05 in relative values. The relative change is negative, as in the experiments, for low values of β_{2Hz} and high values of β_{8Hz}. E: Relative change in the 8 Hz F1 is positive, as in the experiments, for low values of β_{2Hz} and high values of β_{8Hz}. F: Negative values in D are multiplied by positive values in E, and the absolute value of the result is shown as a contour plot, with values increasing toward lower right corner as indicated by lighter grays. The toy model behaves as in the experiments for low values of β_{2Hz} and high values of β_{8Hz}.

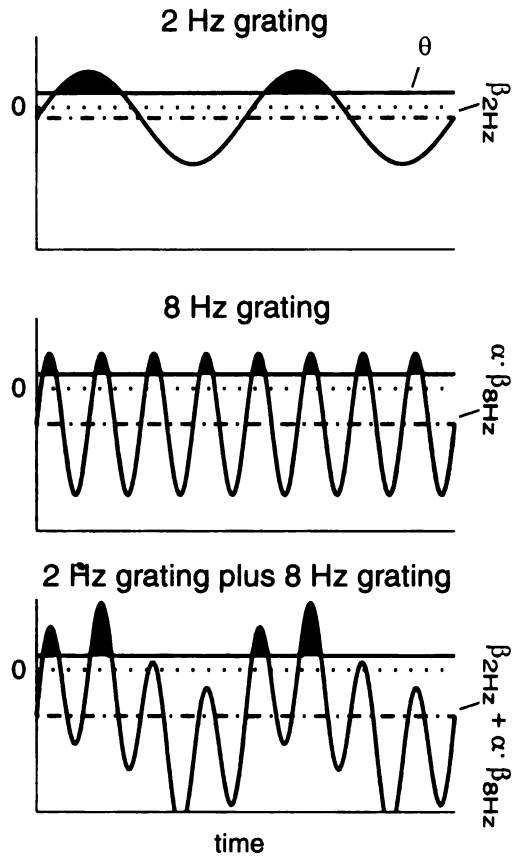

Figure 1.13:

Model of the input and response to single gratings with a temporal frequency of 2 and 8 Hz and to the superposition of the two gratings. The solid curves are the inputs as a function of time, the solid horizontal line is the threshold, θ, the dash-dotted line is the inhibitory DC, β_{2Hz} and $\alpha\beta_{8Hz}$ in the toymodel, subtracted from zero, the dotted line. The black part of the curve above threshold is the response of the cell. Since the inhibitory DC component is larger for higher temporal frequencies, β_{8Hz} is larger than β_{2Hz}, the input at 8 Hz need a higher amplitude, α, (a higher contrast) to give the same F1 response. Adding the two gratings results in a DC equal to the sum of the two single gratings, $\beta_{2Hz} + \alpha\beta_{8Hz}$, resulting in a decrease of the 2 Hz F1 component and an increase of the 8 Hz F1 component. (The values chosen in this figure are for display only and do not correspond to those used to obtain the results in the simulations).

frequency F1 increases, when the two sinusoids are added together. Next we fix the threshold at 0.2, and find that across all values of α, the same basic result is obtained (Fig. 1.12C).

Finally we examine the dependence of the results on the two β's, that is, on the size of the negative DC offset evoked by the two gratings, for fixed values of the threshold and relative amplitude. (Fig. 1.12D-F). Small or negative values of β_{2Hz} and high (positive) values of β_{8Hz} yield changes in the experimentally observed directions: for these values of the β's, the 2 Hz F1 is decreased (negative "2 Hz F1 difference" in Fig. 1.12D) and the 8 Hz F1 is increased (positive "8 Hz F1 difference" in Fig. 1.12E) when the two sinusoids are added together. To better ascertain the parameter range over which each F1 is changed in the appropriate direction, we multiply the negative region of the 2 Hz change (positive values set to zero) with the positive region of the 8 Hz change (negative values set to zero), and take the absolute value of the result; contours of this result are shown in Fig. 1.12F. The contours increase with approach toward the lower right corner, that is, as β_{8Hz} increases and β_{2Hz} decreases. (The parameter region that gives the desired result increases when the threshold is decreased or the relative 8 Hz amplitude is increased, not shown.) Thus, we conclude that it is critical to the observed result that an 8 Hz grating evoke a larger negative DC, relative to its F1, than a 2 Hz grating. (This occurs in our full model due to the slow time course

of NMDA conductances, which lowers the F1/DC ratio for higher frequencies; see Discussion.)

Reid et al. (1992) studied the superposition of 8 counter-phase gratings of increasing temporal frequencies. As in the two-grating paradigm of Dean et al. (1982), they found that the modulation of low temporal frequencies is depressed and that of high temporal frequencies is enhanced in the superposition relative to that of the constituent sinusoids. Again for drifting gratings, we examined the F1 responses of our full model at each of 8 stimulus frequencies, in response to each of the 8 individual sinusoids alone and in response to their superposition (Fig. 1.14). As in the

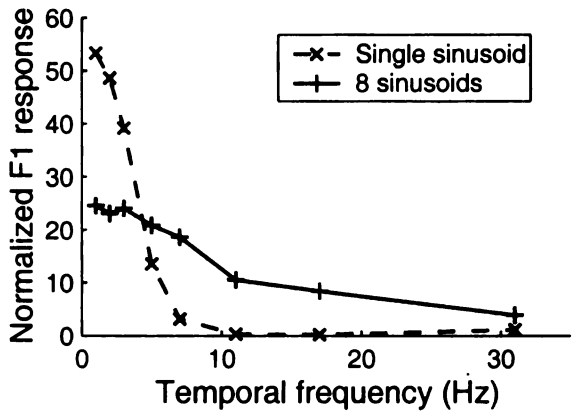

Figure 1.14:

Normalized F1 response to eight single gratings at the preferred orientation, at their respective temporal frequencies (×, dashed line), and to the same temporal frequencies for a superposition of the eight gratings (+, solid line). The contrast of the single gratings are 20% when alone, and 12.5% each when superposed. The normalized F1 response of the low temporal frequencies is higher for the single gratings than for the stimulus of eight superposed gratings, while the effect is reversed for high temporal frequencies, as found by Reid et al. (1992).

experiments, the F1's at lower temporal frequencies are decreased, while those at higher temporal frequencies are increased, in the superposition compared to the single gratings. We find a cross-over point from depression and elevation between 4 and 5 Hz, slightly lower than, but comparable to, the experimentally found cross-over of 6 to 8 Hz (Reid et al., 1992).

1.4 Discussion

We have shown that a simple correlation-based local circuit can account for many aspects of cortical response properties to multiple gratings, including many features of the dependence of suppression or enhancement on a mask grating's orientation, spatial frequency, and temporal frequency, as well as the effects of mixing sinusoids of multiple temporal frequencies. The model predicts that superposition of a mask grating orthogonal to the preferred orientation should cause little change in orientation tuning to a base grating, having a primarily divisive effect on the orientation tuning curve. It also predicts that high-temporal-frequency (*e.g.*, 8 Hz) gratings should evoke a stronger negative DC for a given F1 amplitude than low-temporal-frequency gratings (*e.g.*, 2 Hz).

The circuit model that attains these results (Troyer et al., 1998) rests on two basic assumptions.

First, both the excitation and inhibition received by a simple cell come from other cells of similar preferred orientation (Anderson et al., 2000a; Ferster, 1986), but the excitation and inhibition are evoked by opposite polarities (light or dark) at any given point in the receptive field (Ferster, 1988; Hirsch et al., 1998). Second, the inhibition dominates, rather than balances, excitation in the cortical circuitry. This dominance is supported by experiments showing that even slight movement of a spot stimulus across a subregion boundary is sufficient to cause the spot to evoke net inhibition (Hirsch et al., 1998), as well as by experiments showing that nonspecific shock of the LGN evokes massive inhibition in cortex (Ferster and Jagadeesh, 1992). It is this excess inhibition that accounts for the cross-orientation (or 'second grating') suppression. The model also agrees with recent findings by Freeman et al. (2001) that cross-orientation suppression is not affected by adaptation to a cross-oriented stimulus. The cells in our model do not receive input from cells preferring orientations orthogonal to their own preferred orientation, thus their responses are not affected by the activity of these.

While the model captures a wide array of results, it also fails in two notable ways. First, suppression in experiments is more broadly tuned for mask spatial frequency (also seen in DeAngelis et al., 1992), and is tuned to lower mask temporal frequencies, than in the model. Although recent experiments by Durand et al. (2001) report the high-temporal frequency cutoff of suppression to be between 16 and 20 Hz, similar to our findings. Second, the majority of cells studied experimentally showed no tuning for mask orientation of the base component of response, whereas in the model there is such tuning. It will be important to determine these properties for cells in layer 4, the layer that we are modeling. If they hold in layer 4, it would suggest that two types of improvements are needed in the model. First, inhibitory neurons in the model at present follow the tuning of the LGN input for temporal frequency (and for orientation), and have the same spatial frequency tuning (same Gabor RF shapes) as the excitatory neurons. We may need to consider inhibitory cell models that show stronger responses at low temporal frequencies, and that have broader tuning or a broader variety of tunings for spatial frequency. Second, the tuning for mask orientation of the base response component is a threshold effect: the addition of the untuned base component and the tuned mask component of current, followed by rectification by the spike threshold, yields a tuned base component of the spiking response. Sufficient voltage noise can smooth away many threshold effects, and voltage noise appears comparable in size to stimulus-induced voltage modulations (Anderson et al., 2000b; Arieli et al., 1996; Paré et al., 1998; Tsodyks et al., 1999), suggesting that exploration of higher-noise regimes might remove the threshold-induced tuning.

Cross-orientation suppression in the model depends both on the dominance of inhibition, and on the fact that inhibitory neurons in the model respond to all orientations, although they are orientation-tuned: their tuning curves resemble a tuned hill atop an untuned platform (Troyer et al., 1998). Recent results find two types of inhibitory interneurons in cat V1 layer 4: simple cells that show good orientation tuning, and complex cells that are untuned for orientation (Hirsch

et al., 2000). It is possible that these separately embody the two components of inhibitory tuning – the tuned hill and the untuned platform – that we are attributing to a single class of cells.

1.4.1 Suppression and contrast

The modeled experiments (Bonds, 1989), and other reported results (DeAngelis et al., 1992; Morrone et al., 1982) display a wide range of suppression strengths. There does not seem to be any systematic connection between suppression strengths and cell type (simple/complex), tuning width, cortical position etc. Our cells often required higher contrasts of both base and mask than in experiments to see a given level of response or suppression, although the relative contrast of base vs. mask for a given strength of suppression was often similar. Strength of overall responses can be varied without otherwise altering circuit behavior by varying circuit parameters in a coordinated way (Troyer et al., 1998); thus the most robust issue seems to be the relative contrast required to achieve a given degree of suppression, rather than the absolute contrasts. Furthermore, the relative contrast necessary to achieve a given degree of suppression is also parameter-dependent in the model, depending in particular on the overall strength of inhibition. We have used the model as tuned for other experiments and not altered it to fit these data.

The strength of response and suppression also depends on our LGN model, which is currently very simple: we assume LGN spike-rate responses to the two gratings add linearly, up to rectification. Bonds (1989) shows results from a few LGN cells suggesting sublinear addition. It will be important to determine both the degree to which the DC of the LGN input grows, and the manner in which the F1 of the total LGN input received by a simple cell alters, when a mask grating is added to the base grating.

1.4.2 Modulation changes with multiple gratings

Our model reproduces the qualitative effects of modulation changes for pairs of gratings found by Dean et al. (1982) (with the difference that they used counter-phase gratings in their experiments and we used drifting gratings in the simulations). The simple toy model we considered for this paradigm accords well with this, showing the experimentally observed effect across parameters provided that the 8 Hz grating evokes a stronger negative DC for a given F1 than the 2 Hz grating. This stronger negative DC effect at higher frequencies arises in our full model due to the presence of NMDA conductances in excitatory synapses; the slow time course of these conductances suppresses the high-frequency F1 without altering the DC, resulting in a higher DC/F1 ratio (*e.g.* Krukowski, 2000, Fig. 2.28). We have also found that an additional mechanism not considered here, frequency-dependent synaptic depression (Abbott et al., 1997; Tsodyks and Markram, 1997) in geniculocortical synapses, can play a similar role, by differentially lowering the DC/F1 ratio of low-frequency stimuli (Krukowski, 2000).

Our result for the extension to 8 sine gratings, Fig. 1.14, agrees with the experimentally observed

response amplitudes of cortical cells (Reid et al., 1992). Reid et al. (1992) further reported a decrease in integration time of the response to the 8 sine gratings, as determined by the slope of the curve of response phase vs. temporal frequency; the cells appear to respond faster. They argue that these effects must be of cortical origin. We do not see a change in integration time in our simulations (data not shown). We have found (Kayser et al., 2001a) that increases in contrast can advance the phase of response, due to a number of mechanisms including synaptic depression, spike-rate adaptation, and increases in conductance. We can speculate that such effects might contribute to the experimental result, since there is greater overall contrast in the 8-grating stimulus than in the single-grating stimuli, although we do not see an effect in the present simulations.

1.4.3 Conclusion

Correlation-based or "push-pull" connectivity with dominant inhibition has been shown to account for many experimentally observed properties of layer 4 of cat primary visual cortex. These include contrast-invariant orientation tuning (Troyer et al., 1998), cortical temporal frequency tuning that cuts off at much lower frequency than LGN tuning (Krukowski and Miller, 2001), and various contrast-dependent nonlinearities (Kayser et al., 2001a). The present results suggest that this framework can also explain a range of suppression and enhancement effects observed with multiple-grating stimuli. However, they also suggest some modifications may be needed; in particular, our inhibitory cell models may need to be modified to explain the broader spatial-frequency tuning and lower temporal-frequency tuning of suppression observed experimentally.

Chapter 2

Different roles for simple- and complex cell inhibition

Abstract

We have previously proposed a model of the circuitry underlying simple-cell responses in cat V1 layer 4. We argued that the ordered arrangement of LGN inputs to a simple cell must be supplemented by a component of feedforward inhibition that is untuned for orientation and that responds to high temporal frequencies in order to explain the sharp, contrast-invariant orientation tuning and low-pass temporal frequency tuning of simple cells. The temporal tuning also requires a significant NMDA component in geniculocortical synapses. Recent experiments have revealed cat V1 layer 4 inhibitory neurons with two distinct types of receptive fields (RFs): complex RFs with mixed ON/OFF responses, lacking in orientation tuning; and simple RFs with normal, sharp orientation tuning (although some respond to all orientations). We show that complex inhibitory neurons can provide the inhibition needed to explain simple cell response properties. Given this complex cell inhibition, antiphase or "push-pull" inhibition from tuned simple inhibitory neurons acts to sharpen spatial frequency tuning, lower responses to low-temporal-frequency stimuli and increase the stability of cortical activity.

2.1 Introduction

Understanding the circuitry underlying response properties in primary visual cortex (V1) remains a central problem in systems neuroscience (*e.g.*, Ferster and Miller, 2000) and serves as a model problem for understanding cortical processing.

Hubel and Wiesel (1962) proposed that the orientation selectivity of simple cells in cat V1 layer 4 is shaped by an oriented arrangement of input from cells in the lateral geniculate nucleus (LGN) that are not tuned for orientation. Such an input pattern has been verified experimentally (Alonso et al., 2001; Reid and Alonso, 1995; Tanaka, 1983), but is not sufficient to explain simple-cell response properties. In response to a drifting grating stimulus, the mean LGN input to a simple cell grows with increasing contrast for all orientations, so that the mean input evoked by non-preferred orientations at high contrast exceeds the peak input evoked by the preferred orientation at low contrast (Troyer et al., 1998). Yet orientation tuning bandwidth remains roughly constant across contrasts, a phenomenon known as contrast-invariant orientation tuning (Anderson et al., 2000b; Sclar and Freeman, 1982; Skottun et al., 1987). Similarly, in response to a high-temporal-frequency drifting grating ($\geq$ 20 Hz) that produces little or no response in the great majority of V1 cells (DeAngelis et al., 1993; Freeman et al., 2002; Holub and Morton-Gibson, 1981; Ikeda and Wright, 1975; Movshon et al., 1978; Saul and Humphrey, 1992b), the great majority of LGN cells fire strongly (at levels greater than half their response to their optimal temporal frequency) (Freeman et al., 2002). Thus, a high-contrast, optimally oriented 20-Hz grating should evoke a high mean rate of LGN input to a simple cell (even if mechanisms that act as low-pass filters remove the input's temporal modulation) that exceeds the peak LGN input in response to a sufficiently low-contrast grating of optimal temporal frequency and orientation. Yet almost all simple cells respond to the optimal low-contrast stimulus and not to the 20-Hz high-contrast stimulus.

We have previously suggested a model of cat V1 layer 4 that can account for the contrast-invariant orientation tuning (Troyer et al., 1998), temporal frequency tuning (Krukowski and Miller, 2001), and other response properties (Kayser et al., 2001b; Lauritzen et al., 2001) of simple cells. The essential idea is that strong feedforward inhibition (inhibition from cortical interneurons driven by LGN inputs) that shows contrast-dependent responses to all orientations, and to all temporal frequencies that drive LGN cells, supplements feedforward excitation from LGN inputs to account for simple cell response properties. Given that most layer 4 cells are simple (Bullier and Henry, 1979; Gilbert, 1977) and given one report of a simple layer 4 inhibitory neuron (Gilbert and Wiesel, 1979), we assumed the inhibitory neurons providing this inhibition would be simple cells. The inhibition and excitation received by a layer 4 simple cell have similar orientation tuning (Anderson et al., 2000a; Ferster, 1986; Martinez et al., 2002), but are arranged in a spatially opponent or "push-pull" relationship: in ON subregions, light evokes excitation and dark evokes inhibition, and vice versa in OFF subregions (Anderson et al., 2000a; Ferster, 1988; Hirsch et al., 1998). Therefore, our model was based on antiphase inhibitory connectivity: an inhibitory simple cell tended to connect to cells

that preferred dark where it preferred light, and vice versa. These inhibitory simple cells were predicted to respond to all orientations in a contrast-dependent manner, though showing a tuned peak of response, and to show temporal frequency tuning like that of LGN cells.

Recently Hirsch et al. (2000) and J. Hirsch, private communication reported results of intracellular in vivo recording of cells that were subsequently filled and reconstructed. A total of 10 anatomically identified inhibitory neurons in cat V1 layer 4 have been recorded. Four had complex RFs with mixed ON/OFF responses throughout the responsive region. These cells showed roughly equal responses to all orientations, with little (2 cells) or no (2 cells) sign of orientation bias. The other six had simple RFs: segregated, oriented ON- and OFF-subregions with push-pull inhibition. These cells were well tuned for orientation in response to high-contrast drifting bars, although 2 showed substantial response to all orientations. Reexamination of previous studies supports the finding that a substantial fraction of cat V1 layer 4 interneurons are complex cells: of 9 previously anatomically identified such neurons, 5 were simple and 3 complex (and one was unoriented center-surround) (Ahmed et al., 1997; Gabbott et al., 1988; Gilbert and Wiesel, 1979; Kisvarday et al., 1985; Martin et al., 1983). The orientation tuning of these complex cells was not discussed. In addition, Azouz et al. (1997) anatomically identified one layer 4 interneuron, which was orientation untuned, although its complex or simple nature was not discussed. These results suggest that the broadly-tuned inhibition we posited indeed exists, but primarily in the form of orientation-untuned complex, rather than simple, inhibitory neurons.

In this paper, we explore the hypothesis that complex inhibitory neurons lacking in orientation tuning, and hypothesized to have temporal tuning that follows that of their LGN inputs, provide the inhibition that explains the contrast-invariant orientation tuning and temporal frequency tuning of simple cells. We also explore the role in this scenario of antiphase inhibition provided by the sharply-tuned simple inhibitory cells. An abstract of this work has appeared previously (Lauritzen and Miller, 2002).

2.2 Materials and Methods

The model we study is similar to a model previously described ("computational model" of Troyer et al., 1998), with the major differences (1) that we have included two types of inhibitory cells: simple inhibitory cells and the complex inhibitory cells recently described by Hirsch et al. (2000), and (2) that we have included NMDA as well as AMPA receptors in excitatory synapses, as in (Krukowski and Miller, 2001) but with a different Mg^{++} concentration. The detailed methods are as in (Troyer et al., 1998) except where otherwise described. Here we present the basics of the model along with the present additions.

2.2.1 Model Input.

The input to our model comes from 7200 LGN X-cells arranged in four overlying 30 × 30 sheets of ON cells and four similar sheets of OFF cells, with ON and OFF lattices offset by one-half square lattice spacing, covering 6.8 × 6.8° of the visual field. We use four overlying sheets because we assume each LGN X-cell receives input from a single retinal ganglion (RG) X-cell, and each RG X-cell projects to 4 LGN X-cells (as in Wörgötter and Koch, 1991; this value is intermediate between values from Sherman, 1985 and Peters and Yilmaz, 1993). LGN firing rates in response to a drifting grating were calculated by assuming rates were sinusoidally modulated, up to rectification at zero rate, about background rates of 10 and 15 Hz for ON and OFF cells respectively. The amplitude of the sinusoidal modulation was chosen so that the first harmonic (F1) of the rectified responses matched experimental values from one published X-cell (Fig. 1 Sclar, 1987). This is the LGN data used in most of our later studies, Kayser et al. (2001b); Krukowski and Miller (2001); Lauritzen et al. (2001); Troyer et al. (2002), but not in our original study, Troyer et al. (1998); this data is used because it is the only published data of which we are aware that includes responses both at multiple temporal frequencies and multiple contrasts. This LGN cell has a high-contrast temporal frequency tuning curve (essentially identical to the curve illustrated in fig. 2.6b) that peaks at 16 Hz, which is on the high end for LGN X-cells (Derrington and Fuchs, 1979; Hamamoto et al., 1994; Lehmkuhle et al., 1980; Saul and Humphrey, 1990; Sclar, 1987), but its overall range of temporal tuning is more typical, *e.g.* the average tuning over all X-cells shows a broad peak extending from 4 to 16 Hz with responses still above half-maximal at 32 Hz (Fig. 5C Sclar, 1987), and almost all LGN cells respond with greater than 1/2 their maximal response to stimuli of 20 Hz or greater (Freeman et al., 2002) (but see (Lehmkuhle et al., 1980; Saul and Humphrey, 1990), who find lower LGN cutoffs). The Sclar data determined the amplitude as a function of temporal frequency and contrast; this amplitude was then scaled by a factor reflecting the spatial frequency of the grating, given by the spatial frequency transfer function computed from the spatial receptive field of LGN cells as given in (Troyer et al., 1998), with the transfer function scaled so that its peak value is 1. Spikes were then generated from these LGN firing rates in a random (Poisson) fashion. Overlying LGN cells have 25% correlation in their spike trains, matching data showing correlations among LGN cells with overlapping RFs (Alonso et al., 1996).

2.2.2 Model architecture.

The model consists of a grid of 40 × 40 excitatory simple cells (E) and two grids of 15 × 15 inhibitory cells, one of simple cells (I_s) and one of complex cells (I_c) (Hirsch et al., 2000). All cells represent layer 4 cells, representing a 2/3 × 2/3 mm patch of cortex, corresponding to 0.75 × 0.75° in visual angle.

Each simple cortical cell was assigned a Gabor-function describing its RF, with orientation given by a measured orientation map from cat V1, spatial frequency of 0.8 cycles/degree, retinotopic

position progressing uniformly across the sheet, and spatial phase assigned randomly to each cell. The precise parameters used for the Gabor functions were those specifying the "broadly tuned" cells in Troyer et al. (1998), reproducing the observed (Anderson et al., 2000a; Ferster et al., 1996) 35^o half-width at half-height of the orientation tuning of intracellular voltage modulations in response to optimal sinusoidal gratings. The connection strength from LGN cells to a cortical simple cell was determined as in Troyer et al. (1998) by a probabilistic sampling of the cell's Gabor function, where positive regions of the Gabor are converted to probabilities of a connection from an ON-cell centered on that point, and negative regions converted to probabilities of OFF-cells connecting.

The complex cell RFs were constructed to have dimensions comparable to the simple cells, but round, by giving them a Gabor envelope with a diameter equal to the geometric mean of the length and width of the simple cells. The LGN connections were determined with the same algorithm as for the simple cells with the difference that a random number was assigned as the phase for each possible connection; that is, a Gabor RF with the preferred orientation given by the orientation map was assumed, but the phase of this RF was chosen randomly for each possible LGN connection to determine the probability of that connection. This caused the cell to receive input from both LGN ON- and OFF-cells at any given retinotopic point, resulting in mixed ON-OFF RFs untuned for orientation, but overall to receive the same amount of LGN input as the simple cells.

Cortical cells were modeled as single-compartment conductance-based integrate-and-fire neurons as in Troyer et al. (1998), and the two types of inhibitory cells had the same biophysical parameters. Each cell received stimulus-independent background excitatory input (Poisson) at a rate of 4000 Hz. This along with the spontaneous activity of the LGN inputs resulted in background firing rates of approximately 0.7 Hz for excitatory cells, 1-2 Hz for simple- and 30-40 Hz for complex inhibitory cells. The spontaneous rate for complex cells is somewhat high, but comparable to rates of around 20 Hz reported for similarly nonspecific inhibitory interneurons in other areas of cortex (Brumberg et al., 1996; Simons and Carvell, 1989; Swadlow, 1989, 1990, 1991, 1994). The rates could probably be decreased without substantial changes in overall model behavior by decreasing the background inputs to complex cells (we kept these identical to all cortical cells for simplicity), or by including inhibitory connections between complex cells (chemical synapses of Galarreta and Hestrin, 2002; Gibson et al., 1999; Tamas et al., 1997, 1998) and/or lowering the strength of LGN inputs to complex cells (we kept the strengths of LGN inputs identical on all cortical cells for simplicity), either of which could be compensated by increasing the synaptic strengths of connections from complex cells, but we have not explored any of these steps.

NMDA-mediated conductances (Krukowski and Miller, 2001; Lauritzen et al., 2001), in addition to the AMPA-mediated conductances, were added to all of the excitatory synapses except for the thalamocortical synapses onto inhibitory cells, which were purely AMPA-mediated following evidence that there is little NMDA in excitatory synapses onto inhibitory cells (Angulo et al., 1999; Ling and Benardo, 1995). The relative strength of NMDA and AMPA conductances were set in

terms of the integrated current (*i.e.*, the total charge transfer) through excitatory conductances when the postsynaptic cell is clamped at the spike-threshold voltage. 75% of the integrated current in all the synapses was mediated by NMDA, which is the value obtained by matching AMPA and NMDA amplitudes to those observed at thalamocortical synapses at the oldest ages studied in thalamocortical slices (Crair and Malenka, 1995), using a physiological level of extracellular Mg^{2+}. NMDA was modeled as in Krukowski and Miller (2001) except that a Mg^{2+} concentration of 1.3mM was used rather than 100 μM as in that reference; the latter figure was an error, and led us to conclude in that reference that over 90%, rather than 75%, of integrated current was carried by NMDA.

The probability of forming a synapse between any pair of simple cells depended on the correlation between their sets of LGN inputs, as in Troyer et al. (1998): the probability of a connection from an excitatory cell monotonically increased with the degree of correlation, while the probability of a connection from an inhibitory cell monotonically increased with the degree of anticorrelation. As shown in Troyer et al. (1998, Fig. 8B), the result is that the distribution of orientation differences between connected cell pairs peaks at zero difference and falls off to zero at differences of about $\pm 30^o$; while the distribution of phase differences peaks at 0 difference for excitatory synapses and at 180^o for inhibitory synapses, and falls off to zero over about $\pm 60^o$ from the peak. The result of this connectivity pattern is that the excitatory currents and inhibitory currents received by a cell in response to preferred-orientation drifting gratings modulate roughly at opposite phases across spatial frequencies (*e.g.* see Fig. 2.4b) and across temporal frequencies (*e.g.* see Krukowski and Miller, 2001, Figs. 1B,C).

Connections from complex cells only depend on the distance between the receptive fields of the two cells, with probability 10% of forming a synapse onto cells less than $\sim 150\mu$m away and zero otherwise. For simplicity, complex cells only receive thalamocortical input; cortical connections onto complex cells are to be explored in further studies. These connectivity rules yield the basic cortical circuit structure within a single iso-orientation column shown in cartoon form in fig. 2.1a. An important feature of the model is that the inhibition is dominant over feedforward excitation, rather than precisely balancing it.

The thalamocortical and E $\rightarrow$ E synapses displayed depression, with $f = 0.563$, $\tau = 99$ msec (LGN), and $f = 0.875$, $\tau = 57$ msec (E $\rightarrow$ E). Here, f is the synaptic efficacy immediately after a presynaptic spike, and τ the time constant of recovery, as in (Abbott et al., 1997). The experimental basis for these depression parameters is discussed in (Kayser et al., 2001b, table 1). Connections onto and from inhibitory cells may also express use dependent changes (Gupta et al., 2000), but these have been omitted for simplicity.

As in Troyer et al. (1998), we define the total synaptic strength of a given type received by a cell by (i) assuming the cell is voltage clamped at threshold; (ii) for each synapse, integrating over time the synaptic current induced by one presynaptic spike; and (iii) summing over all synapses of the

given type. Thus, total synaptic strength is expressed in units of *nA msec*. For simulations using only simple-cell inhibition, $I_s \rightarrow I_s$ connections were set to zero (because $I_s \rightarrow I_s$ connections can create instability in such a network unless they are very weak, (Krukowski, 2000)). The remaining connection strengths were 20 nA msec (LGN); 5 nA msec (E $\rightarrow$ E); 5 nA msec ($I_s \rightarrow$ E) as used previously for networks containing only simple cell inhibition with the synaptic depression parameters used here (Krukowski, 2000). When a mixture of complex- and simple-cell inhibition was included, the total synaptic weight received by a cell from each type of connection were: 25 nA msec (LGN); 4 nA msec ($I_c \rightarrow$ E); 10 nA msec ($I_c \rightarrow I_s$); 8.5 nA msec (E $\rightarrow$ E, I_s); 8 nA msec ($I_s \rightarrow$ E, I_s). For simulations using only complex-cell inhibition, strengths were identical to these except that all connections from I_s cells were set to zero. These strengths were set empirically, in a stepwise manner. First, LGN strengths were set to yield discernible tuning in a network without intracortical connections (this needed to be higher than in the case of simple-cell-inhibition only to overcome the increased inhibition to a preferred stimulus from complex cells); then $I_c \rightarrow$E connections were set to give reasonably sharp orientation tuning of E cells without too much dampening of preferred responses; then E$\rightarrow$E connections were set to give reasonable overall spike rates to a preferred stimulus, and E$\rightarrow I_s$ connections were set equal for simplicity; then $I_c \rightarrow I_s$ connections were increased to yield sharp orientation tuning of I_s cells; finally connections from I_s cells were set to give a reasonable inhibitory current modulation in E-cell responses, and were set equal onto E and I_s cells for simplicity. In simulations of fig. 2.7, as indicated in the text, all intracortical synaptic strengths from I_c and from E cells were increased by 20%; synaptic strengths from LGN and, when present, from I_s remained at default levels.

Each simulation was started with a 'blank screen' for one second with LGN cells firing at their background rates to equilibrate the network, followed by an additional 0.25 seconds with a grating stimulus to suppress transients before actually recording data for 1 second of simulated time as the grating stimulus continued. For all figures except figs. 2.2 and 2.3, simulations were run at 40% contrast with a grating oriented at 128° to avoid artifacts of the grid with the stimulus. Tuning curves were calculated from 20 such simulations (with different random seeds for the Poisson spike trains of the LGN inputs) and from responses of all cells with preferred orientations within ±5° of 128°. To determine orientation tuning curves (figs. 2.2 and 2.3), responses were obtained from 1 repetition of gratings having each of 18 orientations, from 8° to 178° by 10°, at each of the indicated contrasts. Cells were binned by preferred orientation in bins of ±5° around each grating orientation; each bin's tuning curve was determined, and the tuning curves of the different bins were averaged together by equating the central orientation of each bin (representing orientation 0° in fig. 2.2).

2.2.3 Toy model

To assess the stabilizing effect of the push-pull inhibition we constructed a simple model consisting only of current input to a simple cell. The firing rate of the cell is, $r(t) = [I_{ff}(t) + I_{ex}(t) - I_c - I_s(t) - \theta]^+$; with $I_{ff}(t) = [\sin(t)]^+$, the thalamocortical input current; $I_{ex}(t) = r(t) \times w_{ex}$, the excitatory recurrent input current; $I_c = C$, the constant complex cell inhibitory current; and $I_s(t) = [w_s \times \sin(t + \pi)]^+$, the simple inhibitory cell push-pull current. t is time in cycles, θ the firing threshold, w_{ex} the recurrent excitatory input strength, w_s the simple inhibitory cell input strength. $[x]^+ = \{x$ if $x > 0$; 0 otherwise$\}$. In the presented simulations we vary C and w_{ex}, and fix $w_s = 15$, and $\theta = 0$. Changing w_s varies the stable regime for simple cell inhibition, and increasing θ has the same effect as increasing I_c. The value $w_s = 15$ was chosen to make excitatory and inhibitory currents of roughly equal amplitude in fig. 2.8b. Any value of w_s greater than 0 increases the stable area (fig. 2.8c), with a greater increase in area for larger w_s.

2.2.4 Computing the effect of variability in integration times

In the Discussion we state a rough estimate of the effects of variability of LGN integration times (Mukherjee and Kaplan, 1995; Saul and Humphrey, 1990) on the amplitude of temporal modulation of the LGN input to a simple cell. It is obtained as follows. We consider the change in amplitude in changing from 2 to 8 Hz drifting grating stimulation. To simplify, we assume that all of a cell's inputs are perfectly in phase at 2 Hz, and that their integration times are uniformly distributed between $-\tau$ and τ about some central value. As a conservative assumption we will take τ to cover the full range of experimentally observed integration times, even though an individual simple cell receives LGN inputs with correlated temporal response properties (Alonso et al., 2001). Then at 8 Hz the phases will be uniformly distributed between $-\phi$ and ϕ where $\phi = 2\pi\tau(6\text{Hz})$ is in radians. The sum of the inputs at their peak at 8 Hz, ignoring the effects of temporal integration for simplicity, is then proportional to $\int_{-\phi}^{\phi} d\theta \cos(\theta) = 2\sin(\phi)$, whereas the sum at 2 Hz is proportional to $\int_{-\phi}^{\phi} d\theta \cos(0) = 2\phi$. Thus, the ratio of 8-Hz peak modulation amplitude to 2-Hz peak modulation amplitude is $R = \sin(\phi)/\phi$.

To apply this result, we consider a simple cell receiving only input from nonlagged X-cells, because this is the only kind of input considered in this paper, and because most cat V1 cells receive largely or exclusively X-cell input (Ferster, 1990a,b) and the majority have only or nearly only nonlagged-type timing in their receptive fields (Saul and Humphrey, 1992a). Nonlagged X-cells have a range of integration times spanning ± 35 msec (Saul and Humphrey, 1990) or less (Mukherjee and Kaplan, 1995); setting $\tau = .35$ msec yields $R = .73$. Lagged X-cells have a broader range of integration times ((± 50 msec Saul and Humphrey, 1990), yielding $R = .50$. Cells that receive a mix of nonlagged and lagged input appear to receive them in spatially segregated subregions (Saul and Humphrey, 1992a), and could show greater demodulation due to the relative phase shift between nonlagged and lagged inputs, which differ in mean integration time by 70 msec (Saul

and Humphrey, 1990). However such cells are also likely to change their direction selectivity with increasing temporal frequency (Saul and Humphrey, 1992b), thus analysis of the modulation to an optimal stimulus with changing temporal frequency becomes more complicated because the optimal stimulus may change with temporal frequency.

2.3 Results

2.3.1 Model Overview

The model contains three cortical cell types found in cat V1 layer 4: orientation-tuned excitatory and inhibitory simple cells with separate ON and OFF subfields, and inhibitory complex cells untuned for orientation with ON-OFF receptive fields (RFs) (Hirsch et al., 2000). All cells receive thalamocortical input selected probabilistically, the simple cell inputs chosen from ON-center inputs overlying ON-subregions and OFF-center inputs overlying OFF subregions (Alonso et al., 2001; Hubel and Wiesel, 1962; Reid and Alonso, 1995; Tanaka, 1983), and the complex cell inputs chosen from all LGN cells whose RFs overlap. Cortical connectivity is also determined probabilistically, with the most probable connections illustrated in the cartoon in fig. 2.1a. The simple cells form synapses primarily to other cells with similar preferred orientation, according to the correlation of their RFs. Excitatory synapses are formed to cells with correlated RFs (similar preferred orientation and similar absolute spatial phase, meaning that ON-subregions of the two cells tend to overlap in visual space and similarly OFF-subregions tend to overlap), and inhibitory synapses are formed to cells with anti-correlated RFs (similar preferred orientation and opposite absolute spatial phase, meaning that ON-subregions of one cell tend to overlap OFF subregions of the other cell). The complex cells project randomly with equal (10%) probability to all simple cells within 150 μm, and, for simplicity, do not receive any cortical input. The model contains simple cells preferring all orientations and all spatial phases and a range of retinotopic positions. In particular, the relative spatial phase (which refers to the locations of ON and OFF subregions relative to the receptive field center) of each simple cell is assigned randomly; only receptive fields with even symmetry are illustrated in Fig. 2.1, but these are not favored over other relative spatial phases in the model.

We designed the architecture so that complex inhibitory cells would lack orientation tuning, as observed, and the feedforward inhibition from the complex cells would cause both inhibitory and excitatory simple cells to have sharp orientation tuning without responses to orientations orthogonal to the preferred. As described in the Introduction, some simple inhibitory cells, while sharply tuned, respond to all orientations (and thus could provide some of the untuned inhibition needed to explain sharp orientation tuning of other simple cells). Similarly, some excitatory simple cells in cats respond to all orientations (*e.g.* Azouz et al., 1997). For simplicity, we ignore these facts and assume that the only orientation-untuned component of inhibition comes from complex

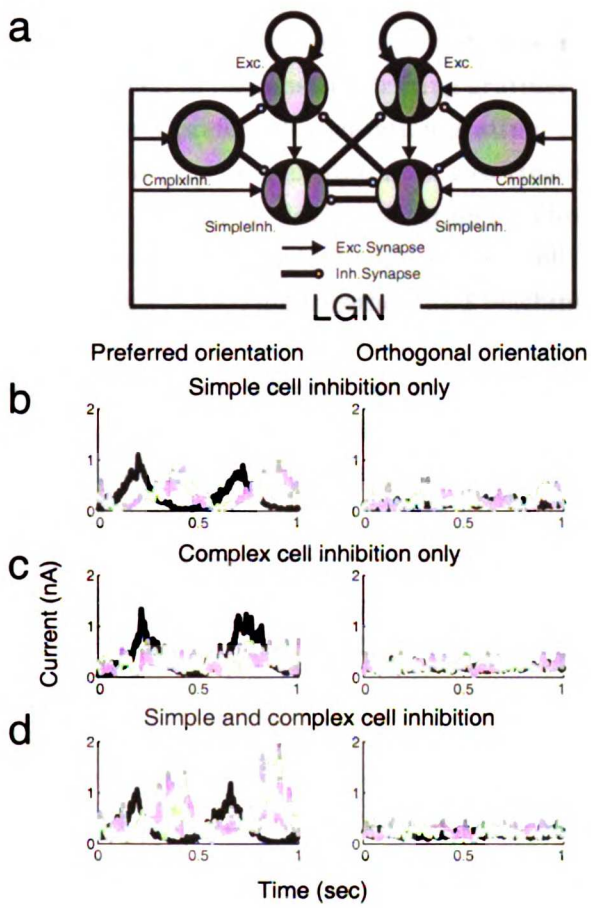

Figure 2.1:

Overview of the model and its behaviour with different types of inhibition. (a) Cartoon of model circuit. (b-d) Example synaptic current traces for a single excitatory cell when stimulating with a drifting grating; excitatory input in black, inhibitory input in gray. Left, cell preferring the orientation of the grating; right, cell preferring the orientation orthogonal to the grating. (b) Simple cell inhibition only. At the preferred orientation, inhibitory current modulates with time in anti-phase with excitatory current. (c) Complex cell inhibition only. Inhibitory current is unmodulated with time. (d) Both simple- and complex cell inhibition. Inhibitory current at the preferred orientation has an unmodulated part arising from the complex cell inhibition and a part modulated with time arising from the simple cell inhibition. The cell can reach threshold when the excitatory synaptic current is larger than the inhibitory synaptic current, so the response at the preferred orientation is similar in all three cases. At the orthogonal orientation the inhibitory current dominates the excitatory current at all times and the cell will not fire.

cells; for further discussion, see section "Model homogeneity versus physiological heterogeneity" of the Discussion.

2.3.2 Background: The LGN Input to a Simple Cell

Before examining the effects of the model circuit, it is useful to review the nature of the LGN input received by a simple cell in response to drifting gratings of various orientations (Troyer et al., 2002, 1998). In response to a preferred-orientation grating, the cell receives LGN input that is strongly temporally modulated (*e.g.*, see excitatory traces (black lines) in Figs 2.1b-d, left, although these include intracortical as well as LGN excitation). This occurs because the preferred-orientation grating causes all the LGN inputs to the simple cell to modulate their firing rates roughly in phase with one another – peaking together, and reaching low or zero firing rates together – so that the temporal modulations of the individual LGN inputs add constructively to produce a strongly modulated total LGN input. In response to a grating oriented orthogonal to the cell's preferred (which we will refer to as the cell's null orientation), the cell instead receives a roughly constant, temporally unmodulated rate of LGN input (excitatory traces in Figs 2.1b-d, right). This input is temporally unmodulated because the null-oriented grating drives different LGN inputs to the cell at different times – some are reaching their peak rates when others are at their lowest rates and others are in the middle – and so the temporal modulations of the individual LGN inputs add destructively. Thus the total LGN input arrives at a constant, temporally unmodulated rate corresponding to the sum of the mean firing rates of all the LGN inputs to the cell. This mean rate of total LGN input is the same for gratings of any orientation, because the mean rates of the individual LGN cells are independent of orientation. Thus, gratings of different orientations are distinguished, not by the mean rate of LGN input they elicit, but by the temporal modulation of that input, with the strongest temporal modulation elicited by a grating of the cell's preferred orientation and little or no modulation at the null orientation.

The mean rate of total LGN input to a simple cell grows with stimulus contrast, because the mean rates of the individual LGN cells grow with contrast. This is a nonlinear effect: because the mean luminance does not change with changes in contrast, the mean response also would not change if LGN responses were linear in the image. It is induced by the fact that LGN firing rates cannot decrease below zero, whereas they can increase to 100 Hz or higher, many times their background level (10-15 Hz, *e.g.* Kaplan et al., 1987).

Because the mean input grows with contrast for all orientations, even a null-oriented stimulus can elicit a high rate of LGN input at high contrast, higher even than the peak of the temporally modulated input elicited by a preferred-orientation grating at sufficiently low contrast. Yet simple cells show contrast-invariant tuning (Anderson et al., 2000b; Sclar and Freeman, 1982; Skottun et al., 1987), so that they respond to their preferred orientation even at very low contrast and often do not respond to the null orientation even at high contrast. This problem is solved by the feedforward inhibition in our model network, as we now examine.

2.3.3 Orientation tuning

In simulations using drifting grating stimuli, we can block the inhibition coming from one of the two inhibitory cell types. If we block the complex cell inhibition, leaving only simple-cell inhibition, we also have to turn off the $I_s \rightarrow I_s$ connections to avoid instabilities (Krukowski, 2000). (Unless these connections are very weak, they lead to a winner-take-all competition between inhibitory cells of similar preferred orientation and opposite spatial phase: between inhibitory cells of two such opposite phases, only the one receiving more LGN input at any given time would be active. Orientation tuning in the simple-cell-only model depends on the graded strength of antiphase inhibition, so such winner-take-all behavior would greatly broaden the orientation tuning of the excitatory cells.)

In this case, excitatory cells stimulated at their preferred orientation receive excitatory and inhibitory synaptic input currents that modulate out of phase with one another, thus allowing the cells to reach threshold and fire at some point in their cycle (fig. 2.1b, left). Cells preferring the orthogonal orientation will receive a temporally unmodulated synaptic input from the LGN, regardless of their preferred phase. Thus, an excitatory cell will receive both temporally unmodulated LGN excitation and temporally unmodulated inhibition from inhibitory neurons of similar preferred orientation and roughly opposite absolute spatial phase, which are equally driven by the LGN stimulus; because the inhibition is dominant, the excitatory cells will not fire (fig. 2.1b, right). This yields contrast-invariant orientation tuning for excitatory cells, while the inhibitory simple cells, which do not receive inhibition, have responses that mirror the tuning of the LGN input: a response component tuned for orientation atop a component untuned for orientation (fig. 2.2a and b).
As previously reported (Krukowski, 2000; Troyer et al., 1998), this result holds and responses are stable for a wide parameter regime.

These inhibitory simple cells are largely simple according to the classical criteria of Hubel and Wiesel (1962), in that they have spatially segregated ON and OFF subregions from which their responses can be largely understood. Furthermore their responses to a preferred-orientation drifting grating have a ratio of first harmonic to mean (F1/DC ratio) greater than 1, another standard criterion for simple-cell behavior (Skottun et al., 1991). However, because they do not themselves receive feedforward inhibition to counter the nonlinear nature of their LGN input, they show several nonlinear response characteristics that are not typical of simple cells: their orientation tuning is not invariant with stimulus contrast (Troyer et al., 1998), and they show a period-doubled response to a counter-phase grating 90^o out of phase with the cell's receptive field (Wielaard et al., 2001).

If we instead block the simple cell inhibition (both onto other simple inhibitory cells and onto simple excitatory cells), leaving only complex-cell inhibition, the inhibitory synaptic current from the complex cells into the excitatory simple cells at the preferred orientation is temporally unmodulated. Since the excitatory synaptic current is temporally modulated, the membrane potential is

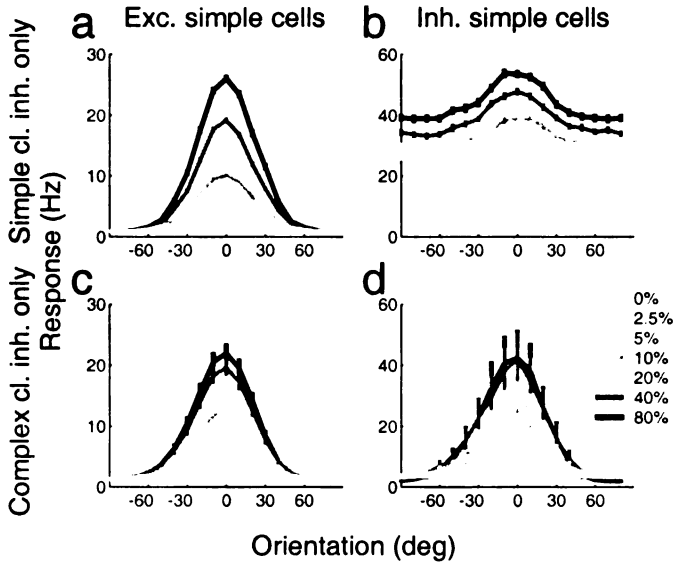

Figure 2.2:

Orientation tuning of cells in the network. (a, b) Simple cell inhibition only. (a) Excitatory simple cells display contrast-invariant orientation tuning. (b) Inhibitory simple cells have a component tuned for orientation atop a component untuned for orientation, thus they have a response to all orientations that increases with contrast. (c, d) Complex cell inhibition only. Both excitatory simple cells (c) and inhibitory simple cells (d) display contrast-invariant orientation tuning. Complex cells are untuned for orientation by design. When both complex- and simple-cell inhibition are included, simple cell responses remain as in (c, d) (not shown). Error bars in this and subsequent figures are ± 1 standard error of the mean. Here and in subsequent figures tuning curves show the mean (DC) response of the cells. Tuning of the first harmonic (F1) of the response is similar in all cases.

still able to periodically reach threshold so the cell will respond (fig. 2.1c, left). For cells preferring the orthogonal orientation, both synaptic currents are unmodulated, so that the dominant inhibition prevents responses (fig. 2.1c, right). The only difference from the previous case (fig. 2.1b, right) is that the inhibitory synaptic current is now coming from the complex inhibitory cells rather than from the simple inhibitory cells. The inhibitory simple cells receive the same type of input, both excitatory and inhibitory, as the excitatory simple cells, so both types of simple cells now display contrast-invariant orientation tuning (fig. 2.2c and d).

If both types of inhibition are used, there is an extra contribution of temporally modulated inhibitory synaptic current at the preferred orientation (fig. 2.1d left). This extra current is antiphase with the excitatory synaptic current at the preferred orientation, and goes away at non-preferred orientations (because the inhibitory simple cells do not respond at these orientations, fig. 2.2d) and so does not affect the orientation tuning curves, which remain the same as in figs. 2.2c,d (not

shown).

Achievement of sharp, contrast-invariant orientation tuned responses via complex-cell inhibition requires relatively tight tuning of inhibitory strength (fig. 2.3). If the complex-cell inhibition

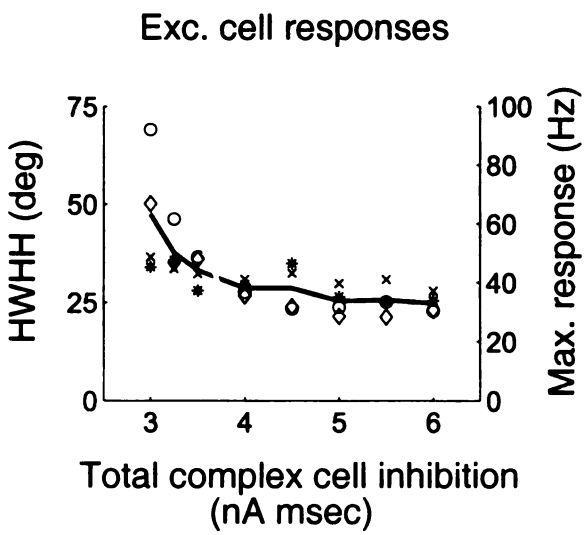

Figure 2.3:

Tuning of the excitatory cell responses as a function of complex cell inhibition, for constant excitatory strength and no simple cell inhibition. Left axis and black curve show half-width at half height of the orientation tuning curve (* 10% contrast, × 20% contrast, ∘ 40% contrast, ◇ 80% contrast). Orientation tuning is lost when the inhibition is below about 3.5 na msec. For high levels of inhibition the response to low contrasts is close to the spontaneous activity of the cells, so the orientation tuning appears broader. Right axis and gray curve show the response to a preferred-orientation stimulus at 80% contrast. This response decreases sharply with inhibition, and has a physiologically realistic level of 20-40Hz for complex cell inhibition around 4 nA msec, a level that also produces contrast-invariant orientation tuning. 4nA msec is the value used in the simulations.

is too weak, responses at non-preferred orientations are not suppressed and orientation tuning becomes very wide (fig. 2.3, black line). If the complex-cell inhibition is too strong, responses at preferred orientations are suppressed, so overall responses become very weak (fig. 2.3, gray line), and contrast-invariance of tuning is lost at low contrasts. Only a relatively narrow range of complex-cell inhibitory strengths around the value of 4 nA-msec used in our simulations achieves sharp contrast-invariant tuning with realistic response levels. This is quite different from the case in which inhibition comes only from simple cells. In that case, because simple-cell inhibition is antiphase to excitation, even very strong inhibition does not interfere with preferred-orientation responses, so a wide range of inhibitory strengths give realistic responses (Troyer et al., 1998). Physiologically, homeostatic mechanisms (Turrigiano and Nelson, 2000) can adjust the overall level of a cell's inhibition (and excitation) to keep its firing rate within a reasonable range, so such mechanisms may

provide the relatively fine tuning of overall inhibitory strength required by complex-cell inhibition.

2.3.4 Spatial frequency tuning

Given complex-cell inhibition, what role does simple-cell inhibition play? For simple-cell inhibition to play a role in shaping the responses of the cells, it must interfere with the excitatory drive underlying responses. At the preferred orientation and spatial frequency, the antiphase simple-cell inhibition is significant only during temporal phases in which complex-cell inhibition already dominates excitation, and so it has little effect. However, if the spatial frequency of the stimulating drifting grating does not match the spatial frequency preference of the cells (roughly given by the spatial frequency component of the Gabor filter, 0.8 cycles/degree), then simple-cell inhibition can impact responses. For example, for a drifting grating stimulus of 0.4 cycles/degree, simple-cell inhibition rises (fig. 2.4b) at times when complex cell inhibition and excitation are comparable

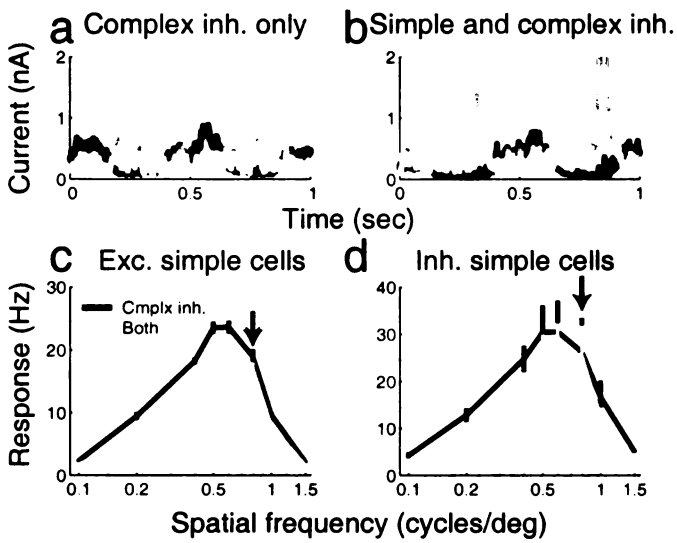

Figure 2.4:

Spatial frequency tuning of simple cells is sharpened by simple cell inhibition. (a, b) Excitatory (black) and inhibitory (gray) synaptic currents vs. time for a grating at a low spatial frequency (0.4 cycles/degrees). (a) Complex cell inhibition only. (b) Simple- and complex cell inhibition. The modulated component of the inhibition interferes in time with the excitatory current, thus decreasing the firing rate of the cells. (c) Response of the excitatory simple cells when stimulating with gratings of different spatial frequencies. Complex cell inhibition only in black; simple- and complex cell inhibition in gray. Arrow shows frequency of the Gabor function defining simple cell receptive fields. Adding simple cell inhibition suppress the response for frequencies away from this Gabor frequency, thus sharpening the spatial frequency tuning of the simple cells. (d) Response of inhibitory simple cells, conventions as in (c).

(fig. 2.4a), so that responses away from the preferred spatial frequency are somewhat suppressed by the addition of simple-cell inhibition (fig. 2.4c,d). Thus, the simple-cell inhibition serves to sharpen the spatial frequency tuning of the simple cells.

To study how this inhibition serves to sharpen the spatial frequency tuning, we examined the dependence of spatial frequency tuning on the strength of simple-cell inhibition. The half-width at half height (HWHH) of the spatial frequency tuning curve decreases with increasing simple-cell inhibitory strength until this strength reaches around 8 nA msec, the default level of simple-cell inhibitory strength used in our simulations with a mix of simple- and complex-cell inhibition, at which point the HWHH reaches a plateau level (fig. 2.5). This sharpening is primarily due to an

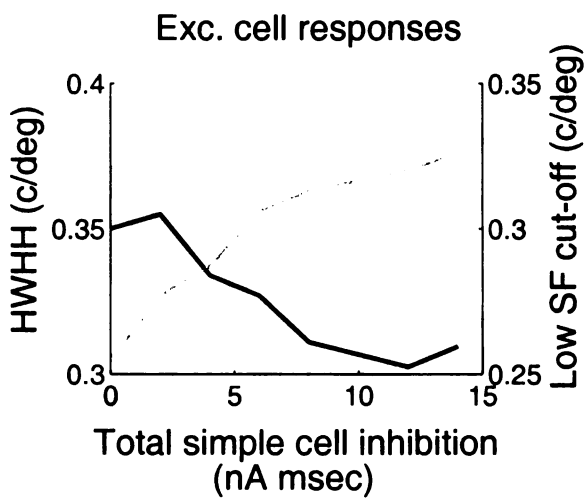

Figure 2.5:

Spatial frequency tuning as a function of the simple cell inhibition. Left axis and black curve show half-width at half height of the spatial frequency tuning curve of the excitatory simple cells. It decreases with increasing simple cell inhibition up to a plateau level. Right axis and gray curve show the low spatial frequency cut-off of the cells. It increases similarly to the decrease in the half-width at half height, indicating that it is the main contributor to the sharpening of the spatial frequency tuning.

increase in the low spatial frequency cut-off of the cells, defined as the spatial frequency below the peak at which spike response is 50% of the peak response. There was no systematic change in the high spatial frequency cut-off with simple cell inhibition (not shown). So there is a maximal level of simple cell inhibition beyond which further increases do not further sharpen spatial frequency tuning, and this sharpening is mainly achieved by reducing the response to gratings of low spatial frequency.

2.3.5 Temporal frequency tuning

We have previously shown that the model with only simple-cell inhibition can explain the fact that cortical neurons have temporal frequency high-cutoffs at much lower frequencies than LGN cells (Krukowski and Miller, 2001). The explanation relied on two elements: NMDA-receptor-mediated conductances (which we will abbreviate simply as "NMDA") in synapses from LGN to excitatory cells act as a low-pass filter, reducing the temporal modulation of the excitatory input at higher

frequencies and thus largely reducing this input to its mean; and the dominant inhibition prevents responses to the mean excitation. Note that this explanation requires that some inhibitory neurons respond to the high temporal frequencies that drive LGN cells.

This explanation of temporal frequency tuning also works with complex-cell inhibition, and in this case is even more powerful: because complex-cell inhibition is not modulated at the opposite phase as the excitation, less demodulation of the excitation is required for the inhibition to dominate the excitation, and so temporal frequency high-cutoffs occur at lower frequencies than in the previous model. Assuming that NMDA constitutes 75% of the current in LGN synapses onto excitatory cells, which corresponds to observations in rat thalamocortical slices (Crair and Malenka, 1995), the resulting temporal frequency tuning of excitatory simple cells shows little or no response above 4 Hz (fig. 2.6a). The complex inhibitory cells, in contrast, have temporal frequency

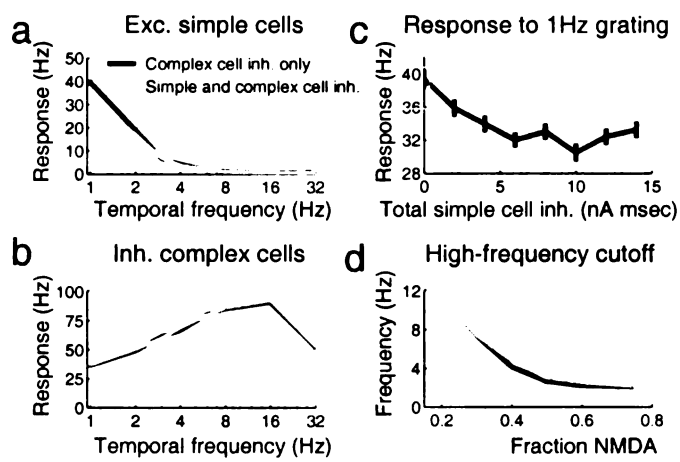

Figure 2.6:

Temporal frequency tuning of simple cells is not dependent on simple cell inhibition. (a) Response of the excitatory simple cells when stimulating with gratings of increasing temporal frequency. Black, only complex-cell inhibition; gray, both simple- and complex-cell inhibition. Temporal frequency cut-off is similar in both cases. Temporal frequency cut-off for inhibitory simple cells is the same (not shown). (b) Temporal frequency tuning for the complex inhibitory cells follows the tuning of the LGN input. (c) Response to stimulation with a drifting grating at 1 Hz for increasing simple cell inhibition. The response decreases until simple cell weights reach around 6 nA msec, and then levels off. (d) The high temporal frequency cut-off as a function of the NMDA fraction in the thalamocortical synapses. The cut-off is similar both for complex cell inhibition only (black) and combined simple- and complex cell inhibition (gray).

tuning that follows that of our model LGN input, cutting off above 16 Hz (fig. 2.6b). Defining the high-frequency cutoff as the temporal frequency above the peak at which the mean spike response is reduced to 50% of the peak response, the cutoff of simple cells is close to 2 Hz. This is on the

low side, but still within the range of cells reported experimentally (*e.g.*, Freeman et al., 2002; Movshon et al., 1978). Decreasing the fraction of NMDA in the thalamocortical synapses to the excitatory cells decreases the demodulation of the excitatory input at higher temporal frequencies, and hence causes the high-frequency cutoff to increase (fig. 2.6d). If the proportion of NMDA is halved from the amount we have assumed, then the cutoff is around 6 Hz, which is a representative experimental cutoff value for cortical cells (DeAngelis et al., 1993; Freeman et al., 2002; Holub and Morton-Gibson, 1981; Ikeda and Wright, 1975; Movshon et al., 1978; Saul and Humphrey, 1992b). In simulations without NMDA, we find that cortical temporal tuning closely follows LGN tuning (not shown).

Addition of simple-cell inhibition up to about 6 nA msec causes a decrease in the response to gratings at low temporal frequencies (fig. 2.6c). Because the simple-cell inhibition does not affect the response at higher temporal frequencies, it does not have a significant effect on the temporal frequency cut-off (fig. 2.6d).

Temporal frequency tuning of inhibitory simple cells in the model is largely identical to that of excitatory simple cells (not shown). This is easily understood since the inhibitory simple cells in the model receive the majority of their excitatory drive from excitatory simple cells, and so their overall tuning follows that of this excitatory drive. We have not included NMDA in LGN synapses onto inhibitory cells, so the LGN-driven component of excitation does not demodulate with increasing temporal frequency and hence yields tuning like that of the LGN inputs, adding a small excitatory component at higher temporal frequencies to inhibitory simple-cell responses. Both factors, the relative strength of their feedback vs. feedforward excitatory drive and the proportion of NMDA, if any, in their LGN synapses, shape the temporal frequency tuning of inhibitory simple cells. Since these are not well experimentally constrained, we cannot make strong predictions as to the exact temporal frequency tuning of the inhibitory simple cells, other than to point out how it will be controlled by these two factors.

2.3.6 Network stability

The network including only simple cell inhibition is stable for a fairly large parameter regime (Troyer et al., 1998). Here we show that the network including only complex cell inhibition is fragile and prone to at least one form of instability, and that simple cell inhibition can help to expand the stable parameter regime.

If we increase all intracortical synaptic weights, both excitatory and inhibitory, by 20% in a network with only complex-cell inhibition, a drifting grating of one orientation evokes tonic firing from cells preferring all orientations (fig. 2.7a). The recurrent excitatory synaptic current builds up over time, resulting in uncontrolled firing (fig. 2.7c and e). Adding simple cell inhibition restores the network to a stable firing state (fig. 2.7b, d, f). The increased inhibitory synaptic current from the simple cells acts to 'reset' the network during non-responsive phases of the stimulus, shutting

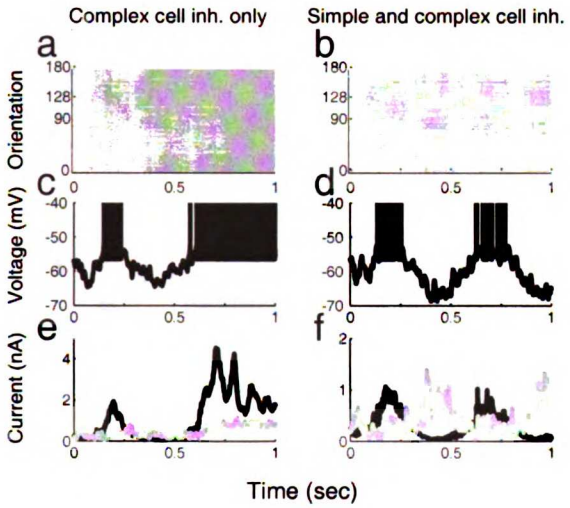

Figure 2.7:

Simple cell inhibition can stabilize otherwise unstable network. (a, c, e) Complex cell inhibition only, (b, d, f) Simple- and complex cell inhibition. (a, b) Raster plots of all excitatory cells arranged according to their preferred orientation. While the activity of the network spreads to all orientations for complex cell inhibition only, adding simple cell inhibition can restrict the activity to cells only at the preferred orientation of the grating. (c) Membrane potential, and (e) synaptic current for a single cell; excitatory current black, inhibitory current gray. Excitatory synaptic current increases and is not shut off again. (d, f) Same as (c, e) with addition of simple cell inhibition. The addition of antiphase-modulated inhibition is enough to shut off excitatory current.

down overactive cells and stabilizing the network.

To explore the conditions for this stabilization effect to occur, we constructed a toy model of a simple cell receiving four input currents: a thalamocortical input modulated with time, a recurrent excitatory input proportional to the activity of the cell, a complex-cell inhibitory input that is constant with time, and an antiphase simple-cell inhibitory input modulated with time. The response of the cell, r, is the difference between its excitatory and inhibitory inputs, rectified over a threshold, θ. For fixed threshold and simple cell inhibitory strength we can determine the stability of the model for a range of excitatory recurrent strengths and inhibitory complex strengths. Defining the stable regime as one in which the response of the cell is larger than a minimum response, but does not grow indefinitely, we can compare the size of the stable regime with- and without simple cell inhibition (fig. 2.8c). For both scenarios, the minimum desired activity is found for the same parameters, since simple-cell inhibition is out of phase with excitation. But the size of the parameter regime in which the activity does not grow indefinitely is significantly increased when including antiphase simple-cell inhibition. For the fixed parameters used here, the ratio of the area of the two stable regimes is about 2:1. The degree of this increase depends on the strength of the simple-cell inhibition, but even very weak simple-cell inhibition causes an increase in area of the

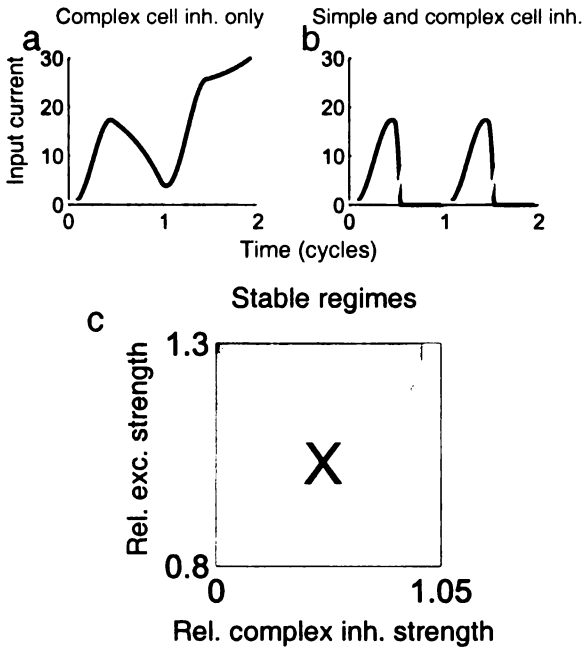

Figure 2.8:

In a toy model, stable parameter regime is increased by simple cell inhibition. (a, b) Excitatory input current (black) and inhibitory input current (gray) to a cell. While excitatory current can grow without bound with complex inhibition only, simple cell inhibition resets the excitatory current on each cycle, thus stabilizing network activity. (c) Stability of the response as a function of complex inhibitory strength C and excitatory strength w_{ex} for fixed simple inhibition strength. White, parameter regime in which responses to preferred orientation are too low (< 2); light gray, stable response for both types of inhibition; medium gray, uncontrolled response for complex inhibition only, but stable for simple- plus complex inhibition; dark gray, unstable for both types of inhibition. Adding simple cell inhibition significantly increases the stable parameter regime of the toy model. X marks the case shown in (a, b): $C = 0.5$, $w_{ex} = 1.022$.

stable regime (not shown). So qualitatively we can conclude that simple-cell inhibition increases the size of the stable regime, though we cannot draw a parameter-free conclusion as to the size of this increase. Comparing the relative size of the inhibitory and excitatory traces in fig. 2.7f to those in fig. 2.8b indicates that the simple-cell inhibitory strength in the toy model that achieves a 2:1 increase in stability is comparable to the strength in the full model.

2.4 Discussion

We have shown that feedforward inhibition from complex inhibitory cells that are untuned for orientation, as observed by Hirsch et al. (2000) in cat V1 layer 4, can combine with feedforward excitation from LGN inputs to explain the sharp, contrast-invariant orientation tuning of layer 4 simple cells. Assuming that these inhibitory cells follow the LGN inputs in their temporal frequency tuning, and given NMDA-receptor-mediated conductances in LGN synapses, this can also explain the low-pass temporal frequency tuning of simple cells. However, the parameter regime where this is achieved is restricted. Given complex cell inhibition, antiphase simple-cell inhibition acts to somewhat sharpen the spatial-frequency tuning of simple cells, to reduce their responses to low-

temporal-frequency stimuli, and to help stabilize the network, somewhat expanding the allowable parameter regime.

2.4.1 Model Predictions

Predictions of the model include:

1. Simple cells receiving significant thalamic excitation should receive a comparable level of orientation-untuned inhibition, yielding detectable conductance changes in response to a stimulus oriented perpendicular to the preferred. Such conductance changes were seen in some but not all simple cells studied by Anderson et al. (2000a); cells receiving little thalamic input could inherit their tuning from cells receiving such input and hence would not require such conductance changes.

2. Complex inhibitory cells should have temporal frequency tuning like that of the LGN inputs, responding to high temporal frequencies to which few other cortical cells respond. This gains some support from results in rabbit somatosensory (Swadlow, 1989, 1991) and motor (Swadlow, 1994) cortex that suspected interneurons follow much higher temporal frequencies of peripheral stimulation than other cortical cells.

3. Thalamocortical synapses onto excitatory cells should include a significant NMDA-receptor-mediated component. This agrees with slice studies of thalamocortical synapses (Crair and Malenka, 1995; Gil and Amitai, 1996) and with some (Miller et al., 1989) but not other (Fox et al., 1989) studies of V1 physiology.

In addition, assumptions as to circuit structure need testing. We assumed that simple inhibitory cells in layer 4 receive strong LGN input that is specifically arranged like that of other simple cells (Alonso et al., 2001; Reid and Alonso, 1995; Tanaka, 1983) and make connections that tend to be antiphase (Anderson et al., 2000a; Ferster, 1988; Hirsch et al., 1998); and that complex inhibitory cells in layer 4 receive strong LGN input that is nonspecific, and project nonspecifically to other cortical cells.

2.4.2 Complex-cell feedforward inhibition as a solution to the problem posed by the LGN inputs

The problem posed by the LGN inputs to a simple cell is that the mean rate of LGN input grows with contrast both at non-preferred orientations and at high temporal frequencies, yet most excitatory simple cells do not respond to these stimuli. The solution we have proposed is that broadly-tuned feedforward inhibition cancels this mean input, allowing responses only to the peaks of temporally modulated excitatory input. This inhibition might arise from orientation-untuned complex cells (this paper) or simple cells that respond to all orientations (previous work). Since Hirsch (private

communication) found a minority of inhibitory simple cells respond strongly to all orientations (see Introduction), both types of inhibitory cells may actually contribute; we have focused on a single type for simplicity.

We argue that a significant part of this inhibition must be feedforward, for two reasons. First, in response to the positive pulse of LGN input evoked by transient non-preferred stimuli such as a high-contrast flashed bar or grating of the cell's null orientation, the inhibition must arrive in time to prevent spiking (*e.g.*, see Felsen et al., 2002; Gillespie et al., 2001, for evidence that many cat V1 cells do not respond to such stimuli). The stimulus evokes a positive pulse of input because it excites some LGN inputs to the simple cell and inhibits others, and those that are excited can raise their firing rates much more strongly than those that are inhibited can lower theirs. Fast-spiking inhibitory cells have higher resistances and lower thresholds than excitatory cells (McCormick et al., 1985) and thus can respond very rapidly (*e.g.*, within 0-1 msec after thalamic action potentials reach cortex in rabbit somatosensory cortex, Swadlow, 1995), hence these cells can spike in time to prevent spiking in excitatory cells (Somers et al., 1995). Consistent with this, shocks to LGN elicit in LGN-recipient cortical cells a short depolarization followed, before spike threshold is reached, by a massive hyperpolarization (*e.g.*, Ferster and Jagadeesh, 1992) induced by inhibitory neuronal firing. Second, the required inhibition seems likely to be driven by LGN rather than cortical excitation because it must be driven by stimuli that excite LGN cells but do not excite most cortical cells. However, the minority of excitatory simple cells that do respond to the stimulus – a very small minority in the case of high-temporal-frequency stimuli (Freeman et al., 2002) – might provide this excitatory drive for steady-state rather than transient stimuli. The inhibitory cells may of course also receive excitation from cortical cells; we only argue that the LGN-driven component of inhibition seems necessary and is sufficient to shape simple cell orientation and temporal-frequency tuning.

The solution via complex-cell inhibition requires relatively fine tuning of overall complex-inhibitory strength. However, no further specificity of these connections is needed – it suffices that complex cells receive topographic but otherwise nonspecific LGN input and project nonspecifically to nearby cortical cells. Thus, homeostatic mechanisms that can control overall inhibitory strength (Turrigiano and Nelson, 2000) could suffice to guide development of this inhibition. Hebbian mechanisms can guide development of inhibitory and excitatory simple-cell connections (Kayser and Miller, 2002).

The inclusion of complex-cell inhibition is consistent with experiments suggesting a "push-pull" arrangement of excitation and inhibition onto simple cells. Dark elicits inhibition in the RF where light elicits excitation and vice versa (Ferster, 1988; Hirsch et al., 2000). This is consistent with inhibition that is antiphase to excitation, but also with partly or entirely phase-nonspecific inhibition along with phase-specific excitation – excitation, when evoked, overwhelms inhibition, and otherwise inhibition is seen. In response to optimal drifting gratings, the evoked inhibitory

conductance in simple cells shows both a mean or DC component, and a temporal modulation that is nearly antiphase to that of excitatory conductance (Anderson et al., 2000a). This is consistent with a circuit containing only antiphase simple-cell inhibition, because factors that cause inhibitory simple-cell firing rates to increase from background more strongly than they decrease, such as excitatory feedback and the minimum firing rate of zero, induce a DC. However, it is also consistent with a combination of antiphase simple-cell inhibition and complex-cell inhibition.

The orientation tuning of inhibition to simple cells is strongly peaked at the preferred orientation, dropping to low values at the orthogonal orientation (Anderson et al., 2000a; Ferster, 1986; Martinez et al., 2002, but see Monier et al., 2003). This suggests that orientation-tuned simple-cell inhibition is much stronger than orientation-untuned complex-cell inhibition.

2.4.3 Alternative solutions to the problem posed by the LGN inputs

With respect to orientation tuning, an alternative possible source of inhibition is cross-orientation inhibition: inhibition, in response to non-preferred orientations, arising from more distant tuned neurons preferring those orientations. Such inhibition would have to be weak since inhibition driven by the cross orientation is typically weak in layer 4 (Anderson et al., 2000a; Ferster, 1986; Martinez et al., 2002). There is no need to invoke such inhibition given the presence of untuned local inhibition (Hirsch et al., 2000). Such local inhibition can also explain temporal frequency tuning, which could not be explained by cross-orientation inhibition.

Related proposals were made in a model of monkey V1 layer 4 (McLaughlin et al., 2000; Wielaard et al., 2001). In this model, all cortical cells, both excitatory and inhibitory, receive simple-cell patterns of LGN input and nonspecific, inhibition-dominated input from other cortical cells, both excitatory and inhibitory, within a given radius. The result is that cells receive phase-nonspecific feedforward inhibition, similar to our complex cell model. However, the absence of a phase-specific inhibitory component is inconsistent with findings in cats that inhibitory conductance to a drifting bar or grating is temporally modulated, roughly antiphase to excitatory conductance (Anderson et al., 2000a; Ferster, 1986, 1988). Furthermore, this connectivity scheme predicts that cells in linear zones of the orientation map respond to all orientations, while cells near orientation pinwheels show sharp orientation tuning (but see Kang et al., 2003). This is incorrect in cats, where pinwheel and linear zone cells show spiking orientation tuning of the same width (Maldonado et al., 1997; Schummers et al., 2002). Pinwheel cells show broader voltage orientation tuning than linear zone cells (Schummers et al., 2002); while it is unclear whether this holds in layer 4, this is suggestive of a distance-dependent component of connectivity that is excitation- rather than inhibition-dominated, which we have neglected. Finally, this connectivity scheme predicts that simple cells showing sharp orientation tuning should receive roughly equal intracortical inhibition in response to stimuli of all orientations, whereas cat layer 4 simple cells have inhibitory tuning that is strongly peaked at the preferred orientation (Anderson et al., 2000a; Ferster, 1986; Martinez et al., 2002).

Synaptic depression acts in some respects as a high-pass filter (Abbott et al., 1997; Tsodyks and Markram, 1997) and so might eliminates changes in the mean LGN input, leaving only temporal modulations of that input. This could reduce or eliminate the need for feedforward inhibition. Our explorations to date suggest that, while synaptic depression can reduce the stimulus-induced mean LGN input to a simple cell, it cannot eliminate it except at the lowest temporal frequencies (1-2 Hz) with very strong depression ('train' parameters of Kayser et al., 2001b; vs. the weaker 'pulse' parameters used here, which do not eliminate the untuned mean LGN input, *e.g.* see Fig. 2.2b). In the course of a previous study (Kayser et al., 2001b), we found that even with strong ('train') depression, inhibition was required to obtain contrast-invariant orientation tuning. Furthermore, including such strong depression tends to eliminate the differences between stimulus contrasts, so that, after incorporating the contrast saturation of LGN responses (*e.g.*, Cheng et al., 1995; Sclar, 1987), cortical cells tend to saturate at significantly lower contrasts than observed experimentally (Kayser et al., 2001b).

Strong depression might render voltage responses to high-temporal-frequency stimuli small enough that an appropriate threshold could explain the high-frequency cutoff of cortical cells without requiring that such stimuli evoke inhibition. However, preliminary investigations suggest that, in this scenario, an appropriate threshold for high-contrast stimuli will unrealistically suppress responses to low-contrast stimuli.

2.4.4 Inhibitory neurons in other systems and the function of simple inhibitory neurons

Studies in a variety of cortical systems in rodents and rabbits have identified "suspected interneurons" (SINS) in extracellular recording and found that SINS are broadly tuned or untuned for the parameters for which other nearby cells are tuned (Bruno and Simons, 2002; Miller et al., 2001; Simons and Carvell, 1989; Swadlow, 2003; Swadlow and Gusev, 2002; Swadlow, 1988, 1989, 1990, 1991, 1994, 1995; Swadlow and Weyand, 1987). In particular, in rabbit V1, SINS are untuned for orientation and have mixed ON/OFF receptive fields like the complex cells studied here, whereas most other cells are tuned (Swadlow, 1988). The basis of this, at least in rat S1 whisker barrels (layer 4), is that SINS unselectively pool large numbers of functionally diverse thalamic inputs, receiving input on average from 65% of the thalamic neurons representing the same whisker (Bruno and Simons, 2002; Swadlow and Gusev, 2002). The high probability (≥ 0.6) of gap junction connections between nearby interneurons of a given physiological type (fast-spiking or low-threshold-spiking) (Galarreta and Hestrin, 1999, 2001, 2002; Gibson et al., 1999) also suggests that rodent interneurons are functionally nonspecific. (Note that the simple/complex interneuron distinction in cat V1 does not correspond to this FS/LTS distinction, J. Hirsch, private communication.)

These unselective inhibitory neurons receiving unselective thalamic input seem analogous to the complex inhibitory neurons reported by (Hirsch et al., 2000). In contrast, simple inhibitory

neurons, which have equally selective orientation tuning and subregion structure as their excitatory neighbors, are likely to receive specifically arranged ON and OFF LGN inputs like other simple cells (Reid and Alonso, 1995; Tanaka, 1983). It seems unlikely that they could show extensive gap junction coupling without losing their phase specificity, since simple cells of all preferred spatial phases are likely to be present in a local region (*e.g.*, DeAngelis et al., 1999). We suggest that the complex-cell interneurons correspond to the rodent and rabbit SINS, while simple-cell interneurons either correspond to an as yet unreported type of interneuron in, or are an evolutionarily new type of interneuron not found in, rodents and rabbits.

If simple-cell interneurons are evolutionarily new, the question arises what function they serve. The answers we have found here – sharpening spatial frequency tuning, reducing low-temporal-frequency responses and increasing network stability – are not large effects. The question remains open.

2.4.5 Model homogeneity versus physiological heterogeneity

In our model, all LGN cells have identical response properties except for ON vs. OFF structure and retinotopic position, and all cortical cells receive LGN inputs specified by an identical Gabor function except for orientation, phase and retinotopic position. In reality, there is much variability in LGN spatial (Cheng et al., 1995; So and Shapley, 1981) and temporal (Derrington and Fuchs, 1979; Freeman et al., 2002; Hamamoto et al., 1994; Lehmkuhle et al., 1980; Mukherjee and Kaplan, 1995; Saul and Humphrey, 1990; Sclar, 1987) response properties and in cortical Gabor filters (DeAngelis et al., 1999, 1993; Jones and Palmer, 1987) and temporal response properties (Albrecht, 1995; DeAngelis et al., 1999, 1993; Freeman et al., 2002; Ikeda and Wright, 1975; Movshon et al., 1978; Saul and Humphrey, 1992b). By ignoring this diversity, we are able to focus on basic principles: how feedforward inhibition can eliminate the orientation-untuned and high-temporal-frequency mean LGN input to yield sharp orientation tuning and, along with thalamocortical NMDA receptors, low-pass temporal frequency tuning.

These same principles would apply in the presence of response heterogeneity. However, heterogeneity might lessen the problem to be solved. For example, some simple cells respond to all orientations (*e.g.* Azouz et al., 1997), suggesting that they receive less feedforward inhibition relative to feedforward excitation (and perhaps less recurrent excitation to keep response strength in a reasonable range) and/or have more broadly tuned Gabor functions describing their LGN inputs. Simple cells with lower temporal frequency cutoffs might receive LGN inputs with lower cutoffs; consistent with this, Alonso et al. (2001) found significant correlation between the temporal properties of a cortical cell and its LGN inputs. This could lessen the amount of NMDA and/or strength of inhibition needed to explain the discrepancy between LGN and cortical cell tuning. However, a significant discrepancy would almost certainly remain, given the large overall difference between LGN and cortical temporal tuning (Freeman et al., 2002). Variation in integration times of LGN

inputs would cause dispersal in phase of LGN responses at higher temporal frequencies, yielding temporal demodulation of LGN input and thus reducing the required NMDA. However, one can estimate (see Methods) that this decrease in amplitude between 2 and 8 Hz should be 27% or less for the majority of V1 cells. In contrast, NMDA levels that mimic cortical tuning (1/2 our default level, see Results) yield 60% diminution under comparable conditions (LGN firing rate amplitudes constant across frequency; no synaptic depression), suggesting significant NMDA would remain required. Diversity in cortical temporal tuning could be explained by inter-cell diversity in the tuning or the range of integration times of LGN inputs, in the degree of NMDA on thalamocortical synapses, and/or in the strength of feedforward inhibition received. In sum, the principles found here would not be undermined by considering heterogeneity, and conversely they suggest means by which heterogeneity might be achieved.

Thalamic-recipient simple cells receiving relatively little feedforward inhibition should (1) respond well to all orientations and (2) have higher temporal frequency cutoffs than typical. Although each response property can have other causes, it would be intriguing to search for a correlation between these response properties in layer 4 cells.

Chapter 3

Effects of noise and its correlations

Abstract

The orientation tuning bandwith of cells in V1 is invariant to contrast stimulus. We have previoulsy shown that this can arise from the combination of feedforward LGN input and dominant feedforward inhibition. Recent results from Ferster's group suggest that the combination of voltage noise and contrast-invariant tuning of the mean membrane potential yields contrast-invariant spike responses. In a single cell model we have found that balanced or dominant intracortical inhibition is necessary for the voltage tuning to become contrast invariant, and that as expected, voltage noise converts this voltage tuning into contrast-invariant spiking tuning.

Here we introduce the physiological noise levels in a network model of spiking neurons and verify the single cell results. Further we show that increased synchronization of the noise between the cells decreases the spontaneous activity of the cells, while it increases their gain as well as shifts their temporal-frequency tuning in the presence of visual stimuli.

The orientation selectivity of the spiking of cells in primary visual cortex (V1) remains constant with contrast, a phenomenon known as contrast-invariant orientation tuning. Understanding the circuitry underlying these response properties remains a central problem in systems neuroscience (*e.g.*, Ferster and Miller, 2000) and serves as a model problem for understanding cortical processing.

Recent results from the Ferster group reveal that the combination of voltage noise and contrast-invariant tuning of the voltage yields contrast-invariant spike responses. We have previously shown that the voltage fluctuations in the Ferster group's raw data are reasonably described by an Ornstein-Uhlenbeck process and, in a single-cell model, that the contrast-invariant spike tuning is only achieved when the inhibition received by a cell balances or dominates the excitatory input to it (Palmer and Miller, 2002, 2003). This inhibition is required to cancel the untuned mean (DC) component of the LGN input and thus allow voltage tuning to be contrast-invariant. However, in a single-cell model the voltage DC did not show the orientation tuning seen in Ferster's data.

Here we include the in vivo noise level in a large-scale network model previously introduced (Lauritzen and Miller, 2003a). We show that the network connectivity can provide the contrast-invariant voltage tuning, including an orientation-tuned voltage DC, and verify that this yields contrast-invariant spike tuning. We further address the effect of correlation of noise in the network and find that the contrast-invariance of orientation tuning is stable even for large correlations between the membrane potential fluctuations of individual cells. Correlations in the noise input to the network has two different effects on the membrane potential of the cells in the presence and absence of stimuli: in the absence of stimuli they reduce the amplitude of the noise fluctuations and lower the mean. These effects occur because the increased correlation of the inhibition in the network acts to suppress fluctuation-induced responses. Both effects work to reduce the firing rate of the cells. In the presence of stimuli, correlations of the noise input increase the gain of the cells.

An abstract of this work has appeared previously (Lauritzen and Miller, 2003b).

3.1 Materials and Methods

The model we study is similar to a model previously described (Lauritzen and Miller, 2003a) (which was a modification of a previous model (Troyer et al., 1998)), with the major differences (1) that we have included physiological noise conductances governed by the Ornstein-Uhlenbeck process, and (2) that we have introduced different levels of correlation between the noise conductances of the cells in the model. The detailed methods are as in (Lauritzen and Miller, 2003a) except where otherwise described. Here we present the basics of the model along with the present additions.

3.1.1 Model Input.

The input to our model comes from 7200 LGN X-cells arranged in four overlying 30 × 30 sheets of ON cells and four similar sheets of OFF cells, with ON and OFF lattices offset by one-half square

lattice spacing, covering 6.8 × 6.8° of the visual field. We use four overlying sheets because we assume each LGN X-cell receives input from a single retinal ganglion (RG) X-cell, and each RG X-cell projects to 4 LGN X-cells (as in Wörgötter and Koch, 1991; this value is intermediate between values from Sherman, 1985 and Peters and Yilmaz, 1993). LGN firing rates in response to a drifting grating were calculated by assuming rates were sinusoidally modulated, up to rectification at zero rate, about background rates of 10 and 15 Hz for ON and OFF cells respectively. The amplitude of the sinusoidal modulation was chosen so that the first harmonic (F1) of the rectified responses matched experimental values from one published X-cell (Fig. 1 Sclar, 1987). We used this data as it, to our knowledge, is the only published data that includes responses both at multiple contrasts and temporal frequencies. This data determined the amplitude as a function of temporal frequency and contrast; this amplitude was then scaled by a factor reflecting the spatial frequency of the grating, given by the spatial frequency transfer function computed from the spatial receptive field of LGN cells as given in (Troyer et al., 1998), with the transfer function scaled so that its peak value is 1. Spikes were then generated from these LGN firing rates in a random (Poisson) fashion. Overlying LGN cells have 25% correlation in their spike trains, matching data showing correlations among LGN cells with overlapping RFs (Alonso et al., 1996).

3.1.2 Model architecture.

The model consists of a grid of 40 × 40 excitatory simple cells (E) and two grids of 15 × 15 inhibitory cells, one of simple cells (I_s) and one of complex cells (I_c) (Hirsch et al., 2003). All cells represent layer 4 cells, representing a 2/3 × 2/3 mm patch of cortex, corresponding to 0.75 × 0.75° in visual angle.

Each simple cortical cell was assigned a Gabor-function describing its RF, with orientation given by a measured orientation map from cat V1, spatial frequency of 0.8 cycles/degree, retinotopic position progressing uniformly across the sheet, and spatial phase assigned randomly to each cell. The precise parameters used for the Gabor functions were those specifying the "broadly tuned" cells in Troyer et al. (1998), reproducing the observed (Anderson et al., 2000a; Ferster et al., 1996) 35^o half-width at half-height of the orientation tuning of intracellular voltage modulations in response to optimal sinusoidal gratings. The connection strength from LGN cells to a cortical simple cell was determined as in Troyer et al. (1998) by a probabilistic sampling of the cell's Gabor function, where positive regions of the Gabor are converted to probabilities of a connection from an ON-cell centered on that point, and negative regions converted to probabilities of OFF-cells connecting.

The complex cell RFs were constructed to have dimensions comparable to the simple cells, but round. The LGN connections were determined with the same algorithm as for the simple cells with the difference that a random number was assigned as the phase for each possible connection, resulting in mixed ON-OFF RFs untuned for orientation, with the same amount of LGN input as the simple cells(Lauritzen and Miller, 2003a).

Cortical cells were modeled as single-compartment conductance-based integrate-and-fire neurons as in Troyer et al. (1998), and the two types of inhibitory cells had the same biophysical parameters. Each cell received stimulus-independent background excitatory (AMPA) and inhibitory (GABA A and B) conductances, mimicking membrane potential fluctuations observed *in vivo*. These were created by adding fluctuating noise conductances to the cells (Palmer and Miller, 2002, 2003). The noise conductances were made up of a part constant in time, g_x^{bkgnd} (AMPA and GABA A only), and a part fluctuating in time, η_x, governed by the Ornstein-Uhlenbeck process (Uhlenbeck and Ornstein, 1930):

$$d\eta_x(t) = -\kappa\eta_x(t)dt + \sqrt{D_x}dW(t),$$

where D is the diffusion constant, $dW(t)$ is Gaussian white noise, and the term $-\kappa\eta_x(t)$ represents decay with a characteristic time scale $1/\kappa = 34$ ms (Palmer and Miller, 2002, 2003). x = AMPA, GABA A or GABA B indicate the type of conductance. This gives an update rule (Destexhe et al., 2001):

$$\eta_x(t+\delta t) = e^{-\kappa\delta t}\eta_x(t) + \sqrt{\frac{D_x}{2\kappa}(1-e^{2\delta t\kappa})}N(0,1),$$

where $N(0,1)$ is a Gaussian white noise process with mean zero and unit standard deviation. We define two diffusion terms, as well as two background conductances, one excitatory and one inhibitory. Noise parameters are chosen to achieve voltage fluctuations as measured intracellularly by David Ferster's group, with a standard deviation around 4 mV for excitatory cells. The noise input is the same for all cell types resulting in voltage fluctuations with standard deviations of 4-5 mV for inhibitory simple cells and 7-8 mV for inhibitory complex cells. The fluctuations in the model are larger than for excitatory cells since the inhibitory cells have different biophysical properties and the complex inhibitory cells do not receive intracortical input. To our knowledge there is no data reporting noise fluctuations for any of the inhibitory cell types, so we kept the noise conductances the same for all three cell types for simplicity. The values were as follows: $D_{AMPA} = 0.7\cdot10^{-15}S^2/s$, $D_{GABAA} = D_{GABAB} = 4.2\cdot10^{-15}S^2/s$, $g_{AMPA}^{bkgnd} = g_{GABAA}^{bkgnd} = 0.2\cdot10^{-9}S$. The inclusion of both types of inhibitory conductances with reversal potentials $V_{Cl} = -70mV$ (GABA A) and $V_{Cl} = -90mV$ (GABA B) is in accordance with (Palmer and Miller, 2002, 2003). Further, all of the three total conductances were rectified at zero to avoid negative conductances.

The correlations in the noise input were created by simply making a fraction of the noise conductances common to all cells in the network and the rest individual for each cell. This rather crude choice of correlations was inspired by findings from Paré et al. (1998), who reported that intracellular recordings of cat pyramidal neurons *in vivo* were correlated with the overall fluctuations of the local field potential measured with EEG, indicating that *all* cells in a small area of cortex get somehow correlated inputs. Other studies reveal that cells with similar, overlapping receptive fields receive correlated input (Lampl et al., 1999). In our noise correlations we have not included this type of correlations, but the structure of the connections in the model result in such a correlation pattern. However, we tested other types of correlations: correlation of noise to excitatory cells and

correlation of input to inhibitory cells, but uncorrelated between the populations; only correlations and/or noise to one type of cells. All these gave qualitatively the same type of results as with the above correlations and will not be discussed further.

The noise conductances with 0% correlation along with the spontaneous activity of the LGN inputs resulted in background firing rates of approximately 0.7 Hz for excitatory cells, 3 Hz for simple- and 15-20 Hz for complex inhibitory cells. The spontaneous rate for complex cells is comparable to rates of around 20 Hz reported for similarly nonspecific inhibitory interneurons in other areas of cortex (Brumberg et al., 1996; Simons and Carvell, 1989; Swadlow, 1989, 1990, 1991, 1994).

NMDA-mediated conductances (Krukowski and Miller, 2001; Lauritzen et al., 2001), in addition to the AMPA-mediated conductances, were added to all of the excitatory synapses except for the thalamocortical synapses onto inhibitory cells, which were purely AMPA-mediated following evidence that there is little NMDA in excitatory synapses onto inhibitory cells (Angulo et al., 1999; Ling and Benardo, 1995). The relative strength of NMDA and AMPA conductances were set in terms of the integrated current (*i.e.*, the total charge transfer) through excitatory conductances when the postsynaptic cell is clamped at the spike-threshold voltage. 35% of the integrated current in all the synapses was mediated by NMDA. This is lower than the the value used previously ((75%) Lauritzen and Miller, 2003a) that was obtained by matching AMPA and NMDA amplitudes to those observed at thalamocortical synapses at the oldest ages studied in thalamocortical slices (Crair and Malenka, 1995), using a physiological level (1.3mM) of extracellular Mg^{2+}. The previously used high levels of NMDA caused a low temporal-frequency cutoff, and decreasing the NMDA to 35% increased the cutoff to more physiological levels. Even though slice experiments (Crair and Malenka, 1995) indicate a 75% fraction of NMDA, some physiological studies indicate that this number might be lower (Fox et al., 1989). Our choice of 35% is purely empirical chosen to be about half of the slice value to get higher temporal-frequency cutoffs while still having a significant amount of the input carried by NMDA-mediated conductances.

The probability of forming a synapse between any pair of simple cells depended on the correlation between their sets of LGN inputs, as in Troyer et al. (1998): the probability of a connection from an excitatory cell monotonically increased with the degree of correlation, while the probability of a connection from an inhibitory cell monotonically increased with the degree of anticorrelation. As shown in Troyer et al. (1998, Fig. 8B), the result is that the distribution of orientation differences between connected cell pairs peaks at zero difference and falls off to zero at differences of about $\pm 30^o$; while the distribution of phase differences peaks at 0 difference for excitatory synapses and at 180^o for inhibitory synapses, and falls off to zero over about $\pm 60^o$ from the peak. The result of this connectivity pattern is that the excitatory currents and inhibitory currents received by a cell in response to preferred-orientation drifting gratings modulate roughly at opposite phases.

Connections from complex cells only depend on the distance between the receptive fields of the

two cells, with probability 10% of forming a synapse onto cells less than 150 μm away and zero otherwise. For simplicity, complex cells only receive thalamocortical input. These connectivity rules yield the basic cortical circuit structure within a single iso-orientation column. An important feature of the model is that the inhibition is dominant over feedforward excitation, rather than precisely balancing it.

The thalamocortical and E $\rightarrow$ E synapses displayed depression, with $f = 0.563$, $\tau = 99$ msec (LGN), and $f = 0.875$, $\tau = 57$ msec (E $\rightarrow$ E). Here, f is the synaptic efficacy immediately after a presynaptic spike, and τ the time constant of recovery, as in (Abbott et al., 1997). The experimental basis for these depression parameters is discussed in (Kayser et al., 2001b, table 1). Connections onto and from inhibitory cells may also express use dependent changes (Gupta et al., 2000), but these have been omitted for simplicity.

As in Troyer et al. (1998), we define the total synaptic strength of a given type received by a cell by (i) assuming the cell is voltage clamped at threshold; (ii) for each synapse, integrating over time the synaptic current induced by one presynaptic spike; and (iii) summing over all synapses of the given type. Thus, total synaptic strength is expressed in units of $nA\ msec$. The total synaptic weight received by a cell from each type of connection were: 42 nA msec (LGN); 16 nA msec ($I_c \rightarrow$ E); 40 nA msec ($I_c \rightarrow I_s$); 12 nA msec (E $\rightarrow$ E, I_s); 10 nA msec ($I_s \rightarrow$ E, I_s). These strengths were set empirically, in a stepwise manner as in (Lauritzen and Miller, 2003a) after the noise parameters had been set to give the right voltage fluctuations at 0% contrast. Because of the increased conductance from the physiological noise levels the connections strengths had to be stronger in this study.

Each simulation was started with a 'blank screen' for one second with LGN cells firing at their background rates to equilibrate the network, followed by an additional 0.25 seconds with a grating stimulus to suppress transients before actually recording data for 1 second of simulated time as the grating stimulus continued. Orientation tuning curve responses were obtained from 1 repetition of gratings having each of 18 orientations, from 8° to 178° by 10°, at each of the indicated contrasts. Cells were binned by preferred orientation in bins of $\pm 5°$ around each grating orientation; each bin's tuning curve was determined, and the tuning curves of the different bins were averaged together by equating the central orientation of each bin (representing orientation 0°). For other figures, simulations were run at a grating oriented at 128° to avoid artifacts of the grid with the stimulus. PSTH's were calculated from 5 such simulations (with different random seeds for the Poisson spike trains of the LGN inputs) and from responses of all cells with preferred orientations within $\pm 5°$ of 128°. For voltage histograms a total of 50 of the above simulations were made and membrane potentials were truncated at threshold and binned for every 0.25ms.

3.2 Results

3.2.1 Model Overview

The model contains three cortical cell types found in cat V1 layer 4: orientation-tuned excitatory and inhibitory simple cells with separate ON and OFF subfields, and inhibitory complex cells untuned for orientation with ON-OFF receptive fields (RFs) (Hirsch et al., 2003). All cells receive thalamocortical input selected probabilistically, the simple cell inputs chosen from ON-center inputs overlying ON-subregions and OFF-center inputs overlying OFF subregions (Alonso et al., 2001; Hubel and Wiesel, 1962; Reid and Alonso, 1995; Tanaka, 1983), and the complex cell inputs chosen from all LGN cells whose RFs overlap. Cortical connectivity is also determined probabilistically. The simple cells form synapses primarily to other cells with similar preferred orientation, according to the correlation of their RFs. Excitatory synapses are formed to cells with correlated RFs (similar preferred orientation and similar absolute spatial phase, meaning that ON-subregions of the two cells tend to overlap in visual space and similarly OFF-subregions tend to overlap), and inhibitory synapses are formed to cells with anti-correlated RFs (similar preferred orientation and opposite absolute spatial phase, meaning that ON-subregions of one cell tend to overlap OFF subregions of the other cell). The complex cells, lacking in orientation tuning (Hirsch et al., 2003), project randomly with equal (10%) probability to all simple cells within 150 μm, and, for simplicity, do not receive any cortical input. The model contains simple cells preferring all orientations and all spatial phases and a range of retinotopic positions. We have previously showed that this model architecture can explain contrast invariant spike tuning as well as other response properties observed in V1 (Lauritzen and Miller, 2003a).

Membrane potential fluctuations observed *in vivo* where created by adding excitatory and inhibitory fluctuating conductances to the cells (Palmer and Miller, 2002, 2003). The noise conductances were made up of a part constant in time, and a part fluctuating in time, resulting in voltage fluctuations as measured (Anderson et al., 2000b) with standard deviations around 4 mV. The fluctuating noise conductances where governed by the Ornstein-Uhlenbeck process (Uhlenbeck and Ornstein, 1930) as Gaussian white noise fluctuations with a decay towards zero on a time scale of 34ms.

Based on findings from Paré et al. (1998), who reported that intracellular recordings of cat pyramidal neurons *in vivo* were correlated with the overall fluctuations of the local field potential measured with EEG, indicating that *all* cells in a small area of cortex get somehow correlated inputs, correlations in the noise input were created by simply making a fraction of the conductances common to all cells in the network and the rest individual for each cell.

3.2.2 No noise correlations

In the absence of visual stimuli simple cells in layer 4 of V1 have a low sponataneous rate (usually less than 1 spike/s), but cells measured *in vivo* show membrane potential fluctuations with a standard deviation around 4 mV (Anderson et al., 2000b). In general *in vivo* fluctuations are much larger than those observed *in vitro* in all cortical areas (e.g. Destexhe et al., 2001; Paré et al., 1998), presumeably from a barriage of cortical input to the cells. Our noise conductances replicates this *in vivo* behaviour (fig. 3.1).

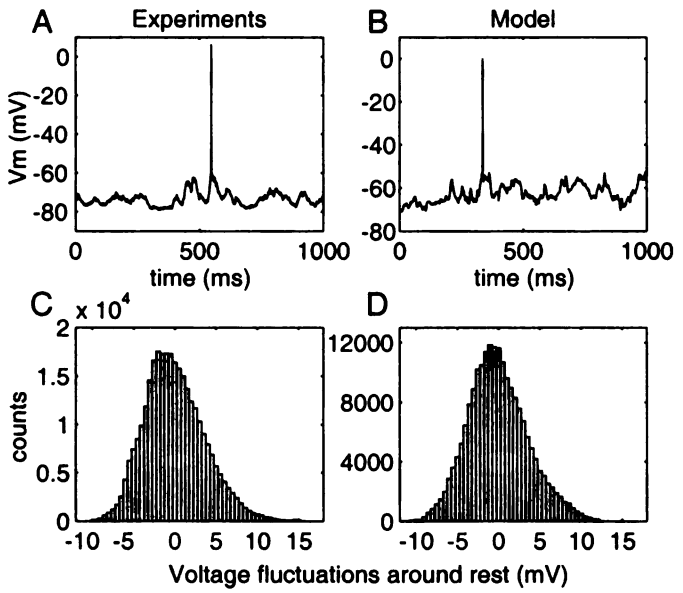

Figure 3.1:
Voltage traces and histogram of voltage fluctuations around the mean for an experimental cell from (Anderson et al., 2000b) (A, C) and a cell in the model (B, D) at 0% contrast (no visual stimulus). Voltage traces are similar and histograms have similar root mean square (RMS) around 4 mV.

In response to a preferred-orientation grating, a cell receives LGN input that is strongly temporally modulated since the grating causes all the LGN inputs to the simple cell to modulate their firing rates roughly in phase with one another so that the temporal modulations of the individual LGN inputs add constructively to produce a strongly modulated total LGN input. In response to a grating oriented orthogonal to the cell's preferred (which we will refer to as the cell's null orientation), the cell instead receives a roughly constant, temporally unmodulated rate of LGN input because the null-oriented grating drives different LGN inputs to the cell at different times, so the temporal modulations of the individual LGN inputs add destructively. This mean rate of total LGN input is the same for gratings of any orientation, because the mean rates of the individual LGN cells are independent of orientation. Thus, gratings of different orientations are distinguished, not by the mean rate of LGN input they elicit, but by the temporal modulation of that input, with the strongest temporal modulation elicited by a grating of the cell's preferred orientation and little or no modulation at the null orientation.

The mean rate of total LGN input to a simple cell grows with stimulus contrast, because the mean rates of the individual LGN cells grow with contrast. This is a nonlinear effect: because the

mean luminance does not change with changes in contrast, the mean response also would not change if LGN responses were linear in the image. It is induced by the fact that LGN firing rates cannot decrease below zero, whereas they can increase to 100 Hz or higher, many times their background level (10-15 Hz, *e.g.* Kaplan et al., 1987).

Because the mean input grows with contrast for all orientations, even a null-oriented stimulus can elicit a high rate of LGN input at high contrast, higher even than the peak of the temporally modulated input elicited by a preferred-orientation grating at sufficiently low contrast. Yet simple cells show contrast-invariant tuning of their firing (Anderson et al., 2000b; Sclar and Freeman, 1982; Skottun et al., 1987) as well as their membrane potential (Anderson et al., 2000b), so that they respond to their preferred orientation even at very low contrast and often do not respond to the null orientation even at high contrast.

In our model this is excess DC input is neutralized by the feedforward inhibition from the complex cells (Lauritzen and Miller, 2003a), so the mean of the membrane potential display contrast-invariant orientation tuning (fig. 3.2 B). Here the total mean (DC) membrane potential at

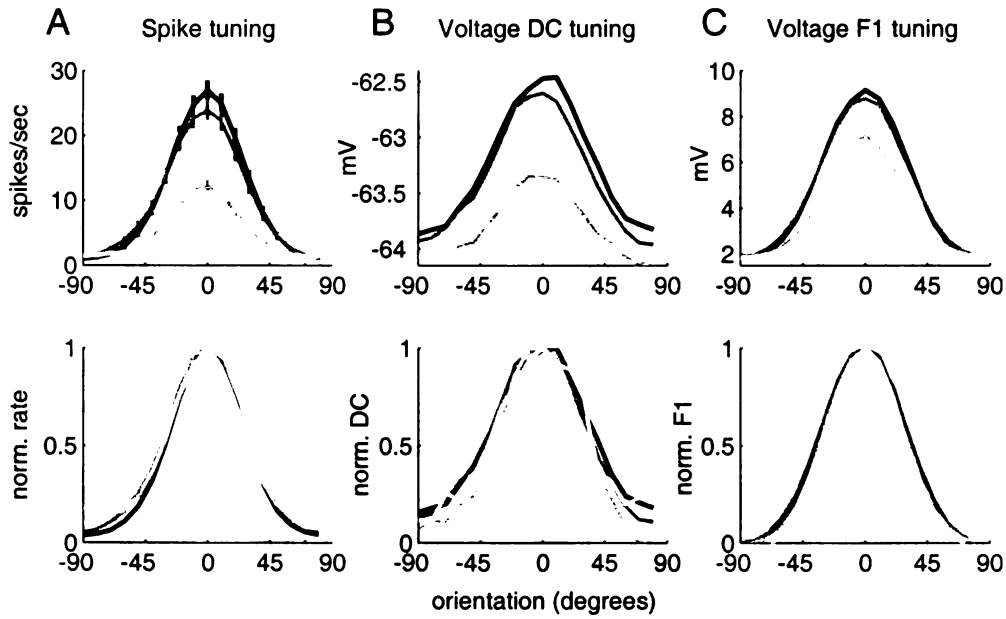

Figure 3.2:

Orientation tuning of the cell responses in the model. Full and normalized responses of the spike tuning (A), mean, DC, of the membrane potential (B), and modulation, F1, of the membrane potential (C). Light gray to black are 2.5%, 10%, 20% and 60% contrasts. All three measurements display contrast-invariant orientation tuning as found by Anderson et al. (2000b). Error bars in (A) and all of the following figures are ± 1 SEM, error bars have been omitted from the rest of the subplots for clarity.

the null orientation is practically constant, while the mean membrane potential at the preferred orientation increase because of cortical amplification. The fundament of the modulation (F1) of the membrane potential (fig. 3.2 C) is made by the LGN input. Given contrast-invarience of the membrane potential, contrast-invariant spike tuning follows naturally (fig. 3.2 A), as also suggested previously (Anderson et al., 2000b; Palmer and Miller, 2002, 2003).

The circular variance of the spike tuning, defined as $1 - F1/DC$, with $DC = \sum_o r(o)$ and $F1 = \sqrt{(\sum_o r(o)\sin(o))^2 + (\sum_o r(o)\cos(o))^2}$, where $r(o)$ is the response at a given orientation, decreases slightly with contrast (fig. 3.3). A decrease in circular variance has been reported in

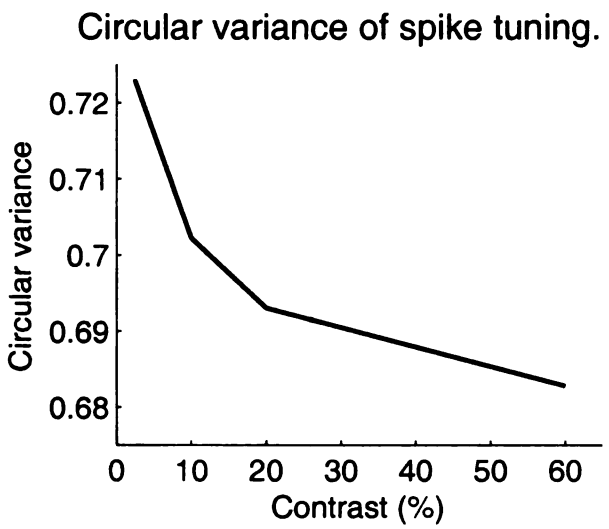

Figure 3.3:
The circular variance of the spike tuning with contrast. We see a small but systematic decrease of circular variance with contrast.

macaque monkey (Shapley et al., 2002) and ferret (M. Usrey, personal communication).

The F1 tuning curves of the excitatory and inhibitory currents onto cortical cells have nearly identical shapes (fig. 3.4 A) as observed in experiments (Anderson et al., 2000a; Ferster, 1986). Similarly, the total input conductance in the model grows by 22% at the nul orientation and 108% at the preferred orientation when the stmulus contrast is increased from 0 to 60% contrast (fig. 3.4 B), in accordance with experimental results showing a 40-300% increase at the preferred orientation and ~20% at the null for simple cells (Anderson et al., 2000a).

3.2.3 Increased noise correlation

In the absence of correlation in the noise conductances the network can explain the basic properties of cortical cell responses discussed above.

If we now increase the noise correlations in the absence of visual stimuli we see two major effects of the behavior of the cells. One, the fluctuations of the membrane potential decrease by ~33% (fig. 3.5 A-D), and, two, the mean of the membrane potential decreases (fig. 3.5 E). The result of these changes is a decrease of the spontaneous rate of the cells in the network (fig. 3.5 F).

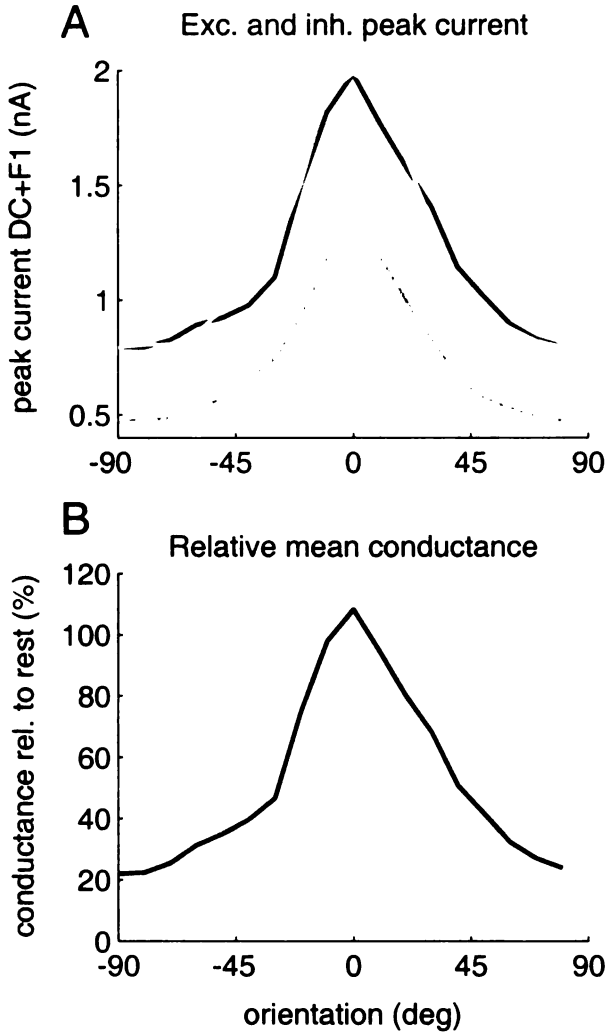

Figure 3.4:

Orientation tuning of the cell input in the model. (A) The orientation tuning of the peak (DC + F1) inhibitory (black) and excitatory (dark gray) current at 60% contrast. Light gray line shows excitatory current scaled and translated to match maxima and minima of the inhibitory current. The excitatory and inhibitory currents have similar orientation tuning. (B) The orientation tuning of the total mean conductance of the cells at 60% contrast relative to the mean conductance at 0% contrast.

If we look at the fluctuations of the synaptic input to the cell with increased noise correlations, one would expect that increased correlations in the cells input would increase the fluctuations of their input as more cells connecting to a given cell would have correlated firing and thus give rise to correlated intracortical inputs. This is the case, both with and without stimuli (fig. 3.6 A-D), but their effects on the membrane potential are different. Without visual stimuli the fluctuations in the membrane potential decrease (fig. 3.5 D). This is easy to understand: The statistics of the outside noise conductance received by a given cell does not change, but the activity of all the cells are more correlated. So when the membrane potential of a cell is close to threshold, so is the membrane potential of most of the other cells, especially the inhibitory cells that would prevent the cell from firing, and since inhibition is dominant this also decreases the mean of the membrane potential. So the excitatory effect of the correlations are basically shielded by the dominant inhibition.

On the other hand, in the presence of visual stimulus, the push-pull connectivity separates the

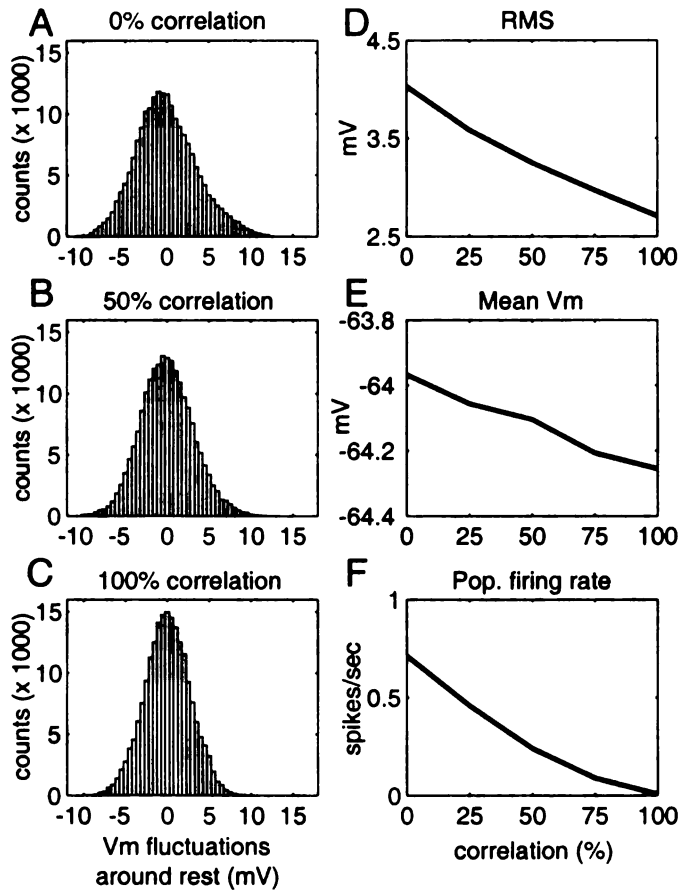

Figure 3.5:

Increased noise correlation reduces the fluctuations and mean of the membrane potential in absence of visual stimuli. Histograms of the voltage fluctuations around the mean of the model cell from fig. 3.1 with noise correlations of 0% (A), 50% (B) and 100% (C) show a decrease in the fluctuations of the membrane potential with increased correlation of the noise conductances. The RMS decreases from around 4 mV with no correlation to around 2.7 mV with 100% correlation (D), and the mean of the membrane potential decreases from -63.97 mV to -64.26 mV in the same interval (E). Similarly the firing rate of all the excitatory cells in the network decreases from ~0.7 spikes/s to 0 spikes/s (F).

arrival of the excitation and (som of) the inhibition, since inhibitory simple cell input arrives at the opposite temporal phase as the one the cell would be firing. So here it is possible to unshield the excitatory effect of the correlations. At points in the stimulus cycle where the membrane potential is close to threshold this causes the cell to fire more frequently, while at the opposite temporal phase, when the cell mainly receive "pull" inhibition, increased noise correlations causes further, noisy, reductions in the membrane potential (fig. 3.6 E-F). Because of this, increased noise correlations yields higher responses to visual stimuli with drifting gratings (fig. 3.7 A), without changing the shape of the mean membrane potential and the spike tuning (fig. 3.7 B-D).

In all, the basic cell responses with increased noise correlation can be explained by the correlation-based connectivity in the cortical model.

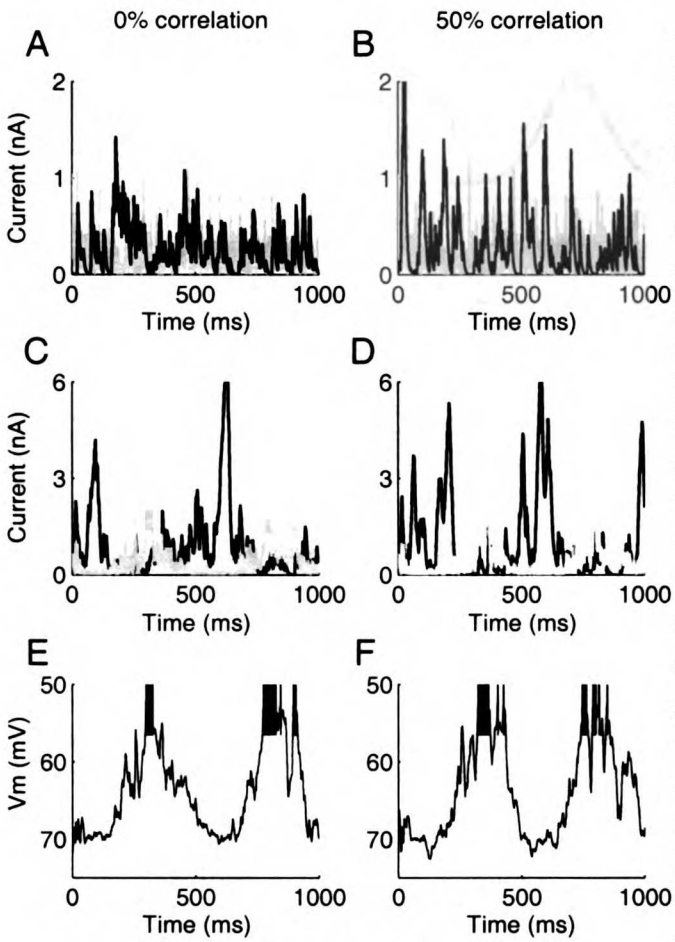

Figure 3.6:

Synaptic currents in a single cell. A-B) Excitatory (gray) and inhibitory (black) synaptic current in a cell in the absence of stimulus for 0 and 50% correlation in the noise. The fluctuatons of the excitatory current is almost entirely thalamocortical, and does not change significantly with increased correlation, while fluctuations of the inhibitory synaptic current increase with correlation. The excitatory current decrease with correlation because of decreased cortical activity (not shown). C-D) Excitatory (gray) and inhibitory (black) synaptic current in a cell when stimulated with a 60% contrast grating at the preferred orientation for 0 and 50% noise correlation. The fluctuations of both currents increase with correlation. E-F) The resulting membrane potential for the above stimulus. The increase in current fluctuations increase the fluctuations in the membrane potential.

3.2.4 Temporal frequency tuning

We have previously suggested a method to explain the temporal frequency high-cutoffs of cortical cells (Krukowski and Miller, 2001; Lauritzen and Miller, 2003a). The explanation relied on two elements: NMDA-receptor-mediated conductances (which we will abbreviate simply as "NMDA") in synapses from LGN to excitatory cells act as a low-pass filter, reducing the temporal modulation of the excitatory input at higher frequencies and thus largely reducing this input to its mean; and some dominant feedforward inhibition responding at high temporal frequencies prevents responses to the mean excitation. This explanation is still valid in the physiological noise regime, but, surprisingly, increasing the correlation in the noise increase the response to stimuli at higher temporal

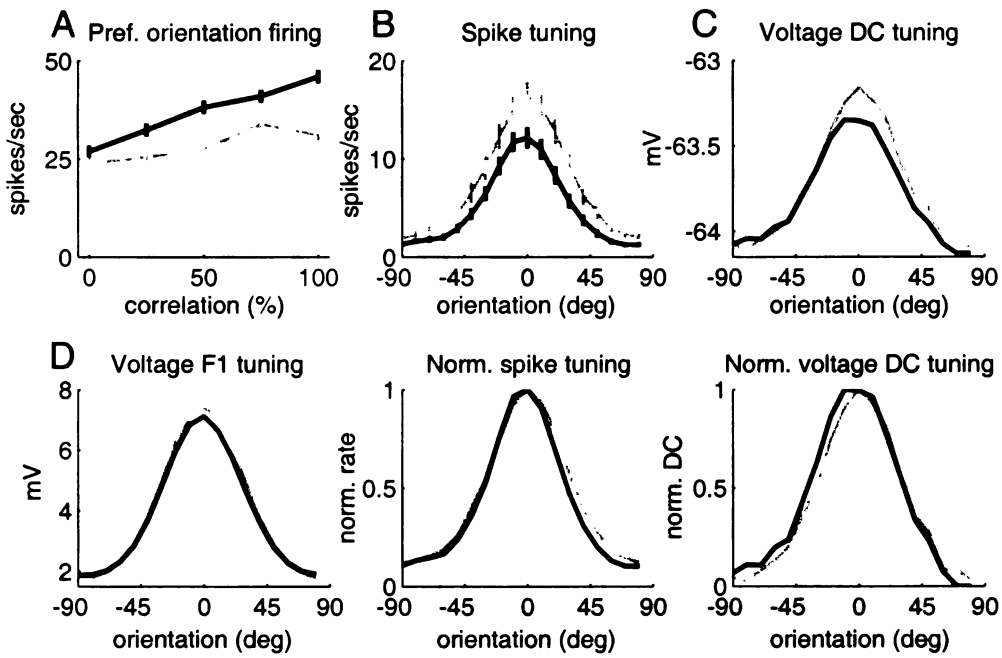

Figure 3.7:

Increased noise correlation increases the response of the cells in presence of visual stimuli. (A) the response at the preferred orientation with increased correlation. Light gray to black are 10%, 20% and 60% contrast respectively. Full and normalized responses of the spike tuning (B), mean, DC, of the membrane potential (C), and full responses of the modulation, F1, of the membrane potential (D) for 0% (black) and 50% correlation (gray) with a stimulus of 10% contrast. The increase in response is multiplicative.

frequencies (fig. 3.8). Defining the high-frequency cutoff as the temporal frequency above the peak at which the mean spike response is reduced to 50% of the peak response, the cutoff of simple cells is close to 3.5 Hz for no noise correlation and increases by ~60% to 5.6 Hz for 100% noise correlations. Both values are within the range of cells reported experimentally (*e.g.*, Freeman et al., 2002; Movshon et al., 1978). This indicates that correlations change the gain of the cells by an uneven amount to different stimuli, and can thus affect the tuning properties of the cells.

3.3 Discussion

We have shown that feedforward inhibition from complex inhibitory cells, untuned for orientation, observed in layer 4 (Hirsch et al., 2003), can combine with feedforward excitation from LGN to explain the sharp contrast-invariant orientation tuning of the membrane potential of layer 4 simple cells. Given the contrast-invariant orientation tuning of membrane potential, physiological noise

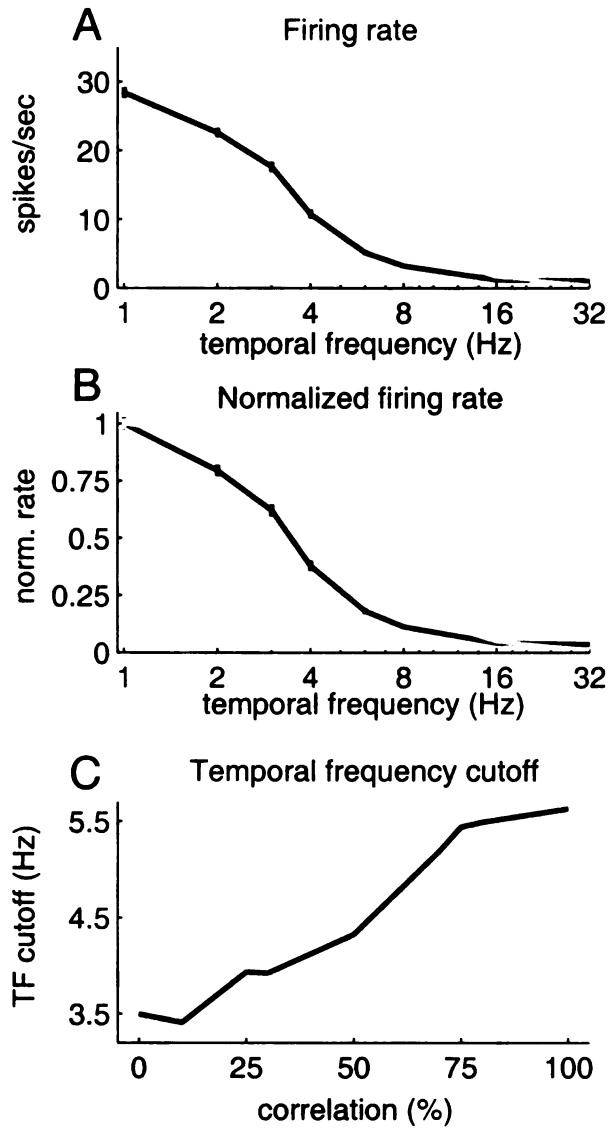

Figure 3.8:

Increased noise correlation increases the temporal-frequency tuning cutoff of the cells in the network. Full (A) and normalized (B) response with increased tempral frequency of a stimulating grating of 60% contrast with 0% (black) and 50% (gray) correlation of the noise input. Temporal-frequency cutoff, defined as the temporal frequency above the peak at which the mean spike response is reduced to 50% of the peak response, of the cells with increased noise correlation (C).

fluctuations can explain contrast-invariance of the spiking orientation tuning. Adding noise correlations in the model gives different results in the presence and absence of visual stimuli: In the absence of stimuli, correlations result in a decrease in the mean and fluctuations of the membrane potential, reducing the firing rate; while in the presence they act to increase both the membrane potential and the firing rates of the cells. The basics of these findings can be explained by the correlation-based circuitry of the network. The temporal frequency tuning of the cells in our network shifts with increased correlations, opening up for the possibility that correlations can alter the receptive field properties of neurons in favor of specific features.

3.3.1 Model Predictions

Predictions of the model include:

1. Simple cells receiving significant thalamic excitation should receive a comparable level of orientation untuned inhibition to provide for contrast invatiance of their voltage tuning, yielding detectable conductance changes in response to non-preferred stimuli. Some cells reported by (Anderson et al., 2000a) show such changes.

2. The spontaneous firing of cells should decrease with increased levels of balanced noise conductances. This have been found in slice experiments (Chance et al., 2002).

3. The spontaneous firing of cells should decrease with increased levels of correlation between their input. In particular, in slice experiments similar to (Chance et al., 2002), correlating the induced excitatory and inhibitory conductances, but fixing the total induced conductance (injected current), would decrease the gain of the cell response to a driving current.

4. The gain of the response to visual stimuli should increase with the correlation of the input to the cells. These cortical correlations could be an effect of top-down influences on V1, such as attention, and will be discussed further in "Correlations in physiology".

3.3.2 Correlations in physiology

The correlations in our cortical model are somewhat artificial, changing the correlation of the induced noise conductances. In cortex we propose these correlation changes induced by top-down influence from higher cortical areas. A classical example is attention; in awake experiments neurons activated by attention to a visual stimulus show increased synchronization and oscillations (*e.g.* Fries et al., 2001). Such oscillations have the same effect on cortical cells as the noise conductances in the model, increasing the gain of their response multiplicatively (McAdams and Maunsell, 1999). However, other results (Martinez-Trujillo and Treue, 2002; Reynolds et al., 2000) show that attention can cause a shift, rather than a gain change, in the contrast response function of these neurons. This is in agreement with our findings that the temporal-frequency tuning changes with increased correlation.

3.3.3 Conclusion

Given basic assumptions of the connectivity on layer 4 of V1 and physiological background conductances, we deduce that intracortical inhibition is necessary for contrast-invariance of voltage orientation tuning that is the basis for contrast-invariance of spike tuning given cortical input-output power laws provided by the physiological noise fluctuations (Anderson et al., 2000b; Hansel and van Vreeswijk, 2002; Miller and Troyer, 2002). Increased correlations in the noise conductance

give qualitatively the same type of response changes as seen in physiology and the main reason for these is an increase in the synaptic conductance fluctuations. So we conclude that an increase in correlation or synchrony in cortex alter responses by changing the gain of the cortical cells (Chance et al., 2002; Murphy and Miller, 2003).

Bibliography

Abbott, L. F., Varela, J. A., Sen, K., and Nelson, S. B. Synaptic depression and cortical gain control. *Science* 275:220–224, 1997.

Ahmed, B., Anderson, J. C., Martin, K. A., and Nelson, J. C. Map of the synapses onto layer 4 basket cells of the primary visual cortex of the cat. *J. Comp. Neurology* 380:230–242, 1997.

Albrecht, D. G. Visual cortex neurons in monkey and cat: Effect of contrast on the spatial and temporal phase transfer functions. *Vis. Neurosci.* 12:1191–1210, 1995.

Alonso, J. M., Usrey, W. M, and Reid, R. C. Precisely correlated firing in cells of the lateral geniculate nucleus. *Nature* 383:815–819, 1996.

Alonso, J. M., Usrey, W. M., and Reid, R. C. Rules of connectivity between geniculate cells and simple cells in cat primary visual cortex. *J. Neurosci.* 21:4002–4015, 2001.

Anderson, J. S., Carandini, M., and Ferster, D. Orientation tuning of input conductance, excitation, and inhibition in cat primary visual cortex. *J. Neurophysiol.* 84:909–926, 2000a.

Anderson, J. S., Lampl, I., Gillespie, D., and Ferster, D. The contribution of noise to contrast invariance of orientation tuning in cat visual cortex. *Science* 290:1968–1972, 2000b.

Angulo, M. C., Rossier, J., and Audinat, E. Postsynaptic glutamate receptors and integrative properties of fast-spiking interneurons in the rat neocortex. *J. Neurophysiol.* 82:1295–1302, 1999.

Arieli, A., Sterkin, A., Grinvald, A., and Aertsen, A. Dynamics of ongoing activity: explanation of the large variability in evoked cortical responses. *Science* 273:1868–1871, 1996.

Azouz, R., Gray, C. M., Nowak, L. G., and McCormick, D. A. Physiological properties of inhibitory interneurons in cat striate cortex. *Cerebral Cortex* 7:534–545, 1997.

Bonds, A. B. Role of inhibition in the specification of orientation selectivity of cells in the cat striate cortex. *Vis. Neurosci.* 2:41–55, 1989.

Brumberg, J. C., Pinto, D. J., and Simons, D. J. Spatial gradients and inhibitory summation in the rat whisker barrel system. *J. Neurophysiol.* 76:130–140, 1996.

Bruno, R.M. and Simons, D.J. Feedforward mechanisms of excitatory and inhibitory cortical receptive fields. *J. Neurosci.* 22:10966–75, 2002.

Bullier, J. and Henry, G. H. Laminar distribution of first-order neurons and afferent terminals in cat striate cortex. *J. Neurophysiol.* 42:1271–1281, 1979.

Carandini, M. and Heeger, D. J. Summation and division by neurons in visual cortex. *Science* 264:1333–1336, 1994.

Carandini, M., Heeger, D. J., and Movshon, J. A. Linearity and normalization in simple cells of the macaque primary visual cortex. *J. Neurosci.* 17:8621–8644, 1997.

Carandini, M., Heeger, D. J., and Movshon, J. A. Linearity and gain control in V1 simple cells. In: *Cerebral Cortex, Vol. 13: Models of cortical circuits*, edited by P.S. Ulinski, E. G. Jones, and A. Peters. Kluwer Academic/Plenum New York, 1999, pp. 401–443.

Carmignoto, G. and Vicini, S. Activity-dependent decrease in NMDA receptor responses during development of the visual cortex. *Science* 258,:1007–1011, 1992.

Chance, F.S., Abbott, L.F., and Reyes, A.D. Gain modulation from background synaptic input. *Neuron* 35:773–782, 2002.

Cheng, H., Chino, Y. M, Smith, E. L. 3rd, Hamamoto, J., and Yoshida, K. Transfer characteristics of lateral geniculate nucleus X neurons in the cat: Effects of spatial frequency and contrast. *J. Neurophysiol.* 74:2548–2557, 1995.

Chung, S. and Ferster, D. Strength and orientation tuning of the thalamic input to simple cells revealed by electrically evoked cortical suppression. *Neuron* 20:1177–89, 1998.

Crair, M. C. and Malenka, R. C. A critical period for long-term potentiation at thalamocortical synapses. *Nature* 375:325–328, 1995.

Dean, A. F., Tolhurst, D. J., and S., Walker N. Non-linear temporal summation by simple cells in cat striate cortex demonstrated by failure of superposition. *Exp. Brain Res.* 45:456–458, 1982.

DeAngelis, G. C., Ghose, G. M., Ohzawa, I., and Freeman, R. D. Functional micro-organization of primary visual cortex: receptive field analysis of nearby neurons. *J. Neurosci.* 19:4046–4064, 1999.

DeAngelis, G. C., Ohzawa, I., and Freeman, R. D. Spatiotemporal organization of simple-cell receptive fields in the cat's striate cortex. I. General characteristics and postnatal development. *J. Neurophysiol.* 69:1091–1117, 1993.

DeAngelis, G. C., Robson, J. G., Ohzawa, I., and Freeman, R. D. Organization of suppression in receptive fields of neurons in cat visual cortex. *J. Neurophysiol.* 68:144–163, 1992.

Derrington, A. M. and Fuchs, A. F. Spatial and temporal properties of x and y cells in the cat lateral geniculate nucleus. *J. Physiol.* 293:347–364, 1979.

Destexhe, A., Rudolph, M., Fellous, J.M., and Sejnowski, T.J. Fluctuating synaptic conductances recreate in vivo-like activity in neocortical neurons. *Neurosci.* 107:13–24, 2001.

Durand, S., Freeman, T. C. B., Kiper, D. C., and Carandini, M. Probing the sources of cross-orientation suppression in cat visual cortex using fast stimuli. *Perception (suppl.)* (abstract), in press, 2001.

Felsen, G., Shen, Y., Yao, H., Spor, G., Li, C., and Dan, Y. Dynamic modification of cortical orientation tuning mediated by recurrent connections. *Neuron* 36:945–54, 2002.

Ferster, D. Orientation selectivity of synaptic potentials in neurons of cat primary visual cortex. *J. Neurosci.* 6:1284–1301, 1986.

Ferster, D. Spatially opponent excitation and inhibition in simple cells of the cat visual cortex. *J. Neurosci.* 8:1172–1180, 1988.

Ferster, D. X- and Y-mediated current sources in areas 17 and 18 of cat visual cortex. *Vis. Neurosci.* 4:135–145, 1990a.

Ferster, D. X- and Y-mediated synaptic potentials in neurons of areas 17 and 18 of cat visual cortex. *Vis. Neurosci.* 4:115–133, 1990b.

Ferster, D., Chung, S., and Wheat, H. Orientation selectivity of thalamic input to simple cells of cat visual cortex. *Nature* 380:249–252, 1996.

Ferster, D. and Jagadeesh, B. EPSP-IPSP interactions in cat visual cortex studied with in vivo whole-cell patch recording. *J. Neurosci.* 12(4):1262–1274, 1992.

Ferster, D. and Miller, K. D. Neural mechanisms of orientation selectivity in the visual cortex. *Ann. Rev. Neurosci.* 23:441–471, 2000.

Fox, K., Sato, H., and Daw, N. The location and function of NMDA receptors in cat and kitten visual cortex. *J. Neurosci.* 9:2443–2454, 1989.

Freeman, T.C., Durand, S., Kiper, D.C., and Carandini, M. Suppression without inhibition in visual cortex. *Neuron* 35:759–71, 2002.

Freeman, T. C. B., Durand, S., Kiper, D. C., and Carandini, M. Probing the source of cross-orientation suppression in primary visual cortex. *Inv. Opth. Vis. Sci.* 42:S726, 2001.

Fries, P., Reynolds, J. H., Rorie, A. E., and Desimone, R. Modulation of oscillatory neuronal synchronization by selective visual attention. *Science* 291:1560–1563, 2001.

Gabbott, P. L. A., Martin, K. A. C., and Whitteridge, D. Evidence for the connection between a clutch cell and a corticotectal neuron in area 17 of the cat's visual cortex. *Proc. R. Soc. London [Biol.]* 233:385–391, 1988.

Galarreta, M. and Hestrin, S. A network of fast-spiking cells in the neocortex connected by electrical synapses. *Nature* 402:72–5, 1999.

Galarreta, M. and Hestrin, S. Electrical synapses between GABA-releasing interneurons. *Nat. Rev. Neurosci.* 2:425–33, 2001.

Galarreta, M. and Hestrin, S. Electrical and chemical synapses among parvalbumin fast-spiking GABAergic interneurons in adult mouse neocortex. *Proc. Nat. Acad. Sci. USA* 99:12438–43, 2002.

Gibson, J. R., Beierlein, M., and Connors, B. W. Two networks of electrically coupled inhibitory neurons in neocortex. *Nature* 462:75–79, 1999.

Gil, Z. and Amitai, Y. Adult thalamocortical transmission involves both NMDA and non-NMDA receptors. *J. Neurophysiol.* 76:2547–2554, 1996.

Gilbert, C. D. Laminar differences in receptive field properties of cells in cat primary visual cortex. *J. Physiol.* 268:391–421, 1977.

Gilbert, C. D. and Wiesel, T. N. Morphology and intracortical projections of functionally characterised neurones in the cat visual cortex. *Nature* 280:120–125, 1979.

Gillespie, D. C., Lampl, I., Anderson, J. S., and Ferster, D. Dynamics of the orientation-tuned membrane potential response in cat primary visual cortex. *Nature Neurosci.* 4:1014–1019, 2001.

Gupta, A., Wang, Y., and Markram, H. Organizing principles for a diversity of GABAergic interneurons and synapses in neocortex. *Science* 287:273–278, 2000.

Hamamoto, J., Cheng, H., Yoshida, K., Smith, E. L. 3rd, and Chino, Y. M. Transfer characteristics of lateral geniculate nucleus X neurons in the cat: Effects of temporal frequency. *Exp. Brain Res.* 98:191–199, 1994.

Hansel, D. and van Vreeswijk, C. How noise contributes to contrast invariance of orientation tuning in cat visual cortex. *J. Neurosci.* 22:5118–5128, 2002.

Heeger, D. J. Normalization of cell responses in cat striate cortex. *Vis. Neurosci.* 9:181–198, 1992.

Heeger, D. J., Simoncelli, E. P., and Movshon, J.A. Computational models of cortical visual processing. *Proc. Natl. Acad. Sci. USA* 93:623–627, 1996.

Hirsch, J. A., Alonso, J.-M., Pillai, C., and Pierre, C. Simple and complex inhibitory cells in layer 4 of cat visual cortex. *Soc. Neurosci. Abstr.* 26:1083, 2000.

Hirsch, J. A., Alonso, J.-M., Reid, R. C., and Martinez, L.M. Synaptic integration in striate cortical simple cells. *J. Neurosci.* 18:9517–9528, 1998.

Hirsch, J. A., Martinez, L. M., Pillai, C., Alonso, J.-M., Wang, Q, and Sommer, F.T. Functionally distinct inhibitory neurons at the first stage of visual cortical processing. *Nature Neuroscience* p. in press, 2003.

Holub, R. A. and Morton-Gibson, M. Response of visual cortical neurons of the cat to moving sinusoidal gratings: Response-contrast functions and spatiotemporal interactions. *J. Neurophysiol.* 46:1244–1259, 1981.

Hubel, D. H. and Wiesel, T. N. Receptive fields, binocular interaction and functional architecture in the cat's visual cortex. *J. Physiol.* 160:106–154, 1962.

Ikeda, H. and Wright, M. J. Spatial and temporal properties of sustained and transient neurones in area 17 of the cat's visual cortex. *Exp. Brain Res.* 22:363–383, 1975.

Jahr, C. E. and Stevens, C. F. Voltage dependence of NMDA-activated macroscopic conductances predicted by single-channel kinetics. *J. Neurosci.* 10:3178–3182, 1990.

Jones, J. P. and Palmer, L. A. The two-dimensional spatial structure of simple receptive fields in cat striate cortex. *J. Neurophysiol.* 58:1187–1211, 1987.

Kang, K., Shelley, M., and Sompolinsky, H. Mexican hats and pinwheels in visual cortex. *PNAS* 100:2848–53, 2003.

Kaplan, E., Purpura, K., and Shapley, R. M. Contrast affects the transmission of visual information through the mammalian lateral geniculate nucleus. *J. Physiol.* 391:267–288, 1987.

Kayser, A. S. and Miller, K. D. Opponent inhibition: A developmental model of layer 4 of the neocortical circuit. *Neuron* 33:131–142, 2002.

Kayser, A. S., Priebe, N. J., and Miller, K. D. Contrast-dependent nonlinearities arise locally in a model of contrast-invariant orientation tuning. *J. Neurophysiol.* 2130-2149, 2001a.

Kayser, A. S., Priebe, N. J., and Miller, K. D. Contrast-dependent nonlinearities arise locally in a model of contrast-invariant orientation tuning. *J. Neurophysiol.* 85:2130–2149, 2001b.

Kisvarday, Z. F., Martin, K. A. C., Whitteridge, D., and Somogyi, P. Synaptic connections of intracellularly filled clutch cells: a type of small basket cell in the visual cortex of the cat. *J. Comp. Neurol.* 241:111–137, 1985.

Krukowski, A. E., 2000. *A model of cat primary visual cortex and its thalamic input.* PhD thesis University of California, San Francisco.

Krukowski, A. E. and Miller, K. D. Thalamocortical NMDA conductances and intracortical inhibition can explain cortical temporal tuning. *Nature Neuroscience* 4:424–430, 2001.

Lampl, I., Reichova, I., and Ferster, D. Synchronous membrane potential fluctuations in neurons of the cet visual cortex. *Neuron* 22:361–374, 1999.

Lauritzen, T. Z., Krukowski, A. E., and Miller, K. D. Local correlation-based circuitry can account for responses to multi-grating stimuli in a model of cat V1. *J. Neurophysiol.* 86:1803–1815, 2001.

Lauritzen, T. Z. and Miller, K. D. Contributions of simple- and complex-cell inhibition to simple cell responses in cat v1. *Abstract Viewer/Itinerary Planner. Washington, DC: Society for Neuroscience. Online* Program No. 456.1, 2002.

Lauritzen, T. Z. and Miller, K. D. Different roles for simple- and complex cell inhibition in V1. *J. Neurosci.* 23:10201–10213, 2003a.

Lauritzen, T. Z. and Miller, K. D. Effects of noise on the tuning of responses in V1. *Abstract Viewer/Itinerary Planner. Washington, DC: Society for Neuroscience. Online* Program No. 910.17, 2003b.

Lehmkuhle, S., Kratz, K. E., Mangel, S. C., and M., Sherman S. Spatial and temporal sensitivity of x- and y-cells in dorsal lateral geniculate nucleus of the cat. *J. Neurophys.* 43:520–541, 1980.

Lester, R. A., Clements, J. D., Westbrook, G. L., and Jahr, C. E. Channel kinetics determine the time course of NMDA receptor-mediated synaptic currents. *Nature* 346:565–567, 1990.

Ling, D. S. F. and Benardo, L. S. Recruitment of $GABA_A$ inhibition in rat neocortex is limited and not NMDA dependent. *J. Neurophysiol.* 74:2329–2335, 1995.

Maldonado, P. E., Gödecke, I., Gray, C. M., and Bonhoeffer, T. Orientation selectivity in pinwheel centers in cat striate cortex. *Science* 276:1551–1555, 1997.

Martin, K. A. C., Somogyi, P., and Whitteridge, D. Physiological and morphological properties of identified basket cells in the cat's visual cortex. *Exp. Brain Res.* 50:193–200, 1983.

Martinez, L.M., Alonso, J.M., Reid, R.C., and Hirsch, J.A. Laminar processing of stimulus orientation in cat visual cortex. *J. Physiol.* 540:321–33, 2002.

Martinez-Trujillo, J. and Treue, S. Attentional modulation strength in cortical area MT depends on stimulus contrast. *Neuron* 35:365–370, 2002.

McAdams, C. and Maunsell, J. Effects of attention on orientation-tuning functions of single neurons in macaque cortical area V4. *J. Neurosci.* 19:431–441, 1999.

McCormick, D. A., Connors, B. W., Lighthall, J. W., and Prince, D. A. Comparative electrophysiology of pyramidal and sparsely spiny stellate neurons of the neocortex. *J. Neurophysiol.* 54:782–805, 1985.

McLaughlin, D., Shapley, R., Shelley, M., and Wielaard, D. J. A neuronal network model of macaque primary visual cortex (V1): Orientation selectivity and dynamics in the input layer 4cα. *Proc. Natl. Acad. Sci. USA* 97:8087–8092, 2000.

Miller, K. D., Chapman, B., and Stryker, M. P. Visual responses in adult cat visual cortex depend on N-methyl-D-aspartate receptors. *Proc. Natl. Acad. Sci. USA* 86:5183–5187, 1989.

Miller, K. D., Simons, D. J., and Pinto, D. J. Processing in layer 4 of the neocortical circuit: New insights from visual and somatosensory cortex. *Curr. Opin. Neurobiol.* 11:488–497, 2001.

Miller, K. D. and Troyer, T. W. Neural noise can explain expansive, power-law nonlinearities in neural response functions. *J. Neurophysiol.* 87:653–659, 2002.

Monier, C., Chavane, F., Baudot, P, Graham, L.J., and Fregnac, Y. Orientation and direction selectivity of synaptic inputs in visual cortical neurons: a diversity of combinations produces spike tuning. *Neuron* 37:663-80, 2003.

Morrone, M. C., Burr, D. C., and Maffei, L. Functional implications of cross-orientation inhibition of cortical visual cells. I. Neurophysiological evidence. *Proc. R. Soc. Lond. B* 216:335–354, 1982.

Movshon, J. A., Thompson, I. D., and Tolhurst, D. J. Spatial and temporal contrast sensitivity of neurones in areas 17 and 18 of the cat visual cortex. *J. Physiol.* 283:101–120, 1978.

Mukherjee, P. and Kaplan, E. Dynamics of neurons in the cat lateral geniculate nucleus: In vivo electrophysiology and computational modeling. *J. Neurophys.* 74:1222–1243, 1995.

Murphy, B. K. and Miller, K. D. Multiplicative gain changes are induced by excitation or inhibition alone. *J. Neurosci* in press:–, 2003.

Palmer, S. and Miller, K. D. The effects of inhibitory gain and conductance fluctuations in a simple model for contrast invariant orientation tuning in cat V1. *Abstract viewer/itinerary planner, number 456.1 Washington DC: Society for Neuroscience.*, 2002.

Palmer, S. and Miller, K. D. The effects of inhibitory gain and conductance fluctuations in a simple model for contrast invariant orientation tuning in cat V1. *in preparation*, 2003.

Paré, D., Shink, E., Gaudreau, H., Destexhe, A., and Lang, E. J. Impact of spontaneous synaptic activity on the resting properties of cat neocortical pyramidal neurons in vivo. *J. Neurophysiol.* 79:1450–1460, 1998.

Peters, A. and Yilmaz, E. Neuronal organization in area-17 of cat visual cortex. *Cerebral Cortex* 3:49–68, 1993.

Reid, R. C. and Alonso, J. M. Specificity of monosynaptic connections from thalamus to visual cortex. *Nature* 378:281–284, 1995.

Reid, R. C., Victor, J. D., and Shapley, R. M. Broadband temporal stimuli decrease the integration time of neurons in cat striate cortex. *Vis. Neurosci.* 9:39–45, 1992.

Reynolds, J., T, Pasternak, and Desimone, R. Attention increases sensitivity of V4 neurons. *Neuron* 26:703–714, 2000.

Saul, A. B. and Humphrey, A. L. Spatial and temporal response properties of lagged and nonlagged cells in cat lateral geniculate nucleus. *J. Neurophysiol.* 64:206–224, 1990.

Saul, A. B. and Humphrey, A. L. Evidence of input from lagged cells in the lateral geniculate nucleus to simple cells in cortical area 17 of the cat. *J. Neurophysiol.* 68:1190–1208, 1992a.

Saul, A. B. and Humphrey, A. L. Temporal frequency tuning of direction selectivity in cat visual cortex. *Vis. Neurosci.* 8:365–372, 1992b.

Schummers, J., Marino, J., and Sur, M. Synaptic integration by V1 neurons depends on location within the orientation map. *Neuron* 36:969–978, 2002.

Sclar, G. Expression of "retinal" contrast gain control by neurons of the cat's lateral geniculate nucleus. *Exp. Brain Res.* 66:589–596, 1987.

Sclar, G. and Freeman, R. D. Orientation selectivity in the cat's striate cortex is invariant with stimulus contrast. *Exp. Brain Res.* 46:457–461, 1982.

Sengpiel, F., Baddeley, R. J., Freeman, T. C. B., Harrad, R., and C., Blakemore. Different mechanisms underlie three inhibitory phenomena in cat area 17. *Vision Res.* 38:2067–2080, 1998.

Shapley, R. M., Johnson, E. N., Hawken, M. J., and Kang, K. Orientation selectivity and stimulus contrast in macaque V1. *Program No. 720.6. 2002 Abstract Viewer/Itinerary Planner. Washington, DC: Society for Neuroscience.*, 2002.

Sherman, S. M. Functional organization of the W-, X-, and Y-cell pathways in the cat: A review and hypothesis. *Progr. Psychobiol. Physiol. Psychol.* 11:233–314, 1985.

Simons, D. J. and Carvell, G. E. Thalamocortical response transformation in the rat vibrissa/barrel system. *J. Neurophysiol.* 61:311–330, 1989.

Skottun, B. C., Bradley, A., Sclar, G., Ohzawa, I., and Freeman, R. D. The effects of contrast on visual orientation and spatial frequency discrimination: A comparison of single cells and behavior. *J. Neurophysiol.* 57:773–786, 1987.

Skottun, B. C., De Valois, R. L., Grosof, D. H., Movshon, J. A., Albrecht, D. G., and Bonds, A. B. Classifying simple and complex cells on the basis of response modulation. *Vision Res.* 38:1079–86, 1991.

So, Y. T. and Shapley, R. Spatial tuning of cells in and around lateral geniculate nucleus of the cat: X and Y relay cells and perigeniculate interneurons. *J. Neurophysiol.* 45:107–120, 1981.

Somers, D., Nelson, S. B., and Sur, M. An emergent model of orientation selectivity in cat visual cortical simple cells. *J. Neurosci.* 15:5448–5465, 1995.

Swadlow, H.A. Fast-spike interneurons and feedforward inhibition in awake sensory neocortex. *Cereb. Cortex* 13:25–32, 2003.

Swadlow, H.A. and Gusev, A.G. Receptive-field construction in cortical inhibitory interneurons. *Nat. Neurosci.* 5:403–4, 2002.

Swadlow, H. A. Efferent neurons and suspected interneurons in binocular visual cortex of the awake rabbit: Receptive fields and binocular properties. *J. Neurophysiol.* 59:1162–1187, 1988.

Swadlow, H. A. Efferent neurons and suspected interneurons in S-1 vibrissa cortex of the awake rabbit: Receptive fields and axonal properties. *J. Neurophysiol.* 62:288–308, 1989.

Swadlow, H. A. Efferent neurons and suspected interneurons in S-1 forelimb representation of the awake rabbit: Receptive fields and axonal properties. *J. Neurophysiol.* 63:1477–1498, 1990.

Swadlow, H. A. Efferent neurons and suspected interneurons in second somatosensory cortex of the awake rabbit: Receptive fields and axonal properties. *J. Neurophysiol.* 66:1392–1409, 1991.

Swadlow, H. A. Efferent neurons and suspected interneurons in motor cortex of the awake rabbit: Axonal properties, sensory receptive fields, and subthreshold synaptic inputs. *J. Neurophysiol.* 71:437–453, 1994.

Swadlow, H. A. Influence of VPM thalamic afferents on putative inhibitory interneurons in S1 of the awake rabbit: evidence from cross-correlation, microstimulation and latencies to peripheral sensory stimulation. *J. Neurophysiol.* 73:1584–1599, 1995.

Swadlow, H. A. and Weyand, T. G. Corticogeniculate neurons, corticotectal neurons, and suspected interneurons in visual cortex of awake rabbits: Receptive-field properties, axonal properties, and effects of eeg arousal. *J. Neurophysiol.* 57:977–1001, 1987.

Tamas, G., Buhl, E. H., and Somogyi, P. Massive autaptic self-innervation of GABAergic neurons in cat visual cortex. *J. Neurosci.* 17:6352–6364, 1997.

Tamas, G., Somogyi, P., and Buhl, E. H. Differentially interconnected networks of GABAergic interneurons in the visual cortex of the cat. *J. Neurosci.* 18:4255–4270, 1998.

Tanaka, K. Cross-correlation analysis of geniculostriate neuronal relationships in cats. *J. Neurophysiol.* 49:1303–1318, 1983.

Troyer, T. W., Krukowski, A. E., and Miller, K. D. LGN input to simple cells and contrast-invariant orientation tuning: An analysis. *J. Neurophysiol.* 87:2741–2752, 2002.

Troyer, T. W., Krukowski, A. E., Priebe, N. J., and Miller, K. D. Contrast-invariant orientation tuning in cat visual cortex: Feedforward tuning and correlation-based intracortical connectivity. *J. Neurosci.* 18:5908–5927, 1998.

Tsodyks, M. V., Kenet, T., Grinvald, A., and Arieli, A. Linking spontaneous activity of single cortical neurons and the underlying functional architecture. *Science* 286:1943–1946, 1999.

Tsodyks, M. V. and Markram, H. The neural code between neocortical pyramidal neurons depends on neurotransmitter release probability. *Proc. Natl. Acad. Sci. USA* 94:719–723, 1997.

Turrigiano, G. G. and Nelson, S. B. Hebb and homeostasis in neuronal plasticity. *Curr. Opin. Neurobiol.* 10:358–364, 2000.

Uhlenbeck, G.E. and Ornstein, L.S. On the theory of the brownian motion. *Phys. Rev.* 36:823–841, 1930.

Wielaard, D. J., Shelley, M., McLaughlin, D., and Shapley, R. How simple cells are made in a nonlinear network model of the visual cortex. *J. Neurosci.* 21:5203–5211, 2001.

Wörgötter, F. and Koch, C. A detailed model of the primary visual pathway in the cat: Comparison of afferent excitatory and intracortical inhibitory connection schemes for orientation selectivity. *J. Neurosci.* 11:1959–1979, 1991.